On Full Duplex Wireless Networks
PHY, MAC and Network Layers Perspective

Al Kadri, Mhd Omar

Awarding institution:
King's College London

On Full Duplex Wireless Networks: PHY, MAC and Network Layers Perspective.

Mhd Omar Alkadri

A Thesis Submitted for the Degree of

Doctor of Philosophy at

King's College London

July 2017

To my beloved wife, son, mother, father and my whole family.

Acknowledgements

First and foremost, I thank God Almighty for giving me the strength, patience, determination and the means to complete my doctoral studies. This wonderful and challenging journey, which started in Jul. 2013, would not have been possible without the guidance and support of several individuals. I owe my deepest gratitude to Prof. Arumugam Nallanathan for his continuous support, insightful guidance, and inspirational mentorship. Thank you Sir, for everything you did for me, I have learnt a lot from you.

Special thanks to Prof. Hamid Aghvami, Dr. Vasilis Friderikos, Prof. Mischa Dohler, Dr Mohammad Reza Nakhai, Dr. Adnan Aijaz, and Dr. Yansha Deng for their helpful guidance and useful advice regarding my research.

I would also like to thank my examiners, Prof. Pei Xiao (University of Surrey) and Dr. Cong Ling (Imperial College London), for making my viva a sincerely enjoyable experience, as well as for their valuable suggestions which have led to significant improvements in the presentation and quality of this thesis.

I am particularly grateful to all my current and previous colleagues at CTR, including Yaqub, Ehsan, Christoforos, Giorgos, Sunila, Gao, Massimo, Maria, Enric, Alex, Syed, Mati, Shuyu, Menglan, Nasreen, Ayda, Racha, Hayder, Mohammad, Waleed, Kostas, Hadi, Hisham, Javier, and

Zainab. Thank you all for the invaluable technical and psychological support you have extended to me and for making my PhD journey immensely memorable.

I would also like extend my deepest gratitude to the School of Natural and Mathematical Sciences, King's College London for their distinguished GTS studentship, as my PhD would not have been possible without it.

Last, but not the least, I wish to thank my beloved wife and my whole family, for standing by me in ups and downs. To them I owe all the success in my life.

Abstract

In conventional half-duplex (HD) wireless communications systems, bidirectional communications between a pair of nodes is achieved with either frequency division duplexing (FDD) or time division duplexing (TDD). The former technique employs different frequency bands for the uplink (UL) and downlink (DL), whereas, in the latter technique, a single channel is shared in the time domain for both UL and DL. Such techniques however may not be suitable to fulfil the envisioned requirements of next generation wireless systems. Historically, simultaneous transmission and reception in wireless communications was deemed infeasible in practice due to the so called self-interference (SI), which is the interference generated by the transmitter of a radio on its own receiver. Recent developments in SI cancellation techniques have led to the practical realization of FD radios. FD technology has a number of attractive features, for example, it can potentially double (theoretically) the ergodic capacity, reduce the feedback delay, decrease the end-to-end delay, improve the network secrecy and increase the efficiency of network protocols.

Motivated by these developments, first in this study, a two-tier heterogeneous cellular networks (HCNs) wherein the first tier comprises half-duplex (HD) macro base stations (BSs) and the second tier consists of FD small cells. Advocating for the use of small cells as a strong candidate to deploy FD technology, for its low-powered nature and ease of

deployment. The study is conducted through a stochastic geometry approach, we characterize and derive the closed-form expressions for the outage probability and the rate coverage.

Furthermore, we move up the layers of the protocol stack and present an energy-efficient medium access control (MAC) protocol for distributed full-duplex (FD) wireless network, termed as Energy-FDM. The key aspects of the Energy-FDM include energy-efficiency, co-existence of distinct types of FD links, throughput improvement, and backward comparability with conventional half-duplex (HD) nodes.

Finally, we present a cross-layer aided routing protocol, termed as X-FDR, for multi-hop FD wireless networks. X-FDR exploits a Physical (PHY) layer model capturing imperfection of SI cancellation. At the medium access control (MAC) layer, X-FDR adopts an optimized MAC protocol which implements a power control mechanism without creating the hidden terminal problem. X-FDR exploits the unique characteristics of FD technology at the network layer to construct energy-efficient and low latency routes in the network.

Contents

List of Figures

List of Tables

Acronyms

3GPP	3rd generation partnership project.
ABS	almost blank subframes.
ACK	acknowledgement.
ADC	analog to digital converter.
AODV	ad-hoc on-demand distance vector.
AWGN	additive white Gaussian noise.
BS	base station.
CDF	cumulative distribution function.
CDMA	code division multiple access.
CR	cognitive radio.
CSI	channel state information.
CSMA/CA	carrier sense multiple access/collision avoidance.
CSMA/CD	carrier sense multiple access/collision detection.
CTS	clear to send.
D2D	device-to-device.
DAC	digital to analog converter.

DCF distributed coordination function.

DIFS double inter-frame spacing.

DL downlink.

DSL digital subscriber line.

eICIC enhanced inter-cell interference coordination.

EIFS extended inter-frame spacing.

FD full-duplex.

FDD frequency division duplexing.

FT first transmission.

GP ground plane.

GPRS general packet radio service.

GSM global system for mobile.

HCN heterogeneous cellular network.

HD half-duplex.

HetNet heterogeneous network.

HPPP homogeneous Poisson point process.

ICI inter-cell interference.

ICIC inter-cell interference coordination.

IDC international data corporation.

IEEE institute of electrical and electronics engineers.

LAN	local area network.
LTE	3GPP long term evolution.
M2M	machine-to-machine.
MAC	medium access control.
MIMO	multiple-input-multiple-output.
MM	millimetric.
MMSE	minimum mean square error.
NACK	negative acknowledgement.
NAV	network allocation vector.
OFDMA	orthogonal frequency division multiple access.
PDF	probability density function.
PHY	physical.
QoS	quality of service.
RERR	route error.
RF	radio frequency.
RREP	route reply.
RSI	residual self-interference.
RTS	ready to send.
RUPD	route update.
SC	small cell.

SI self-interference.

SIFS short inter-frame spacing.

SINR signal to interference and noise ratio.

SNR signal to noise ratio.

ST second transmission.

TDD time division duplexing.

TS transmission flag.

UL uplink.

WLAN wireless local area network.

Wi-Fi wireless fidelity.

Chapter 1

Introduction

Wireless radios are rapidly becoming an essential part of every day's life. With laptops connecting to hotspot access points, smart phones streaming videos wirelessly through cellular networks, and high definition (HD) video group calls, users are increasingly demanding higher speeds and wider availability from their providers. There are several predictions on how the growth of data will reach by 2020, and the amount of connected devices there will be. According to IDC's Digital Universe study [1]. The amount of data is expected to reach 44 zetabytes (ZB) by 2020, compared to 4.4 ZB in 2013, with 10 times multiplication factor, doubling the amount of data almost every two years, as demonstrated in Fig. 1.1. Such growth results mainly from the growing number of M2M applications, such as smart meters, video surveillance, healthcare monitoring, sensors, device-to-device (D2D) communications, vehicular communications, transportations, and package or asset tracking, etc. In another study done by Cisco [2], the predicted amount of connected devices in 2020 is expected to reach 50 Billion, with an average of 6.6 devices per person, compared to 12.5 Billion devices in 2010 with an average of 1.8 devices per person as shown in Fig 1.2. Those predictions may not nec-

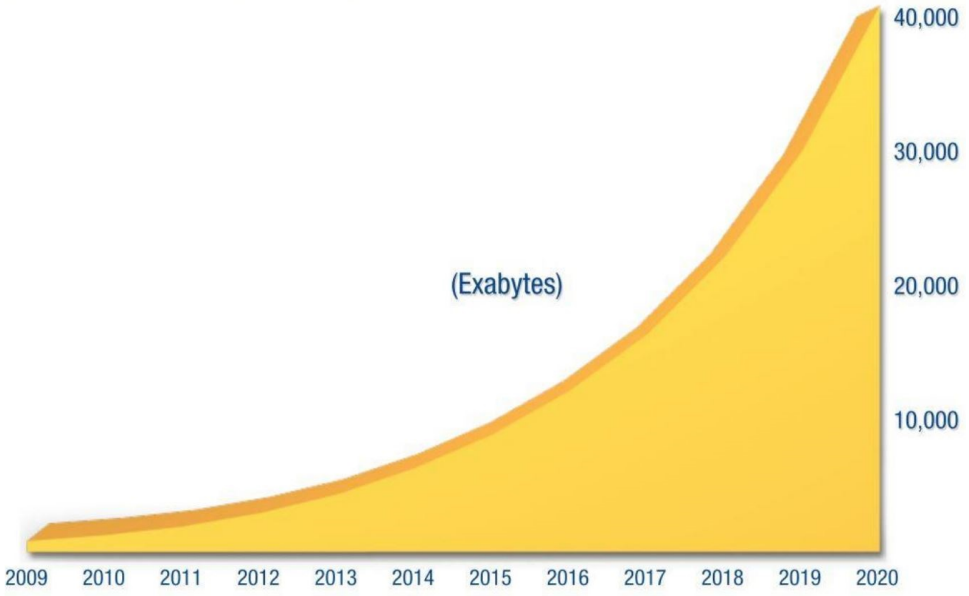

Figure 1.1: Predicted data growth by 2020.
Source: IDC's Digital University Study, December 2012.

essarily become a reality or represent exactly how things are going to be, however, it indicates a clear trend of imminent growth that must be properly addressed.

This means that the devices trying to connect through wireless channels is bound to increase, necessitating further research into addressing the problems and challenges accompanied with the expected densification and the change of requirements.

The challenges in wireless communications originate mainly from the shared and broadcast nature of the wireless medium. Which means that the devices attempting to communicate or access the network in a specific area, need to contend for the wireless channel, requiring adequate access mechanisms to share the medium efficiently, especially with the increasing scarcity of the spectrum. Therefore, different technologies had been proposed to meet the requirements of next generation wireless communications and address the problems of spectrum scarcity, capacity and availability. Proposed solutions included cognitive radios [3], millimetre

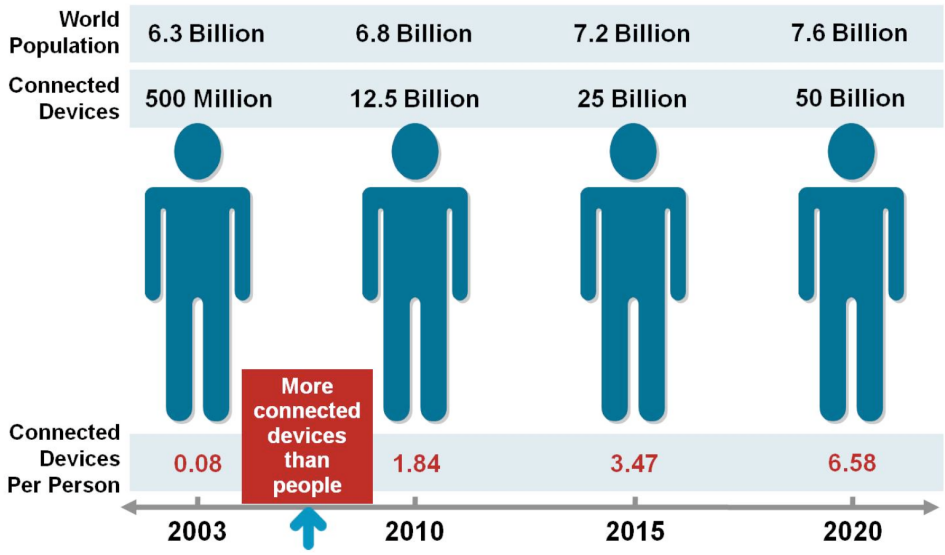

Figure 1.2: Predicted number of connected devices by 2020.
Source: Cisco IBSG, April 2011.

(MM) wave communications [4], and D2D communications [5].

One important and promising solution that recently attracted attention of both academic and industrial communities, is Full-Duplex (FD) technology.

FD communications offer many appealing features and advantages which made it a strong candidate to achieve the requirements of next generation wireless communication. Features of FD technology include theoretically doubling the capacity of the network [6, 7], reducing feedback delay [8], decreasing end-to-end delay [9], improving network secrecy [10], and increasing the efficiency of higher layers network protocols [11]), in addition to the possibility of merging FD technology with other proposed solutions to accomplish significant improvements in the performance of wireless networks. This made research on FD technology a necessity, and significantly intriguing.

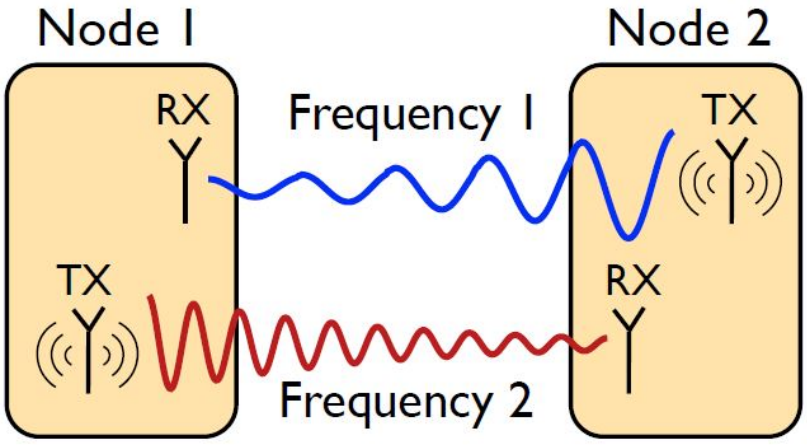

Figure 1.3: Frequency division duplexing.

1.1 Current Wireless Communications

Current wireless communication systems perform bi-directional communications between a pair of nodes by using duplexing techniques and isolated sprecturm resources for uplink and downlink. The main duplexing techniques are frequency division duplexing (FDD) and time division duplexing (TDD).

FDD uses two different carrier frequencies to achieve simultaneous transmission, one frequency for uplink and another spatially isolated frequency for downlink, as illustrated in Fig. 1.3. With this technique, Nodes 1 and 2 can exchange data at the same time, while using two different frequencies. This provides spacial isolation between the two nodes and prevents them from interfering with each other. Many networks use FDD as a standard to enable bi-directional uplink and downlink transmissions. Examples include 4G Long Term Evolution (LTE) network [12], Global System for Mobile (GSM) [13], Code Division Multiple Access (CDMA2000) cellular networks [14] and Digital Subscriber Line (DSL) connections [15]. The use of two separate frequencies indeed achieve simulation communication, however it could be rather costly in

terms of spectrum allocation, and economical cost inefficiency as well, since service providers will have to purchase and license two frequencies to achieve successful communications via FDD.

In TDD, nodes divide access in time slots as shown in Fig. 1.4. When Nodes 1 and 2 attempt to communicate with each other, they allocate different time slots to each node, which may also be done by the access point in centralized topologies. Afterwards, the nodes take turns in sending data to each other based on the assigned time slots. Consequently, the interference is prevented by allowing a single transmission at a time, dividing the single frequency channel in terms of time slots. TDD is simple to implement and does not accommodate the complexity of orthogonality that FDD has, therefore, many data networks adopts it as a duplexing scheme, especially in ad-hoc networks where frequency use is not tightly controlled. Using TDD achieve bi-directional transmissions, however, it is not simultaneous and therefore is known as half duplexing, additionally, it can lead to other problems across the network, like the hidden terminal problem, when nodes think the spectrum that include a receiving node is idle, and starts a new transmission that collides with an ongoing one. Examples of TDD usage include wireless Local Area Networks (WLAN 802.11) [16] and Bluetooth (802.15) [17], in addition to mobile communications.

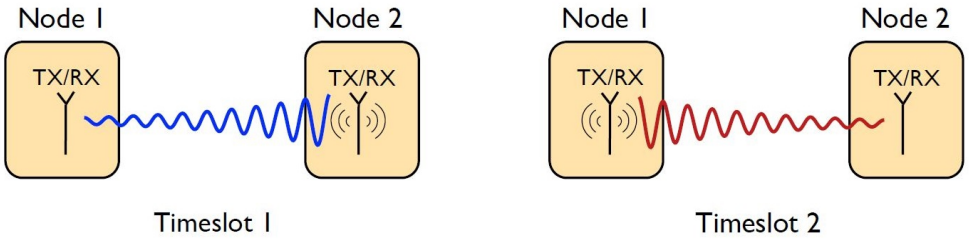

Figure 1.4: Time division duplexing.

1.2 Inband Single Channel Full Duplex

To mitigate the inherited problems of TDD and FDD, a radio that can transmit and receive simultaneously using a single carrier frequency is required. However, until recently, simultaneous transmission and reception in wireless communications was deemed infeasible in practice due to the immense self-interference (SI), which is the interference generated by the transmitter of a radio on its own receiver as illustrated in Fig 1.5. With such overwhelming self-interference, that could measure hundreds of thousands of times compared to the desired signal, the receiver of Node 1 is unable to decode any signals that Node 2 is transmitting to Node 1.

> "It is generally not possible for radios to receive and transmit on the same frequency band because of the interference that results. Thus, bidirectional systems must separate the uplink and downlink channels into orthogonal signaling dimensions, typically using time or frequency dimensions."
>
> - Andrea Goldsmith, "Wireless Communications," Cambridge Press.

This SI formed the biggest challenge of the practicality of FD. How-

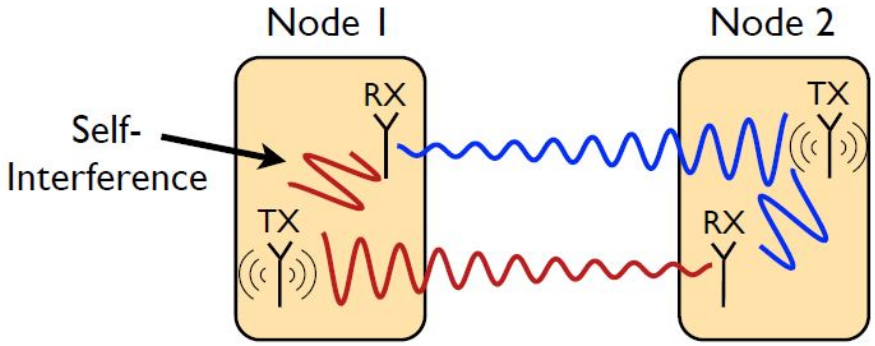

Figure 1.5: Self-Interference of nodes on their own receivers.

ever, recent developments in SI cancellation techniques have led to the practical realization of FD radios. The major developments of SI cancellation and different proposed schemes are discussed in Chapter 2.

Full-duplex mode is one of the technologies that is being thoroughly investigated as an enabling technology of the next generation wireless communication. Several different organizations have already demonstrated the feasibility of FD from a technical point of view. In fact, a start-up company established by researchers from Stanford university, called 'Kumu Networks'[1], had specialized in FD wireless communications and secured more $45.43 millions of investments by big providers to accelerate the practical realization of FD[2]. Investors include Cisco, Verizon Ventures, Deutsche Telekom, along with previous investors NEA, Third Point Ventures and Khosla, among many others, who are already carrying out trials of FD technology in different phases. This confirms the significant interests of big industry players in FD technology and consequently could indicate an imminent future implementation.

1.2.1 Benefits of Full Duplex

There are numerous features and potential benefits that FD technology can provide to meet the requirements of next generation wireless communications. Benefits include

- Theoretically **doubling the ergodic capacity** [6, 7, 18, 19], allowing both uplink and downlink nodes to communicate simultaneously on the same frequency, compared to the time alternating TDD-based systems, or utilize both licensed frequencies of FDD-based systems in both direction at the same time.

[1] http://www.kumunetworks.com.
[2] http://www.fiercewireless.com/tech/kumu-networks-brings-full-duplex-to-mwc.

- **Reducing the feedback delay**, since reception of feedback signaling, such as control signals, channel state information (CSI), acknowledgement (ACK) messages, resource allocation information, etc., during data transmission enables shorter air interface latency in feedback information [8].

- **Decreasing the end-to-end delay**. An FD-capable relay can transmit as soon as it receives the data, instead of having to wait for the previous transmission to complete before it can forward the received data [9, 20].

- **Improving the network secrecy**. A bystanding node that is not involved in the FD communication will receive two mixed signals at the same time, making it significantly difficult to decode the intended signal for an eavesdropping attack or packets sniffing [10, 21].

- **Increasing the efficiency of network protocols** like medium access control [11]. Actually, it is significantly important to account for FD capabilities in the protocols of higher layers, since most legacy protocols prevent simultaneous transmissions for collisions avoidance.

- FD technology **can be merged with many emerging technologies** to achieve higher performance, like cognitive radios (CR), device-to-device (D2D) communications, massive MIMOs, small cells (SC), ad-hoc networks, vehicular and machine-to-machine (M2M) communications.

1.2.2 Challenges of Full Duplex

The most important challenge in terms of FD hardware implementation, is the difficulty of designing a self-interference cancellation mechanism that could, ideally, perfectly omit the signal originating from the transmitter of the FD node. Many imperfect SI cancellation schemes had been proposed, however, it is rather difficult to handle SI of nodes with high transmission power like macro base stations. With the realization of FD technology, additional challenges arises, like addressing its capabilities and limitations at the PHY layer, and address the increased inter-user interference, with providing tractable frameworks to evaluate the performance gain. Other challenges also occur in higher layers to address the FD capabilities with maintaining backward compatibility with HD nodes. Energy consumption in FD networks is also an important challenge to be addressed, owing to additional hardware and processing capabilities of nodes. Therefore, novel designs of higher layer protocols shall be provided to reap the full benefits of FD technology.

1.3 Thesis Contribution

1.3.1 Key Outcomes

The contributions of this thesis cover different aspects of FD communications. The key outcomes of this research in the form of novel frameworks, solutions, algorithms, and protocol enhancements are summarized below.

- Considering FD technology in heterogeneous cellular networks (HCNs), a tractable model for the interference coordinated two-tier HCN with FD small cells was presented, wherein tier 1 comprises legacy HD macrocells and tier 2 consists of FD small cells. By explicitly

accounting for spatial distribution of base stations, self-interference, transmit power, cell association, uplink power control and ABS factor, the signal-to-interference noise (SINR) expressions for users in the corresponding two tiers were provided. Specifically, the underlying model captures the DL scenario for tier 1 and both UL and DL scenarios for tier 2, since tier 1 and tier 2 operate in HD and FD mode, respectively. Advocating for the use of FD in small cells as their low powered nature and ease of deployment.

- Based on the considered system model for two-tier HCN with FD small cells, the closed-form expressions for outage probability and rate coverage of different tiers were derived. The final expressions explicitly account for interference coordination, and a comprehensive performance evaluation through numerical as well as simulation studies were provided. investigating the impact of various design parameters on network performance in various scenarios.

- For FD technology of wireless distributed networks, an energy efficient FD medium access control (MAC) protocol was presented, while particularly accounting for the peculiarities of FD environments such as bi-directional and uni-directional links (explained in Chapter 4). The protocol operation of [22] is adapted for the proposed energy saving technique. The proposed protocol, termed as Energy-FDM, particularly focuses on reducing the transmission power of data and acknowledgement (ACK) packets to achieve energy efficiency. It also ensures operability of both bi-directional and uni-directional links, maintains backwards compatibility with co-existing HD nodes, and achieves high throughput by using FD while addressing the hidden node problem. The proposed proto-

col is analysed through a stochastic geometry based approach for accurate and realistic performance evaluation.

- Based on the proposed protocol, A cross-layer aided energy efficient FD routing protocol was proposed termed as X-FDR (explained in Chapter 5). Further modifications on the adopted MAC protocol were made for compatibility. X-FDR accounts for the residual self-interference (RSI) in the SINR expressions of the nodes, which is the interference caused by the imperfection of interference cancellation mechanisms. It also accounts for the MAC retransmission attempts to reconcile more realistic scenarios. A novel route cost metric was proposed, aiming to minimize the energy consumption of the route and decrease the end-to-end latency.

- We propose the use of several FD features in X-FDR, like the ability to sense the medium while transmitting, which provides immediate reaction towards channel errors. This consequently enables nodes to send a burst of packets, sized by the minimum buffer size β_{min} of nodes on the selected route, and wait for an acknowledgement packet (ACK) for the last received packet only, instead of acknowledging the reception of each packet. It also employs immediate forwarding, where an FD node does not have to wait for the reception of the full packet before it starts forwarding. This feature reduces the end-to-end delay of the transmitting stream and increases network availability.

- Novel processes for route discovery and route maintenance were proposed for X-FDR, aiming to reduce the delays caused by new route discovery, by initiating route discovery at the node where the communicating link breaks, then resuming the transmission by the

node that received the full burst of data.

1.3.2 List of Publications

The publications [3] related to the main contributions of this thesis are stated as follows. The chapter relevance of different publications is given in Table 1.1.

1. **M. O. Al-Kadri**, A. Aijaz and A. Nallanathan, "Ergodic Capacity of Interference Coordinated HetNet with Full-Duplex Small Cells" European Wireless 2015, pp. 1-6 Budapest, Hungary, May, 2015.

2. **M. O. Al-Kadri**, Y. Deng, A. Aijaz and A. Nallanathan, " Outage Probability of Heterogeneous Cellular Networks with Full-Duplex Small Cells" IEEE GLOBECOM 2016, pp. 1-6, Washington DC, USA, December, 2016.

3. **M. O. Al-Kadri**, Y. Deng, A. Aijaz and A. Nallanathan, " Modeling and Analysis of Two-Tier Heterogeneous Cellular Networks with Full-Duplex Small Cells" IEEE Access, Accepted for publication in 15 Mar. 2017.

4. **M. O. Al-Kadri**, A. Aijaz and A. Nallanathan, "An Energy-Efficient Full-Duplex MAC Protocol for Distributed Wireless Networks," IEEE Wireless Communications Letters, vol. 5, no. 1, pp. 44-47, February, 2016.

5. **M. O. Al-Kadri**, A. Aijaz, Y. Deng and A. Nallanathan, "X-FDR: A Cross-Layer Routing Protocol for Multi-hop Full-Duplex

[3] The numbering associated with this section does not refer to the Bibliography section of this thesis.

Table 1.1: Publications related to individual chapters

Chapters	Journals	Conferences
Chapter 3	(3)	(1), (2)
Chapter 4	(4)	-
Chapter 5	(5)	-

Wireless Networks" Submitted to IEEE Wireless Communications Magazine in 18 Jun. 2017.

1.4 Outline of the Thesis

The reminder of the thesis is structured as follows. Chapter 2 provides the preliminaries and related works on the required technical background for understanding the research area addressed. The main contributions of the study are related to three distinct area about FD technology: Modelling and analysis of two-tier heterogeneous cellular networks, with case study of outage and rate coverage probabilities, provided in Chapter 3. Proceeding to a higher layer in the protocol stack, specifically, the MAC layer, an energy efficient FD MAC protocol that accounts for different FD link types is presented in Chapter 4. Further, proceeding higher up to the network layer, Chapter 5 presents a cross-layer aided FD routing protocol for distributed multihop wireless networks. Since each contribution chapter addresses a unique research problem, concluding remarks are presented therein. Based on the overall picture of research conducted in the thesis, the main conclusions and potential future work are presented in Chapter 6.

Chapter 2

Preliminaries and Related Work

2.1 Full Duplex Technology

2.1.1 Basic concept of FD technology

The concept of in-band full-duplex (FD) technology is the use of the same time and spectral resources to conduct communications and exchange information. In contrast to the current systems, which operate in half-duplex mode, in one direction at a time, or in out-of-band full-duplex mode using two separate frequencies for each direction. This approach allows nodes to communicate simultaneously using the same frequency band, theoretically doubling the spectral efficiency of a system. However, the biggest challenge for the practical realization of FD systems is the self-interference (SI). SI is caused by the strong transmitted signal of a node at its own receiver, causing interference to itself when transmitting on the same frequency band that is significantly higher than the intended signal. SI can be millions to billions of times stronger (60-90 dB) than a received signal [23, 24]. For example, a radio with a transmit power

of 20 dBm and a noise floor of approximately -90 dBm needs to cancel nearly 110 dB of SI to ensure that its own transmissions do not disrupt the reception. If a cancellation mechanism was presented to cancel this SI, the signal becomes theoretically decodable. The main idea of SI cancellation lies in the fact that the transmitted signal is perfectly known at the transmitter, hence it can be used to totally suppress the SI at the receiving end. However, several non-linearities in the radio frequency (RF) chain and errors in the channel estimations may occur, negatively affecting this cancellation processes. Those reasons lead to the belief that in-band FD radio systems are not practically feasible. However, recent advances in the SI cancellation techniques (Briefed in Sec. 2.2), have lead to the practical realization of FD communications.

Historically, several SI cancellation mechanisms had been proposed, however, FD technology were deemed infeasibly costly at times as it required altering established systems to adapt with FD, or an unnecessary luxury at other times, since networks used to fulfil their expectations. However, this belief is not dominant any more for different reasons, like the recent widespread realization that most traditional approaches to enhance spectral efficiency such as advances in modulation, coding, and multiple-input-multiple-output (MIMO) technology, have been exhausted by now, leaving system designers willing to explore different and non-traditional approaches. The bigger drive nonetheless, might be the architectural progression towards short-range systems, like small cell networks and Wi-Fi access points, where the transmission power and their cell-edge path loss is significantly less than its traditional base stations counterparts, making SI cancellation problem much more manageable. This shift towards smaller cells, along with the significant needs of service providers for capacity expansion, more bandwidth and wider coverage, in

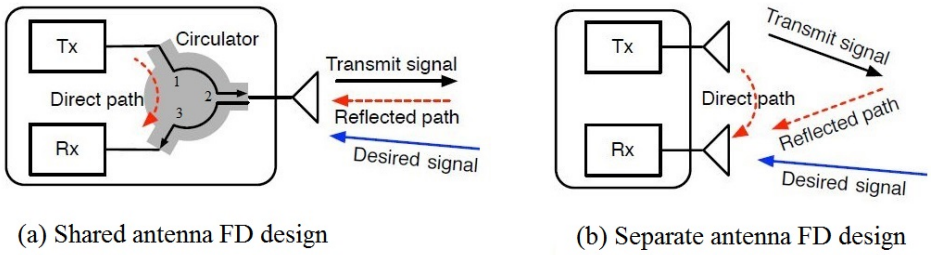

(a) Shared antenna FD design

(b) Separate antenna FD design

Figure 2.1: Two methods of FD antenna design.

addition to the emergence of new rising technologies that could exploit FD capabilities, have sparked a renewed interest in FD technology.

2.1.2 FD radio design

There are two design methods for separating the transmit and receive signals for FD radios antenna design, which are shared antennas and separated antennas. Fig. 2.1(a) demonstrate the basic structure for shared antenna FD radio using a circulator as a duplexer [23]. An ideal three-port circulator would prevent the leakage of the transmitted signals into the receiving chain. With the use of circulator, FD radio can simultaneously transmit and receive in a frequency band with a shared antenna. However, in a practical environment, the transmitted signal in the circulator does flow from point 1 to point 3, which can affect the intended received signals from port 2 as direct SI, which will required additional SI cancellation techniques.

The second method for separating the transmit and receive signals is by physically separating the antenna components, dedicating a separate antenna for transmitting and receiving. When the number of equipped antennas is 2 or more, the separated antennas can be utilized for FD transmission as shown in Fig. 2.1(b). Contrary to the shared antenna design, each node divides the antennas into groups for simultaneous trans-

mission and reception, allocating the spatial resources into two parts for FD transmission [25–30].

2.1.3 FD transmission topology

There are three fundamental topologies for FD wireless communications, as demonstrated in Fig. 2.2, with the assumption that nodes using FD and HD radios can be equipped with multiple antennas of different quantities. In Fig. 2.2(a), the topology of bi-directional FD transmission is illustrated, where two nodes, a and b, attempt to exchange signals for two-way communication. Let $link_{ab}$ and $link_{ba}$ denote the transmission links from node a to node b and from node b to node a, respectively. If HD transmission is applied for this two-way communication, $link_{ab}$ and $link_{ba}$ will have to utilize separate time or frequency resources for successful transmissions, which reduces spectrum efficiency. However, if the nodes operate in FD mode, they can simultaneously transmit and receive using a single frequency band, leading to the theoretical doubling of the spectrum efficiency.

The second topology is the uni-directional (relay) topology, as illustrated in Fig. 2.2(b). In relay topology, at least three distinctive nodes are involved, a source node s, relay nodes r and a destination node d. When a source node s attempts to transmit data towards a corresponding destination d, it uses one or a series of selected relay nodes. Let $link_{sr}$ and $link_{rd}$ denote the transmission links from source s to relay r, and from relay r to destination d, respectively. If HD transmission is applied to the relay node, $link_{sr}$ and $link_{rd}$ will have to utilize separated resources, where the source and relay nodes transmit their signals via different time or frequency resources. However, using FD transmission mode, the source and relay nodes can simultaneously transmit their

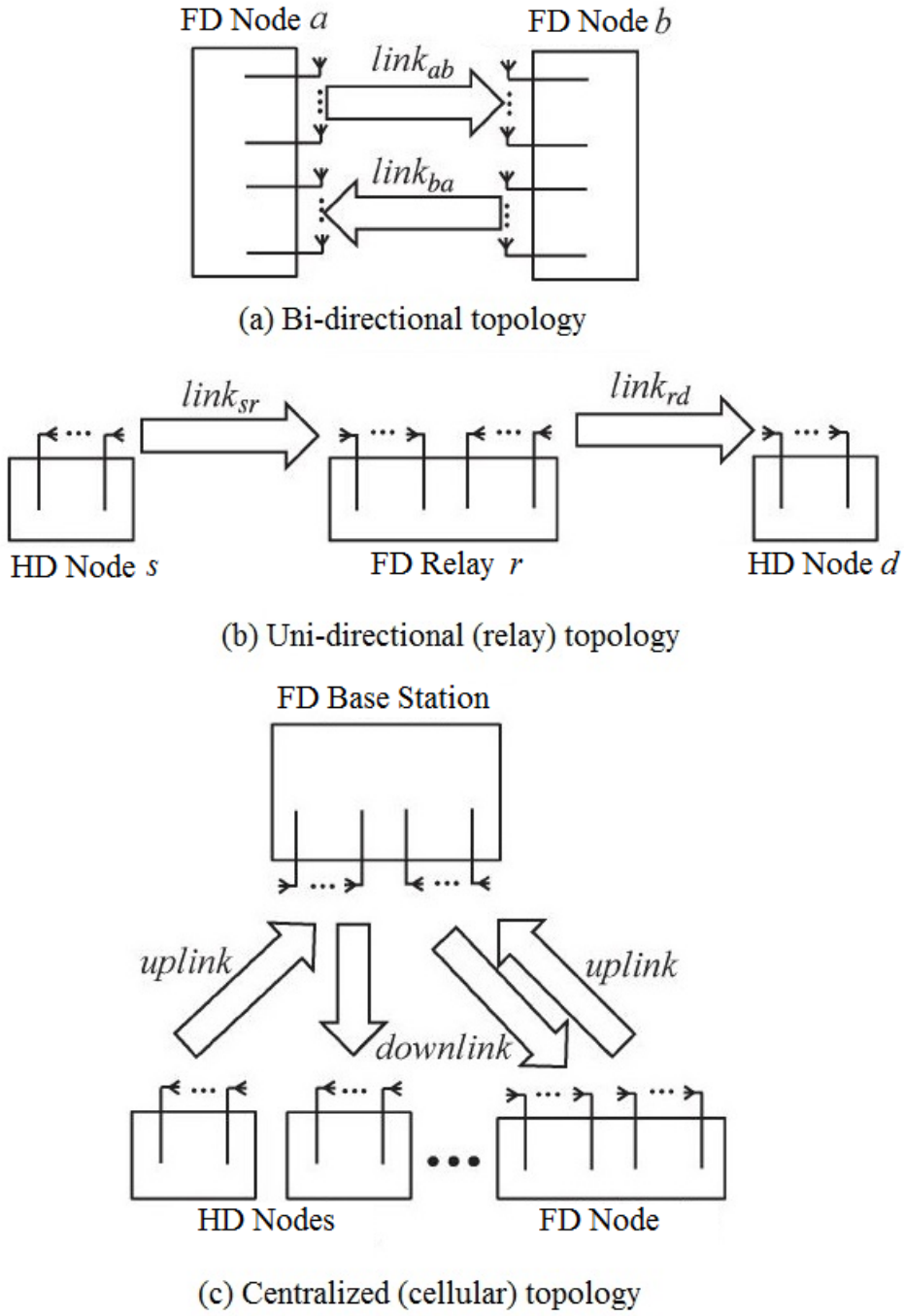

Figure 2.2: FD transmission topologies.

signals using the same frequency band.

Finally, Fig. 2.2(c) demonstrate a centralized (cellular) topology, which consists of a base station (BS) and multiple mobile stations. In this topology, two kinds of data links are defined, uplink and downlink, whereas each individual mobile station transmits its data signals toward a designated BS, and the BS transmits data signals to multiple mobile stations. If HD transmission is adopted at the BS, the uplink and downlink channels are separated orthogonally using either TDD or FDD. However, if BS employs FD transmission, multiple mobile stations can simultaneously communicate with the BS using the same spectrum frequency. Additionally, if mobile stations employ FD technology as well, they can simultaneously transmit and receive data signals with the FD-enabled BS using identical uplink and downlink channels, while an HD mobile station can only communicate with the BS through separate uplink or downlink channel.

2.2 Self-Interference Cancellation Techniques

Self-Interference (SI), is the interference generated by the transmitter of a radio on its own receiver. It forms the key challenge in the realization of FD systems. In order to overcome the strong SI, significant efforts have been devoted to handle this interference. Recent advancements in SI cancellation techniques have made terminals able to suppress sufficient amount of SI, leading to the practical feasibility of FD technology. Techniques for interference cancellation in research can be categorized in three different domains, propagation, analog and digital domain cancellation techniques.

Cancellation in propagation domain is the first step of SI cancellation,

it aims at using the properties of electromagnetic waves, applying insulations between transmitters and receivers. The amount of cancellation achieved in the propagation domain depends on the distance between antennas, the antenna directionality, and the antenna placement on the FD device.

Analog Cancellation is the cancellation performed in analog domain before the received signal passes through the Analog-to-Digital Converter (ADC). It can be done using either active or passive techniques where analog circuit mitigation is performed to increase attenuation on the SI signal. It is used as the second suppression stage of in-band FD architectures. The basic concept is to track the propagation effect of the interfering signal, then subtract it from the received signals using specific electronic processing in the analog domain.

Digital cancellation operates on digital samples. If an FD radio has a good estimate of the phase and amplitude of its transmitted signal at the receive antenna, it can generate the digital samples for its transmitted signal and subtract them from its received samples. In this section, the SI cancellation techniques in the three domains are briefed for a better understanding of how FD radios are achieved.

2.2.1 Propagation Domain

The first step of SI cancellation occurs in the propagation domain. SI cancellation in the propagation domain reduces the power level of the received SI significantly by applying insulations between transmitters and receivers, and allows further SI reduction at the analog and digital domains. There are two different schemes of propagation techniques, based on the design of antennas illustrated in Fig 2.1.

The first FD antenna design, the shared-antenna, consists of using the

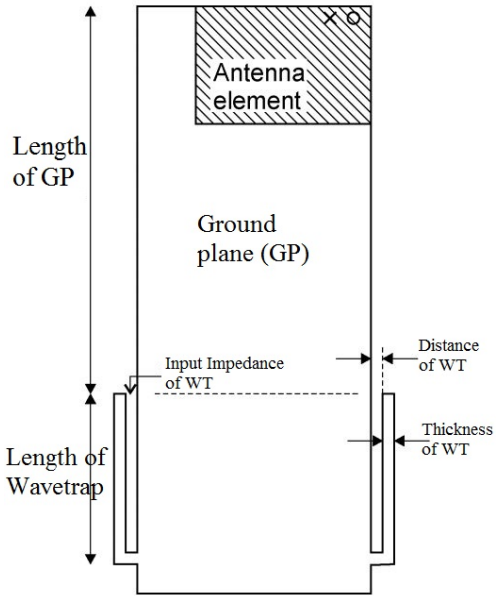

Figure 2.3: SI cancellation in propagation domain using wavetraps.

same antenna for transmission and reception by employing a circulator, which is a circuit that routes the signals from the transmit chain to the antenna and from the antenna to the receive chain [31,32]. For example, in the relay topology, it is common to position antennas back-to-back, which means arraying antennas together that connect each relay end. Moreover, different techniques can be applied like the wavetraps technique [33] as shown in Fig. 2.3, which provide isolation by introducing resonant short circuit transmission lines to the long sides of the chassis edges, achieving effective electrical shortage of the terminal ground plane, similar to the band-gap structures presented in [34], which uses metallic electromagnetic structure which have high surface impedance.

The separated-antenna design, consists of using dedicated antennas to transmit and receive. In this design, it is possible to suppress interference using a variety of ways, like path loss attenuation, increasing the distance between antennas to further increase the attenuation or by placing absorptive shielding between transmitting and receiving an-

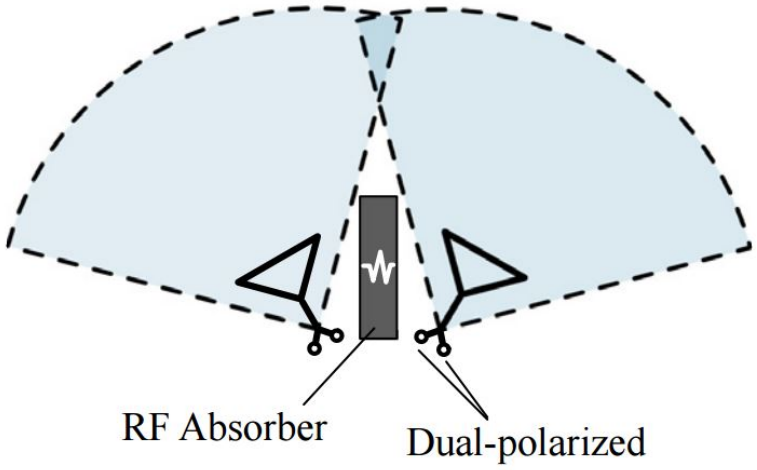

Figure 2.4: SI cancellation in propagation domain using dual polarization and absorptive shielding.

tennas [35–37]. These approaches are limited by the design of the FD devices, which forms a significant challenge in implementing them within commercial products. Another approach to isolate antennas and enhance the SI suppression is the use of cross-polarization [36, 37], for instance, terminals can transmit in vertical polarization and receive in horizontal polarization. Fig. 2.4 [36], illustrate an example of using both dual polarization and an absorptive shielding. Another SI cancellation method in the propagation domain would be to exploit the antenna radiation pattern of directional antennas, then carefully placing the receiving antenna in 'null points' of the transmit antenna array [36, 38, 39]. Another important SI cancellation method is multiple antenna cancellation [39], which employs multiple antennas to make the RF signals add destructively at the receiver antenna as shown in Fig 2.5(a), or to obtain an inverse version of the received RF signal through internal phase shifting by 180^o, and then subtract it at the RF part as shown in Fig 2.5(b).

The majority of SI cancellation schemes in the propagation domain of both antenna designs are passive mechanism with obvious limitations, since they are highly sensitive to environmental conditions and

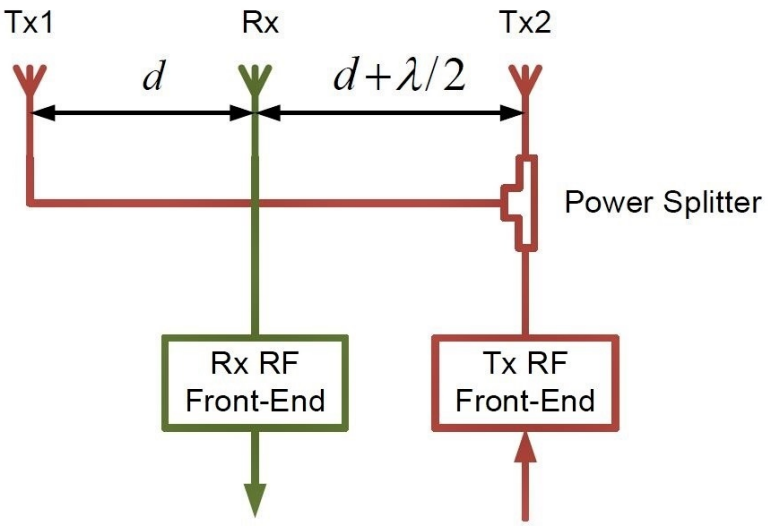

(a) with distance $d+\lambda/2$

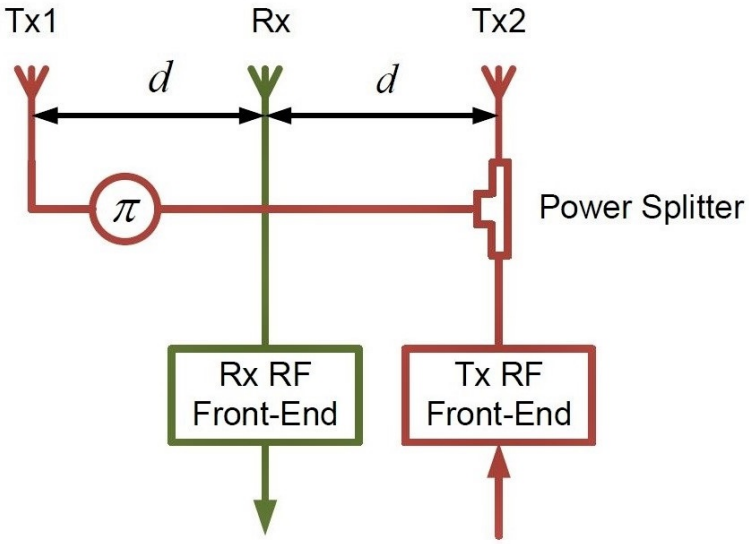

(b) with internal inverter

Figure 2.5: SI cancellation in propagation domain using multiple antenna positioning.

do not track the changes in the signal that naturally suffer different phenomenons over the wireless channel, it can also attenuate and damage the intended signal in addition to the SI. Therefore, it is necessary to track the variations of the signal on the propagation channel and apply further active SI cancellation schemes in the analog and digital domains.

2.2.2 Analog Domain

Analog cancellation is the second suppressing stage in SI cancellation, and the first active SI cancellation phase. The main goal of SI cancellation in the analog domain is to track the propagation effect of the interfering signal, and by means of electronic processing subtract it from the received signal before it enters the analog-to-digital converter (ADC) [24, 35, 40–42]. Moreover, tracking the transmitted signal is also possible in the digital domain, where the interference channel effect by means of gain and phase adjustments is applied, then converted back to analog domain to subtract it from the received signal [27, 35].

There are various analog cancellation schemes proposed, like analog cancellation using vector modulation [43, 44]. Vector modulation enables a modulator to control the angle and amplitude of an input signal, scale it and rotated by an intended value. An input signal is split into two components, in-phase (I) and quadrature phase (Q), where the Q component is 90^o out of phase from the I. The I and Q components are separately scaled using variable amplifiers, and then combined to achieve the desired angular and scaling shift in the input signal. The 90^o phase shift is implemented through delaying the input signal by a quarter wavelength ($\lambda/4$ delay). An example block diagram of a vector modulator using is shown in Fig 2.6, using an existent noise cancellation chip like QHx220. The transmit signal is sampled through an RF signal splitter and inserted

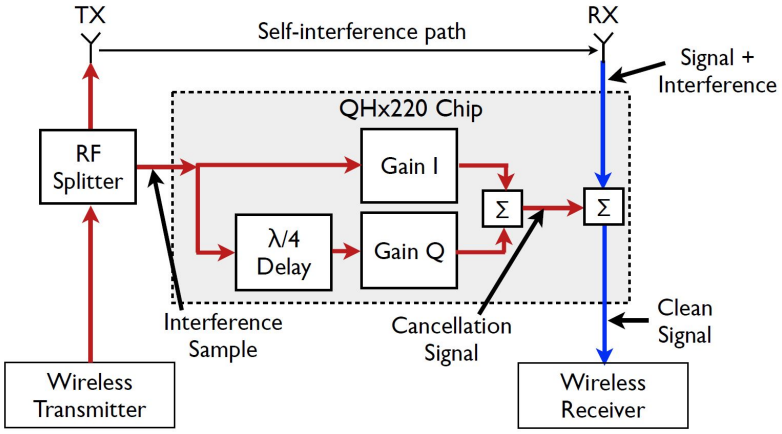

Figure 2.6: SI cancellation in analog domain using vector modulation.

into the interference sample input, then the vector modulator chip adjust I and Q gains to reflect the on-air attenuation and phase change of the transmit signal, creating a cancellation signal that can remove the ambient interference from the input signal. Vector modulation based SI cancellation is limited by the frequency dependence of the $\lambda/4$ delay. Q component has a fixed delay with respect to I component. Therefore, this approach can correctly emulate a 90^o phase shift for a single frequency, while for signals with bandwidth, this delay will only match one frequency of the bandwidth, meaning that this technique suffers from a similar bandwidth constraint as antenna cancellation, and different schemes shall be used for SI cancellation of signals with bandwidths.

All radios that perform SI cancellation by adjusting phase will encounter a bandwidth constraint that bounds its cancellation capabilities. This limits the achieved cancellation by both phase offset cancellation and cancellation using vector modulation. Therefore, to cancel further interference, a radio needs to obtain an inverted signal that forms the perfect negative of the transmitted signal, which can be used to theoretically achieve perfect SI cancellation. FD radios can use a balanced/unbalanced (Baluns) transformer to obtain the inverted signal of SI without phase

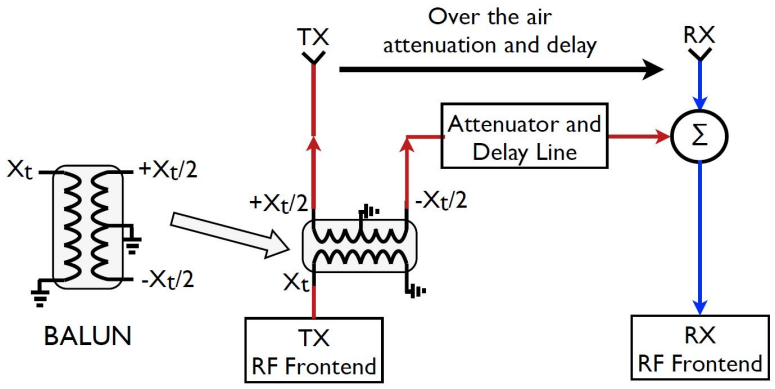

Figure 2.7: SI cancellation in analog domain using signal inversion.

adjustment, and then use the inverted signal to cancel SI [45]. Fig. 2.7 demonstrate the antenna design with the use of Balun transformer to cancel SI. The positive signal is transmitted through the transmit antenna, while the negative signal traverse over a wire to create an SI cancellation signal. A passive variable delay and attenuator is used to match the cancellation signal to the SI at the receiving antenna. Then, the receiver sums the received signal with the generated cancellation signal to omit the residual SI. While signal inversion cancellation scheme can theoretically cancel SI perfectly, there are practical limitations, since the transmitted signal through the air experiences attenuation and delay. To obtain perfect cancellation the FD radio must apply identical attenuation and delay to the inverted signal before the summation occur, which is challenging to achieve in practice. Additionally, the Balun itself may suffer engineering imperfections, like leakage or a non-flat frequency response, necessitating a the third phase of SI cancellation process, the SI cancellation in the digital domain.

2.2.3 Digital Domain

SI cancellation in the digital domain is the third phase of SI cancellation, in order to achieve successful bidirectional communications. There

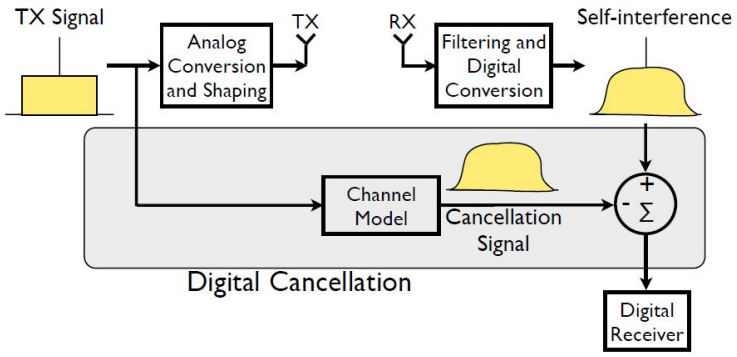

Figure 2.8: Basic SI cancellation in digital domain.

are two main goals for conducting SI cancellation in the digital domain, first, to eliminate the residual SI that remained after the first two phases of SI cancellation took place, and second, to account for the multipath components. Although significant efforts have been devoted for the SI cancellation schemes in the propagation and analog domains, there is still residual SI that negatively affects the reception of the intended signal. Digital cancellation operates on digital samples. If an FD radio has a good estimate of the phase and amplitude of its transmitted signal at the receive antenna, it can generate the corresponding digital samples for its transmitted signal and subtract them from its received samples by applying further complex and heavy signal processing. Fig. 2.8 demonstrate the basic digital cancellation operation.

Digital cancellation on its own is insufficient, it has to be adopted with additional analog SI methods. In literature digital SI cancellation schemes could cancel up to 20-25 dB [46, 47] The limitation is bound by the ADCs, which have a limited dynamic range, and since SI is significantly stronger than the intended received signal, an ADC can quantize away the received signal, making it unrecoverable after digital sampling as shown in Fig 2.9.

There is no standard set of digital cancellation techniques. Research

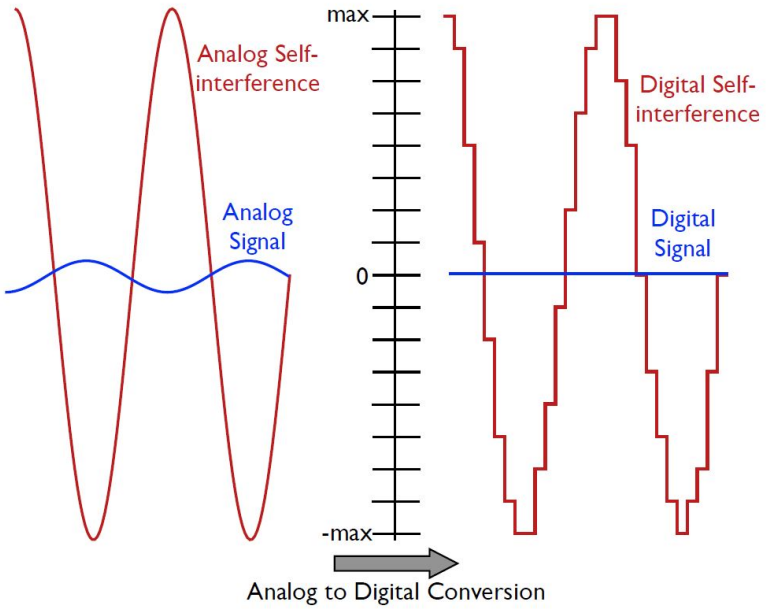

Figure 2.9: Effect of ADC quantization with strong SI signal.

on this area is vastly developing in a rapid pace. Numerous amount of papers have been published recently proposing different ways and techniques to handle the SI issue. An important step in this stage would be to model the channel chain from the transmitter digital-to-analog converter (DAC) to the receiver ADC, so that filtering can be effectively applied. Once that is done, It becomes possible to use different techniques like, perform beamforming for MIMO-capable systems [48], optimal power gain control and allocation, and antenna selection [49–52], minimum mean square error (MMSE) filters and null-space projections [53], and joint decoding [52], etc.

Therefore, for the best SI cancellation results, a selection of different methods and techniques shall be applied on different stages and domains to allow successful decoding of the intended signal, resulting in an efficient operation of FD systems that can transmit and receive simultaneously on the same frequency.

2.3 Related Work

In this section, the related state of the art in FD communications is presented. Since the contribution of this thesis is concerned with different layers of the protocol stack, the related work on different aspects of FD communications is summarized as follows.

2.3.1 Modeling and Analysis of Full Duplex Heterogeneous Networks

Recent studies on modeling and analysis of Heterogeneous Cellular Networks (HCNs), heavily rely on stochastic geometry framework [54–57]. Using these tools, comprehensive modeling and analysis of legacy HCNs has been carried out in [58–61]. In [62], the authors have presented the outage probability, the average ergodic rate, and the minimum average user throughput for a downlink HD multi-tier HCNs. They have concluded that neither the number of BSs nor the tiers affect outage probability or average ergodic rate in an interference-limited full-loaded HCNs with unbiased cell association. These conclusions, however, may not hold in environments which are prone to higher interference, like HCNs comprising FD nodes.

FD-enabled HCNs have been recently attracting growing interest [63]. In [64], the authors have derived the expression for the throughput of hybrid duplex heterogeneous networks composed of multi-tier networks, with access points (APs) operating in each tier, either in bi-directional FD mode or downlink HD mode. The authors have concluded that having tiers with hybrid duplex BSs degrades the performance, while higher throughput was achieved when each tier operates in the same duplex, either HD or FD rather than a mixture of both. This motivates further

research on two-tier HCNs with FD small cells and HD macrocells, instead of considering hybrid scenarios where small cells could be either operating in FD or HD mode.

In [65], authors have derived the downlink rate coverage probability of a user in a single-tier FD small cell network with massive MIMO wireless backhauls.

In [66], authors have introduced an FD-assisted cross-tier inter-cell interference (ICI) mitigation scheme called fICIC, which operates on small cells compared to the standardized eICIC that operates on the macrocells. Such a change might lead to modifications on the current backhaul, affecting feasibility of application. This motivates further investigation on the application of eICIC on FD-enabled HCNs to avoid legacy network modifications.

In [67], the authors consider a hybrid scenario where all BSs operate in FD mode. They derived a closed-form expression for the critical value of the self-interference attenuation power, which is required for the FD users to outperform HD users.

In [68], the authors have considered a single tier mixed small cell network, where BSs operate in either HD or FD, with all users operating in HD. The effect of FD cells on the performance of the mixed system was presented, however, an interference coordination scheme was not considered and only a single tier was investigated.

2.3.2 Full Duplex MAC Protocols for Distributed Wireless Networks

In FD distributed wireless networks, design of medium access control (MAC) layer becomes particularly challenging [69]. Some recent studies have proposed different MAC protocols for FD distributed wireless net-

works. In [70], the authors have proposed an FD MAC protocol, termed as FD-MAC, which adopts the 802.11 RTS/CTS handshaking, and allows the secondary transmission to occur during the same time slots of the primary one, making use of the FD opportunity of the nodes. However, this can only work on bi-directional links, and could require the secondary transmitter to request a new transmission if the secondary transmission was longer than the primary one.

In [71], Radunovic *et al.* have proposed an FD capable MAC protocol termed as ContraFlow. Which is a solution based on self-interference cancellation and scheduling mechanisms that improves spatial reuse, eliminates hidden terminals, and rectifies decentralized coordination inefficiencies among nodes, which lead to fairness improvements. To avoid collisions and solve the hidden node problem in ContraFlow, the primary receiver sends a busy tone even if it has no data to transmit, which is inherently inefficient in terms of power/energy consumption.

In [72], Goyal *et al.* have proposed a distributed MAC protocol that considers both bi-directional and uni-directional links, and adopts to the traffic conditions of the network. However, a new one bit transmission flag (TF) has been introduced to identify the FD opportunity, which may affect the backward compatibility of the protocol with conventional half-duplex (HD) nodes.

Cheng *et al.* have proposed an FD MAC protocol that accounts for uni-directional links and addresses the hidden node problem without the use of busy tone in [22], using their proposed RTS/full duplex clear to send (FD-CTS) access mechanism.

Tamaki *et al.* have proposed a relay FD MAC protocol termed as RFD-MAC, which enable bi-directional and multi-hop FD relay communications [73]. The RFD-MAC protocol is designed based on a syn-

chronous method in [45]. The RFD-MAC increases FD links by overhearing MAC headers, which include 1-bit information concerning the existence of a successive frame, and selecting a secondary transmission node using the gathered information. The gathered information is also used to avoid a collision between the primary and secondary transmissions. This may require modifications to existing HD MAC protocols and may lead to back incompatibility.

In [74], Miura *et al.* have introduced the use of directional antennas in FD protocol and proposed a distributed MAC protocol based on CSMA/CA without the use of RTS/CTS handshaking. The protocol adopts random access, and omits using ACK/NACK to avoid the collisions that may occur by using such procedure. Moreover, Sugiyama *et al.* have proposed a directional asynchronous FD medium access control protocol termed as DAFD-MAC, to avoid interference on primary and secondary transmissions [75]. Although the use of directional antennas mitigates the hidden terminal problem, it makes the protocol incompatible with networks employing omnidirectional antennas.

Energy efficiency has been rarely considered in existing protocols and use maximum transmission power for control and data packets, which is energy-inefficient. Additionally, most proposed protocols assumes perfect SI cancellation at the PHY layer, which has not been achieved yet, and could severely affect the results of the proposed protocol.

2.3.3 Full Duplex Routing Protocols for Distributed Wireless Networks

Research on routing protocols for FD wireless networks is still in infancy. In [76], Fang *et al.* have proposed cross-layer optimization for opportunistic multi-path routing in FD wireless networks. The route selection

problem has been solved under various resource competitions and node constraints. However, the proposed framework assumes perfect SI cancellation.

Kato and Bandai [77] have proposed an on-demand detour routing protocol for directional FD wireless networks. Although the use of directional antennas mitigates the hidden terminal problem, the protocol is not compatible with networks employing omnidirectional antennas.

Ramirez and Aazhang [78] addressed the problem of joint power allocation and routing in FD wireless networks through a modification to Dijkstra's algorithm to maximize network throughput.

In [79], authors have investigated a power optimal routing in fading wireless channels. The fading distribution of the channel is modeled, and the outage capacity of full-duplex decode-and-forward (FD-DF) relaying is taken as QoS constraint. In this QoS routing algorithm, the weighted power sum of relay nodes is minimized while the end-to-end link outage probability is kept below a threshold. The assumed system model employs perfect SI cancellation.

Chapter 3

Modeling and Analysis of HCNs with Full-Duplex Small Cells

3.1 Introduction

FD technology has a number of attractive features e.g., it can potentially double (theoretically) the ergodic capacity [6, 7], reduce the feedback delay [8], decrease the end-to-end delay [9], improve the network secrecy [10] and increase the efficiency of network protocols (e.g., medium access control [11]).

On the other hand, small cells are gaining increasing popularity in the next generation cellular systems. Small cells provide an easy and cost-efficient deployment solution for capacity and coverage improvements over the conventional macro-centric networks [80, 81]. The low-powered nature of small cells make them the ideal candidate for FD deployment considering that the self-interference (SI) is more manageable compared to the conventional high-power macro counterparts, therefore, small cells

forms an energy efficient solution for the deployment of FD technology. This inspires and motivates the investigation for the feasibility and performance gains of FD small cells underlay heterogeneous cellular networks (HCNs).

An important issue for HCNs is the inter-cell interference, which arises due to the dense unplanned deployments of small cells, loud neighbors, and the closed subscriber group access. To mitigate this interference, 3GPP has recently standardized the *enhanced Inter-Cell Interference Coordination* (eICIC) technique in Release 10 [82]. eICIC provides interference cancellation techniques in time, frequency, and power control domains. When the subframes of macro cells and small cells are aligned, their control and data channel overlap with each other. Therefore, eICIC mitigates the interference on the control channel of small cells through *Almost Blank Sub-frames* (ABS) at small cells. During ABS, the macro BSs only transmits the reference signals, which allows small cell BSs to schedule the associated users without interference from the macrocells.

3.2 Contribution

The objective of this chapter is to model and analyze an interference-coordinated two-tier HCN with FD small cells. The key contributions of this chapter can be summarized as follows.

- We formulate a tractable model for the interference coordinated two-tier HCN with FD small cells, wherein tier 1 comprises legacy HD macrocells and tier 2 consists of FD small cells. By explicitly accounting for spatial distribution of base stations, self-interference, transmit power, cell association, uplink power control and ABS factor, we provide signal-to-interference noise (SINR) expressions

for users in the corresponding two tiers. Specifically, the underlying model captures the DL scenario for tier 1 and both UL and DL scenarios for tier 2, since tier 1 and tier 2 operate in HD and FD mode, respectively.

- Based on the system model for two-tier HCN with FD small cells, we derive closed-form expressions for outage probability of different tiers. The final expressions explicitly account for interference coordination.

- We adopt the notion of rate coverage from [28], and derive closed-form expressions for the corresponding two tiers.

- We conduct a comprehensive performance evaluation through numerical as well as simulation studies. We investigate the impact of various design parameters on network performance in various scenarios.

3.3 System Model

We consider a two-tier HCNs, where tier 1 comprises macro BSs operating in HD mode, and tier 2 consists of small cells operating in FD mode, as illustrated in Fig. 3.1. Both tiers are spatially distributed in $\mathbb{R}^2$ following homogeneous Poisson point processes (HPPPs) Φ_{S_1} and Φ_{S_2}, with intensities λ_{S_1} and λ_{S_2}, respectively. All users operate in HD mode. The UL small cell users are spatially located in $\mathbb{R}^2$ following the HPPP Φ_{U_2}, with intensity λ_{u_2}. Assuming that the intensity of DL users is high enough, and each user has data ready for transmission, such that saturated traffic conditions hold. We also assume that each small cell BS serves single active uplink user and single downlink user per channel, and

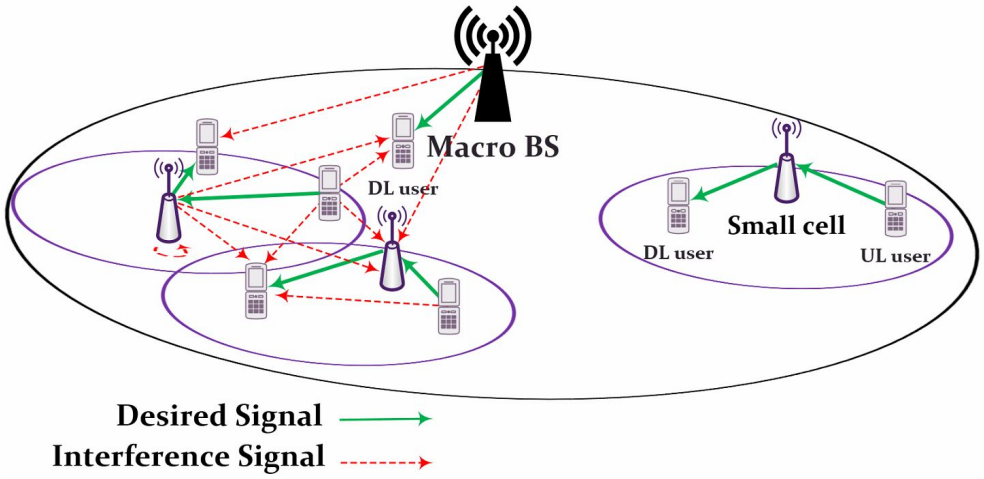

Figure 3.1: Example cells of the system model, where macro BS operates in HD mode, and small cells operate in FD mode.

each macrocell BS serves single active downlink user per channel. This assumption is justified due to the conclusions in [64], that the highest network performance is achieved when each tier in the network operates in the same duplex, rather than having hybrid tiers. We assume that the UL users share the macro DL frequency to minimize the interference on the DL users, considering that the density of small cells is usually significantly higher than the density of macrocells. The full frequency reuse scenario is assumed, such that all the cells use the same frequency band. We assume that the channel coefficients are invariant in each block and vary between different blocks. Moreover, we assume that the channel $h_{i,j}$ between any pair of nodes i and j is impaired by Rayleigh fading, and the path loss is assumed to be inversely proportional to distance with the path loss exponent α.

We assume that the FD small cells are equipped with a single antenna and achieve FD capability through the techniques mentioned in [83], [41]. A node in FD mode receives interference from its transmitted signal, and performs SI interference cancellation. Since the amount of SI depends on the transmission power at the receiver P_{S_2}, we define the residual

self-interference (RSI) power after performing the SI cancellation as [64], [84], [85],

$$RSI = P_{S_2} H_{SI}, \tag{3.1}$$

where $H_{SI} = |h_{SI}|^2$ is the RSI channel gain of the small cell BS, and indicates the SI cancellation capability of that BS, where h_{SI} is the SI channel of the BS. Note that $RSI = 0$ denotes perfect cancellation capability.

The residual self-interfering channel gain H_{SI} in (3.1) needs to be characterized based on the applied SI cancellation algorithm. Here, we consider the digital-domain cancellation, where h_{SI} can be presented as $h_{SI} = h_{SI_c} - \hat{h}_{SI_c}$ where h_{SI_c} and $\hat{h}_{SI_c}$ are the self-interfering channel and its estimate as the self-interference is subtracted using the estimate [64, 84–86], which allows H_{SI} to be modeled as a constant value, such that $H_{SI} = \sigma_e^2$ for the estimation error variance σ_e^2 [64, 84, 86]. Other SI cancellation algorithms, such as analogue domain algorithms [24, 26, 45] or propagation domain algorithms [85, 87, 88] will make the modeling of H_{SI} challenging. Therefore, in our analysis, we consider H_{SI} to be a constant value. Please note that the analysis can still be easily extended to the case of random H_{SI} within our framework. For instance, once the probability density function (PDF) of H_{SI} is available for a certain SI cancellation algorithm, by averaging the analytic results presented in this chapter, over the distribution of H_{SI}, the results for the random H_{SI} can be derived.

We consider the maximum received power cell association rule in the downlink transmission of HCNs, adopting the flexible cell association without biasing [62]. In our case, the association probability $\mathcal{A}$ for the

Table 3.1: Frequently Used Notations

Notation	Definition
Φ_{S_x}	HPPP of base stations in tier x
Φ_{U_x}	HPPP of users in tier x
λ_{S_x}	Spatial density of base stations in tier x
λ_{u_x}	Spatial density of users in tier x
S_x	Base station of tier $x \in (1, 2)$
S_x^*	Associated BS of tier $x \in (1, 2)$
u_x	Users of tier $x \in (1, 2)$
u_x^0	The user at origin of tier $x \in (1, 2)$
RSI	Residual self-interference
P_{Z_y}	Transmission power of $Z \in (S, u)$ of tier $y \in (1, 2)$
$h_{a,b}$	Small scale fading channel coefficient between a and b
$R_{a,b}$	Distance between a and b
α_x	Pathloss exponent in tier $x \in (1, 2)$
I_{Z_y}	Interferences caused by $Z \in (S, u)$ of tier $y \in (1, 2)$
N_0	Additive Gaussian noise
$\mathcal{A}_{S_x}$	Users association probability with BS of tier $x \in (1, 2)$

macrocells and the small cells can be expressed by

$$\mathcal{A}_{S_1} = 1 - \mathcal{A}_{S_2} = 1 - \left(1 + \frac{\lambda_{S_1}}{\lambda_{S_2}} \left(\frac{P_{S_1} B_1}{P_{S_2} B_2}\right)^{2/\alpha_2}\right)^{-1}. \tag{3.2}$$

and

$$\mathcal{A}_{S_2} = \mathbb{P}\left(P^r_{S_2} > P^r_{S_1}\right) = \left(1 + \frac{\lambda_{S_1}}{\lambda_{S_2}} \left(\frac{P_{S_1} B_1}{P_{S_2} B_2}\right)^{2/\alpha_1}\right)^{-1}, \tag{3.3}$$

respectively, In (3.2) and (3.3), $P^r_{S_1}$ and $P^r_{S_2}$ are the received power at the associating user from the macrocell and small cell BSs, respectively. B_1 and B_2 are the bias factor of macrocell and small cell BSs, respectively. Moreover, α_1 and α_2 are the path loss exponents of macrocells and small cells, respectively.

In this work, we assume that the HCNs employs eICIC technique for interference mitigation due to it's wide usage and popularity, with ABS transmission factor of ρ defined as the ratio of ABS transmitted over the total transmitted frames.

3.3.1 Downlink SINR of Macrocell User

For a typical macrocell downlink user located at the origin u_1^0, associated with its serving macrocell BS S_1^*, the SINR is expressed as

$$SINR^{DL}_{u_1} = \frac{P_{S_1} |h_{S_1^*, u_1^0}|^2 R_{S_1^*, u_1^0}{}^{-\alpha_1}}{I^{UL}_{u_2} + I_{S_2} + I^{DL}_{S_1} + N_0}, \tag{3.4}$$

where

$$I_{u_2}^{UL} = \sum_{u_2 \in \Phi_{U_2}} P_{u_2} |h_{u_2,u_1^0}|^2 R_{u_2,u_1^0}{}^{-\alpha_2},$$

$$I_{S_2} = \sum_{S_2 \in \Phi_{S_2}} P_{S_2} |h_{S_2,u_1^0}|^2 R_{S_2,u_1^0}{}^{-\alpha_2},$$

$$I_{S_1}^{DL} = \sum_{S_1 \in \Phi_{S_1} \setminus S_1^*} P_{S_1} |h_{S_1,u_1^0}|^2 R_{S_1,u_1^0}{}^{-\alpha_1}.$$

given $I_{u_2}^{UL}$ is the interference from small cell uplink users, I_{S_2} is the interference from small cell BSs and $I_{S_1}^{DL}$ is the interference from other macrocell BSs.

In (3.4), P_{u_2} is the transmit power of UL user associated with small cell, $h_{S_1^*,u_1^0}$, h_{u_2,u_1^0}, h_{S_2,u_1^0}, and h_{S_1,u_1^0} denote the small scale fading channel coefficient for the channels of the typical downlink user and its serving macrocell BS, small cell users, small cell BSs and other non-associated macrocell BSs, respectively. Moreover, $R_{S_1^*,u_1^0}$, R_{u_2,u_1^0}, R_{S_2,u_1^0}, and R_{S_1,u_1^0} denote the distances between the typical downlink macrocell user and its associated macrocell BS, small cell users, small cell BSs, and other interfering macrocell BSs, respectively.

3.3.2 Downlink SINR of Small Cell User

For a typical small cell downlink user located at the origin u_2^0, associated with its serving small cell BS S_2^*, the SINR expression is given by

$$SINR_{u_2}^{DL} = \frac{P_{S_2} |h_{S_2^*,u_2^0}|^2 R_{S_2^*,u_2^0}{}^{-\alpha_2}}{I_{u_2}^{UL} + I_{S_2} + I_{S_1}^{DL} + N_0}, \tag{3.5}$$

during non ABS transmission, while SINR expression during ABS transmission is given by

$$SINR_{u_2}^{DL\_ABS} = \frac{P_{S_2}|h_{S_2^*,u_2^0}|^2 R_{S_2^*,u_2^0}{}^{-\alpha_2}}{I_{u_2}^{UL} + I_{S_2} + N_0}, \tag{3.6}$$

where

$$I_{u_2}^{UL} = \sum_{u_2 \in \Phi_{U_2}} P_{u_2}|h_{u_2,u_2^0}|^2 R_{u_2,u_2^0}{}^{-\alpha_2},$$

$$I_{S_2} = \sum_{S_2 \in \Phi_{S_2} \setminus S_2^*} P_{S_2}|h_{S_2,u_2^0}|^2 R_{S_2,u_2^0}{}^{-\alpha_2},$$

$$I_{S_1}^{DL} = \sum_{S_1 \in \Phi_{S_1}} P_{S_1}|h_{S_1,u_2^0}|^2 R_{S_1,u_2^0}{}^{-\alpha_1}.$$

given $I_{u_2}^{UL}$ is the interference from small cell uplink users, I_{S_2} is the interference from small cell BSs and $I_{S_1}^{DL}$ is the interference from other macrocell BSs.

In (3.5) and (3.6), $h_{S_2^*,u_2^0}$, h_{u_2,u_2^0}, h_{S_2,u_2^0}, and h_{S_1,u_2^0} denote the small scale fading channel coefficient for the channels of the downlink typical small cell user and its serving small cell BS, small cell users, small cell BSs and macrocell BSs, respectively. Further, $R_{S_2^*,u_2^0}$, R_{u_2,u_1^0}, R_{S_2,u_1^0}, and R_{S_1,u_1^0} denote the distances between the typical small cell downlink user and its associated small cell BS, small cell users, other interfering small cell BSs, and macrocell BSs, respectively.

3.3.3 Uplink SINR of Small Cell BS

We assume that UL users utilize distance-proportional fractional power control of the form $R_x^{\alpha\epsilon}$ [89], where $\epsilon \in [0, 1]$ is the power control factor. Therefore, as users moves closer to the associated BS, the transmit power required to maintain the same received signal power decreases, which is

a key issue for battery-limited users.

For a typical small cell BS in the uplink located at the origin S_2^0, the SINR can be expressed as

$$SINR_{S_2}^{UL} = \frac{P_{u_2}|h_{u_2^*,S_2^0}|^2 R_{u_2^*,S_2^0}{}^{\alpha_2(\epsilon-1)}}{RSI + I_{u_2}^{UL} + I_{S_2} + I_{S_1}^{DL} + N_0}, \tag{3.7}$$

during non ABS transmission, while SINR expression during ABS transmission is given by

$$SINR_{S_2}^{UL\_ABS} = \frac{P_{u_2}|h_{u_2^*,S_2^0}|^2 R_{u_2^*,S_2^0}{}^{\alpha_2(\epsilon-1)}}{RSI + I_{u_2}^{UL} + I_{S_2} + N_0}, \tag{3.8}$$

where

$$I_{u_2}^{UL} = \sum_{u_2 \in \Phi_{U_2}} P_{u_2}|h_{u_2,S_2^0}|^2 R_{u_2,S_2^0}{}^{\alpha_2\epsilon},$$

$$I_{S_2} = \sum_{S_2 \in \Phi_{S_2} \setminus S_2^*} P_{S_2}|h_{S_2,S_2^0}|^2 R_{S_2,S_2^0}{}^{\alpha_2\epsilon},$$

$$I_{S_1}^{DL} = \sum_{S_1 \in \Phi_{S_1}} P_{S_1}|h_{S_1,S_2^0}|^2 R_{S_1,S_2^0}{}^{\alpha_1\epsilon}.$$

given $I_{u_2}^{UL}$ denotes the interference from other small cell uplink users, I_{S_2} is the interference from other small cell BSs and $I_{S_1}^{DL}$ is the interference from macrocell BSs.

When $\epsilon = 1$, the numerator of (3.7) becomes $P_{u_2}|h_{u_2^*,S_2^0}|^2$, with the pathloss completely inverted by the power control, and when $\epsilon = 0$, no channel inversion is performed and all the nodes transmit using the same power.

In (3.7), $h_{u_2^*,S_2^0}$, h_{u_2,S_2^0}, h_{S_2,S_2^0}, and h_{S_1,S_2^0} denote the small scale fading channel coefficient for the channels of small cell uplink BS and its associated small cell uplink user, other interfering small cell uplink users, other small cell BSs and macrocell BSs, respectively. Moreover, $R_{u_2^*,S_2^0}$, R_{u_2,S_2^0},

R_{S_2,S_2^0}, and R_{S_1,S_2^0} denote the distances between the typical small cell uplink BS and its associated small cell uplink user, other interfering small cell uplink users, other small cell BSs and macrocell BSs, respectively.

3.4 Outage Probability Analysis

In this section, we analyze the outage probability of two-tier HCNs with FD small cells, which is a metric that represents the average fraction of the cell area that is in outage at any time. We define the outage probability $\mathbb{O}$ as the probability that the instantaneous SINR of a randomly located user is less than a target SINR τ. Since the typical user is associated with at most one tier, from the law of total probability, the outage probability is given as

$$\mathbb{O} = \sum_{k=1}^{K} \mathbb{O}_k \mathcal{A}_k, \tag{3.9}$$

where $\mathcal{A}_k$ is the per-tier association probability given in (3.3) and (3.2), and $\mathbb{O}_k$ is the outage probability of a typical user associated with k_{th} tier. For a target SINR τ_k and a typical user $\text{SINR}_k(x)$ at a distance x from its associated BS, the outage probability is given by

$$\mathbb{O}_k = \mathbb{E}\left[\mathbb{P}\left[SINR_k(x) < \tau_k\right]\right]. \tag{3.10}$$

Considering the chosen network model of HD macrocells and FD small cells, the expression of the outage probability becomes

$$\mathbb{O} = \mathbb{O}_1^{DL}\mathcal{A}_1 + (\mathbb{O}_2^{DL} + \mathbb{O}_2^{UL})\mathcal{A}_2, \tag{3.11}$$

where $\mathbb{O}_1^{DL}$, $\mathbb{O}_2^{DL}$ and $\mathbb{O}_2^{UL}$ denote the outage probability of macrocell downlink user, small cell downlink user, and small cell uplink BS, respectively, and are derived in the following section.

3.4.1 Outage Probability of Macrocell Downlink User

The probability density function (PDF) of the distance between the typical macrocell user and the associated macrocell BS $R_{S_1^*,u_1^0}$, is given similar to [62] as

$$f_{R_{S_1^*,u_1^0}}(r) = \frac{2\pi\lambda_{S_1}}{\mathcal{A}_{S_1}} r \exp\left\{-\pi \sum_{j=1}^{2} \lambda_j \left(\frac{P_{S_j}}{P_{S_1}}\right)^{\frac{2}{\alpha_j/\alpha_1}}\right\}, \tag{3.12}$$

where $\mathcal{A}_{S_1}$ is given in (3.2).

Theorem 1. *The outage probability $\mathbb{O}_1^{DL}$ in HCNs comprised of HD macrocell and FD small cell, is defined as the probability that the instantaneous SINR of a randomly located macrocell downlink user is lower than a target τ_1, and expressed as*

$$\begin{aligned}\mathbb{O}_1^{DL} =& 1 - \left\{\frac{2\pi\lambda_{S_1}}{\mathcal{A}_{S_1}} \int_0^{\infty} r \exp\Big\{ - r^{\alpha_1} {P_{S_1}}^{-1} N_0 \tau_1 \right. \\ & \left. - \pi\Big((\Psi_1 r^{\frac{2}{\alpha_2/\alpha_1}}) + (\Psi_2 r^{\frac{2}{\alpha_2/\alpha_1}}) + (\Psi_3 r^2)\Big)\Big\} dr\right\},\end{aligned} \tag{3.13}$$

where

$$\begin{aligned}\Psi_1 =& \lambda_{u_2}\left(\frac{P_{u_2}}{P_{S_1}}\right)^{2/\alpha_2} \frac{2\tau_1}{\alpha_2 - 2} {}_2F_1[1, 1 - \frac{2}{\alpha_2}; 2 - \frac{2}{\alpha_2}; -\tau_1], \\ \Psi_2 =& \lambda_{S_2}\left(\frac{P_{S_2}}{P_{S_1}}\right)^{2/\alpha_2} \frac{2\tau_1}{\alpha_2 - 2} {}_2F_1[1, 1 - \frac{2}{\alpha_2}; 2 - \frac{2}{\alpha_2}; -\tau_1], \\ \Psi_3 =& \lambda_{S_1}\left(\frac{P_{S_1}}{P_{S_1^*}}\right)^{2/\alpha_1} \frac{2\tau_1}{\alpha_1 - 2} {}_2F_1[1, 1 - \frac{2}{\alpha_1}; 2 - \frac{2}{\alpha_1}; -\tau_1],\end{aligned}$$

with ${}_2F_1[\cdot]$ denote the Gauss hypergeometric function, and the pathloss exponents $\alpha_j > 2$.

Proof. See Appendix A. □

3.4.2 Outage Probability of Small Cell Downlink User

The PDF of the distance between the typical small cell downlink user and its associated BS $R_{S_2^*,u_2^0}$, is given similar to [62] as

$$f_{R_{S_2^*,u_2^0}}(r) = \frac{2\pi\lambda_{S_2}}{\mathcal{A}_{S_2}} r \exp\Big\{-\pi \sum_{j=1}^{2} \lambda_j (P_{S_j}/P_{S_2})^{\frac{2}{\alpha_j/\alpha_2}}\Big\}. \tag{3.14}$$

Theorem 2. *The outage probability $\mathbb{O}_2^{DL}$ in HCNs comprised of HD macrocell and FD small cell, is defined as the probability that the instantaneous SINR of a randomly located small cell downlink user is lower than a target τ_2, during transmission of both ABS and non-ABS subframes, and expressed as*

$$\mathbb{O}_2^{DL} = 1 - \Bigg\{ \frac{2\pi(1-\rho)\lambda_{S_2}}{\mathcal{A}_{S_2}} \int_0^\infty r \exp\Big\{ - r^{\alpha_2} {P_{S_2}}^{-1} N_0 \tau_2 - \pi\Big((\eta_1 r^2) + (\eta_2 r^{\frac{2}{\alpha_2/\alpha_1}}) + (\eta_3 r^{\frac{2}{\alpha_1/\alpha_2}})\Big)\Big\} dr + \frac{2\pi\rho\lambda_{S_2}}{\mathcal{A}_{S_2}} \int_0^\infty r \exp\Big\{ - r^{\alpha_2} {P_{S_2}}^{-1} N_0 \tau_2 - \pi\Big((\eta_1 r^2) + (\eta_2 r^{\frac{2}{\alpha_2/\alpha_1}})\Big)\Big\} dr \Bigg\}, \tag{3.15}$$

where

$$\begin{aligned}
\eta_1 =& \lambda_{u_2} \left(\frac{P_{u_2}}{P_{S_2}}\right)^{2/\alpha_2} \frac{2\tau_2}{\alpha_2 - 2} {}_2F_1[1, 1 - \frac{2}{\alpha_2}; 2 - \frac{2}{\alpha_2}; -\tau_2], \\
\eta_2 =& \lambda_{S_2} \left(\frac{P_{S_2}}{P_{S_2^*}}\right)^{2/\alpha_2} \frac{2\tau_2}{\alpha_2 - 2} {}_2F_1[1, 1 - \frac{2}{\alpha_2}; 2 - \frac{2}{\alpha_2}; -\tau_2], \\
\eta_3 =& \lambda_{S_1} \left(\frac{P_{S_1}}{P_{S_2}}\right)^{2/\alpha_1} \frac{2\tau_2}{\alpha_1 - 2} {}_2F_1[1, 1 - \frac{2}{\alpha_1}; 2 - \frac{2}{\alpha_1}; -\tau_2],
\end{aligned}$$

for the pathloss exponents $\alpha_j > 2$.

Proof. See Appendix B □

3.4.3 Outage Probability of Small Cell Uplink BS

Since macrocells can only service one DL active user at a time, the UL users can only be associated to the FD small cells. Therefore, we assume that UL users are associated with the small cells based on the flexible association rule, where the PDF of the distance between the UL users and the small cells $R_{S_2,u_2^{UL}}$ is given as

$$f_{R_{S_2,u_2^{UL}}}(r) = e^{-\lambda_2 \pi r^2} 2\pi\lambda_2 r. \tag{3.16}$$

Theorem 3. *The outage probability $\mathbb{O}_2^{UL}$ in HCNs comprised of HD macrocell and FD small cell, is defined as the probability that the instantaneous SINR of a randomly located UL small cell BS is lower than a target τ_3 during both ABS and non-ABS subframes is given by*

$$\begin{aligned}\mathbb{O}_2^{UL} =& 1 - \Bigg\{ 2\pi(1-\rho)\lambda_{S_2} \int_0^\infty r \exp\Big\{ - r^{\alpha_2(\epsilon-1)} {P_{u_2}}^{-1} P_{S_2} \sigma_e^2 N_0 \tau_3 - \pi\Big((\Gamma_1 r^2) + \\ & (\Gamma_2 r^2) + (\Gamma_3 r^{\frac{2}{\alpha_1/\alpha_2}})\Big)\Big\} dr + 2\pi\rho\lambda_{S_2} \int_0^\infty r \exp\Big\{ - r^{\alpha_2(\epsilon-1)} {P_{u_2}}^{-1} P_{S_2} \sigma_e^2 N_0 \tau_3 \\ & - \pi\Big((\Gamma_1 r^2) + (\Gamma_2 r^2)\Big)\Big\} dr \Bigg\},\end{aligned} \tag{3.17}$$

where

$$\begin{aligned}\Gamma_1 =& \lambda_{u_2} \frac{2\tau_3}{\alpha_2 - 2} {}_2F_1[1, 1 - \frac{2}{\alpha_2\epsilon}; 2 - \frac{2}{\alpha_2\epsilon} - \tau_3] \\ \Gamma_2 =& \lambda_{S_2} \left(\frac{P_{S_2}}{P_{u_2}}\right)^{2/\alpha_2\epsilon} \frac{2\tau_3}{\alpha_2 - 2} {}_2F_1[1, 1 - \frac{2}{\alpha_2\epsilon}; 2 - \frac{2}{\alpha_2\epsilon} - \tau_3] \\ \Gamma_3 =& \lambda_{S_1} \left(\frac{P_{S_1}}{P_{u_2}}\right)^{2/\alpha_1\epsilon} \frac{2\tau_3}{\alpha_1 - 2} {}_2F_1[1, 1 - \frac{2}{\alpha_1\epsilon}; 2 - \frac{2}{\alpha_1\epsilon}; -\tau_3],\end{aligned}$$

for $\alpha_j > 2$.

Proof. See Appendix C. □

3.5 Rate Coverage Analysis

In this section, we analyze the rate coverage of two-tier HCNs with FD small cells. The rate coverage is defined in [90] as the probability that a randomly chosen user can achieve a target rate ϖ, which is given by

$$\Theta \triangleq \mathbb{P}\left(\mathcal{R} > \varpi\right). \tag{3.18}$$

Since the DL users can associate with either macro cells or small cells in *open-access* mode, the overall rate coverage for the chosen user in two-tier HCNs is given by

$$\Theta = \rho\mathcal{A}_{S_1}\mathbb{P}\left(\mathcal{R}_{S_1} > \varpi|\mathcal{A}_{S_1}\right) + (1-\rho)\mathcal{A}_{S_2}\mathbb{P}\left(\mathcal{R}_{S_2} > \varpi|\mathcal{A}_{S_2}\right), \tag{3.19}$$

where $\mathcal{A}_{S_1}$ and $\mathcal{A}_{S_2}$ denote the probability that a user is associated with the macrocell or the small cell, and $\mathbb{P}\left(\mathcal{R}_{S_1} > \varpi|\mathcal{A}_{S_1}\right)$ and $\mathbb{P}\left(\mathcal{R}_{S_2} > \varpi|\mathcal{A}_{S_2}\right)$ denote the rate coverage conditioned on the association with the former and the latter, respectively.

The rate achieved by a user associated with the tagged BS in the x^{th}-tier is given by

$$\mathcal{R}_x = \frac{W}{\mathcal{N}_x}\log_2\left(1 + SINR_x\right), \tag{3.20}$$

where W is the bandwidth of the frequency band, $\mathcal{N}_x$ is a random variable which denotes the average number of users associated with the tagged base station in the x^{th}-tier, and $SINR_x$ is the received signal-to-interference-plus-noise-ratio from the serving base station for a user.

3.5.1 Rate Coverage for Macrocell Users in the Downlink

In Rayleigh fading environments, the rate coverage for a macrocell DL user is given by

$$\mathbb{P}\left(\mathcal{R}_{S_1} > \varpi | \mathcal{A}_{S_1}\right) = \mathbb{E}_{\mathcal{N}_{S_1}}\left[\mathbb{P}\left(SINR_{u_1}^{DL} > 2^{\frac{\varpi \mathcal{N}_{S_1}}{W}} - 1 | \mathcal{A}_{S_1}\right)\right]$$
$$= \sum_{n\geq 0} \mathbb{P}\left(\frac{P_{S_1} h_{S_1^*,u_1^0} {R_{S_1^*,u_1^0}}^{-\alpha_1}}{I} > \kappa_1 | \mathcal{A}_{S_1}\right) \mathbb{P}\left(\mathcal{N}_{S_1} = n+1\right), \quad (3.21)$$

where $I = I_{u_2}^{UL} + I_{S_2} + I_{S_1}^{DL} + N_0$ is the cumulative interference from small cell UL users along with macrocell and small cell BSs, and the additive Gaussian noise, and $\kappa_1 = 2^{\frac{\varpi \mathcal{N}_{S_1}}{W}} - 1$.

According to [90], the distribution of the load associated with the x^{th}-tier is given by

$$\mathbb{P}\left(\mathcal{N}_x = n+1\right) = \frac{3.5^{3.5}}{n!} \frac{\Gamma\left(n+4.5\right)}{\Gamma\left(3.5\right)} \left(\frac{\lambda_u \mathcal{A}_x}{\lambda_x}\right)^n \left(3.5 + \frac{\lambda_u \mathcal{A}_x}{\lambda_x}\right)^{-n-4.5}, \quad (3.22)$$

with the mean load $\mathbb{E}\left[\mathcal{N}_x\right] = 1 + 1.28 \frac{\lambda_u \mathcal{A}_x}{\lambda_x}$, where $\Gamma\left(x\right) = \int_0^\infty t^{x-1} e^{-t} dt$ is the Gamma function, and $\mathcal{A}_x$ denotes the association probability of the x^{th}-tier. Hence,

$$\mathbb{P}\left(\frac{P_{S_1} h_{S_1^*,u_1^0} {R_{S_1^*,u_1^0}}^{-\alpha_1}}{I} > \kappa_1 | \mathcal{A}_{S_1}\right)$$
$$= \int_0^\infty \mathbb{P}\left(\frac{P_{S_1} h_{S_1^*,u_1^0} {R_{S_1^*,u_1^0}}^{-\alpha_1}}{I} > \kappa_1\right) f_{R_{S_1^*,u_1^0}}(r)$$
$$= \frac{2\pi\lambda_{S_1}}{\mathcal{A}_{S_1}} \int_0^\infty \mathbb{P}\left(\frac{P_{S_1} h_{S_1^*,u_1^0} {R_{S_1^*,u_1^0}}^{-\alpha_1}}{I} > \kappa_1\right) r$$
$$\times \exp\left\{-\pi \sum_{j=1}^{2} \lambda_j \left(\frac{P_j}{P_{S_1}}\right)^{\frac{2}{\alpha_j/\alpha_1}} r^{\frac{2}{\alpha_j/\alpha_1}}\right\} dr. \quad (3.23)$$

Using the derivation of outage probability for macrocell DL users and (3.22), the final expression for DL rate coverage of macrocell users can be obtained through (3.21).

3.5.2 Rate Coverage for Small Cell Users in the Downlink

Following the same derivation approach, the rate coverage for DL small cell users is given by

$$\begin{aligned}\mathbb{P}\left(\mathcal{R}_{S_2}^{DL} > \varpi | \mathcal{A}_{S_2}\right) &= \mathbb{E}_{\mathcal{N}_{S_2}}\Bigg[\rho\mathbb{P}\left(SINR_{u_2}^{DL\_ABS} > 2^{\frac{\varpi\mathcal{N}_{S_2}}{W}} - 1 | \mathcal{A}_{S_2}\right) \\ &\quad + (1-\rho)\mathbb{P}\left(SINR_{u_2}^{DL} > 2^{\frac{\varpi\mathcal{N}_{S_2}}{W}} - 1 | \mathcal{A}_{S_2}\right)\Bigg] \\ &= \Bigg[(1-\rho)\sum_{n\geq 0}\mathbb{P}\left(\frac{P_{S_2}h_{S_2^*,u_2^0}{R_{S_2^*,u_2^0}}^{-\alpha_2}}{I} > \kappa_2 | \mathcal{A}_{S_2}\right) \\ &\quad + \rho\sum_{n\geq 0}\mathbb{P}\left(\frac{P_{S_2}h_{S_2^*,u_2^0}{R_{S_2^*,u_2^0}}^{-\alpha_2}}{I'} > \kappa_2 | \mathcal{A}_{S_2}\right)\Bigg] \\ &\quad \times \mathbb{P}\left(\mathcal{N}_{S_2} = n+1\right), \end{aligned} \tag{3.24}$$

where $I = I_{u_2}^{UL} + I_{S_2} + I_{S_1}^{DL} + N_0$ denote the cumulative interference from small cell UL users along with macrocell and small cell BSs, receptively. $I' = I_{u_2}^{UL} + I_{S_2} + N_0$ is the cumulative interference during ABS transmission, and $\kappa_2 = 2^{\frac{\varpi\mathcal{N}_{S_2}}{W}} - 1$.

$$\begin{aligned}&(1-\rho)\mathbb{P}\left(\frac{P_{S_2}h_{S_2^*,u_2^0}{R_{S_2^*,u_2^0}}^{-\alpha_2}}{I} > \kappa_2 | \mathcal{A}_{S_2}\right) = (1-\rho) \\ &\times \int_0^\infty \mathbb{P}\left(\frac{P_{S_2}h_{S_2^*,u_2^0}{R_{S_2^*,u_2^0}}^{-\alpha_2}}{I} > \kappa_2\right) f_{R_{S_2^*,u_2^0}}(r).\end{aligned} \tag{3.25}$$

and

$$\rho\mathbb{P}\left(\frac{P_{S_2}h_{S_2^*,u_2^0}R_{S_2^*,u_2^0}{}^{-\alpha_2}}{I'}>\kappa_2|\mathcal{A}_{S_2}\right)=$$
$$\rho\int_0^\infty\mathbb{P}\left(\frac{P_{S_2}h_{S_2^*,u_2^0}R_{S_2^*,u_2^0}{}^{-\alpha_2}}{I'}>\kappa_2\right)f_{R_{S_2^*,u_2^0}}(r). \tag{3.26}$$

Using the load distribution given in (3.22), (3.25) and (3.26), we obtain

$$\frac{2\pi(1-\rho)\lambda_{S_2}}{\mathcal{A}_{S_2}}\int_0^\infty\mathbb{P}\left(\frac{P_{S_2}h_{S_2^*,u_2^0}R_{S_2^*,u_2^0}{}^{-\alpha_2}}{I}>\kappa_2\right)r$$
$$\times\exp\left\{-\pi\sum_{j=1}^{2}\lambda_j(\frac{P_j}{P_{S_2}})^{\frac{2}{\alpha_j/\alpha_2}}r^{\frac{2}{\alpha_j/\alpha_2}}\right\}dr$$
$$+\frac{2\pi\rho\lambda_{S_2}}{\mathcal{A}_{S_2}}\int_0^\infty\mathbb{P}\left(\frac{P_{S_2}h_{S_2^*,u_2^0}R_{S_2^*,u_2^0}{}^{-\alpha_2}}{I'}>\kappa_2\right)r$$
$$\times\exp\left\{-\pi\sum_{j=1}^{2}\lambda_j(\frac{P_j}{P_{S_2}})^{\frac{2}{\alpha_j/\alpha_2}}r^{\frac{2}{\alpha_j/\alpha_2}}\right\}dr.$$

Finally, Using the derivation of outage probability for small cell DL users and (3.22), the final expression for rate coverage of small cell DL users can be obtained through (3.24).

3.5.3 Rate Coverage for Small cell BS in the Uplink

Similarly, the rate coverage for UL small cell BS is given by

$$\mathbb{P}\left(\mathcal{R}_{S_2}^{UL}>\varpi|\mathcal{A}_{S_2}\right)=\mathbb{E}_{\mathcal{N}_{S_2}}\Bigg[\rho\mathbb{P}\left(SINR_{u_2}^{UL\_ABS}>2^{\frac{\varpi\mathcal{N}_{S_2}}{W}}-1|\mathcal{A}_{S_2}\right)$$
$$+(1-\rho)\mathbb{P}\left(SINR_{u_2}^{UL}>2^{\frac{\varpi\mathcal{N}_{S_2}}{W}}-1|\mathcal{A}_{S_2}\right)\Bigg].$$
$$=\Bigg[(1-\rho)\sum_{n\geq0}\mathbb{P}\left(\frac{P_{S_2}h_{u_2^0,S_2^*}R_{u_2^0,S_2^*}{}^{-\alpha_2(\epsilon-1)}}{I+RSI}>\kappa_2|\mathcal{A}_{S_2}\right)$$
$$+\rho\sum_{n\geq0}\mathbb{P}\left(\frac{P_{S_2}h_{u_2^0,S_2^*}R_{u_2^0,S_2^*}{}^{-\alpha_2(\epsilon-1)}}{I'+RSI}>\kappa_2|\mathcal{A}_{S_2}\right)\Bigg]$$
$$\times\mathbb{P}\left(\mathcal{N}_{S_2}=n+1\right), \tag{3.27}$$

where $I = I_{u_2}^{UL} + I_{S_2} + I_{S_1}^{DL} + N_0$ is the cumulative interference from UL small cell users along with macrocell and small cell BSs, and the Gaussian additive noise. $I' = I_{u_2}^{UL} + I_{S_2} + N_0$ is the cumulative interference during ABS transmission.

$$(1-\rho)\mathbb{P}\left(\frac{P_{S_2}h_{u_2^0,S_2^*}R_{u_2^0,S_2^*}{}^{-\alpha_2(\epsilon-1)}}{I+RSI} > \kappa_2|\mathcal{A}_{S_2}\right) = (1-\rho)\int_0^\infty \mathbb{P}\left(\frac{P_{S_2}h_{u_2^0,S_2^*}R_{u_2^0,S_2^*}{}^{-\alpha_2(\epsilon-1)}}{I+RSI} > \kappa_2\right) f_{R_{S_2,u_2^{UL}}}(r). \tag{3.28}$$

and

$$\rho\mathbb{P}\left(\frac{P_{S_2}h_{u_2^0,S_2^*}R_{u_2^0,S_2^*}{}^{-\alpha_2(\epsilon-1)}}{I+RSI} > \kappa_2|\mathcal{A}_{S_2}\right) = \rho\int_0^\infty \mathbb{P}\left(\frac{P_{S_2}h_{u_2^0,S_2^*}R_{u_2^0,S_2^*}{}^{-\alpha_2(\epsilon-1)}}{I+RSI} > \kappa_2\right) f_{R_{S_2,u_2^{UL}}}(r). \tag{3.29}$$

Using the load distribution given in (3.22) and both (3.28) and (3.29) we obtain

$$\begin{aligned}
&2\pi(1-\rho)\lambda_{S_2}\int_0^\infty \mathbb{P}\left(\frac{P_{S_2}h_{u_2^0,S_2^*}R_{u_2^0,S_2^*}{}^{-\alpha_2(\epsilon-1)}}{I+RSI} > \kappa_2\right) r \\
&\times \exp\left\{-\pi\sum_{j=1}^{2}\lambda_j\left(\frac{P_j}{P_{S_2}}\right)^{\frac{2}{\alpha_j/\alpha_2}} r^{\frac{2}{\alpha_j/\alpha_2}}\right\} dr \\
&+ 2\pi\rho\lambda_{S_2}\int_0^\infty \mathbb{P}\left(\frac{P_{S_2}h_{u_2^0,S_2^*}R_{u_2^0,S_2^*}{}^{-\alpha_2(\epsilon-1)}}{I'+RSI} > \kappa_2\right) r \\
&\times \exp\left\{-\pi\sum_{j=1}^{2}\lambda_j\left(\frac{P_j}{P_{S_2}}\right)^{\frac{2}{\alpha_j/\alpha_2}} r^{\frac{2}{\alpha_j/\alpha_2}}\right\} dr.
\end{aligned} \tag{3.30}$$

Finally, Using the derivation of outage probability for UL small cell BS and (3.22), the final expression for rate coverage of UL small cell BS can be obtained through (3.27).

Table 3.2: Parametric Values (unless otherwise specified)

Parameter	Value
$\lambda_x \ \forall x$	$(\pi \times 500^2)^{-1}$
P_{S_1} [dBm]	43 dBm (20 W)
$P_{S,2}$ [dBm]	23 dBm (200 mW)
$P_{u_y} \ \forall y$ [dBm]	23 dBm (200 mW)
W [Hz]	10^7
$\alpha_k \ \forall k$	4
$\tau_n \ \forall n$ [dB]	0 dB
RSI	$P_{S_2} 10^{L_{dB}/10}$
L_{dB} [dB]	-38 dB
ρ	0.3
ϵ	0.2
$B_x \ x \in (1, 2)$	1

3.6 Analytical and Numerical Results

In this section, we evaluate the performance of two-tier HCNs with FD small cells. Specifically, we investigate how different parameters affect network performance in terms of the outage probability and the rate coverage. The simulation methodology comprises independent realization of PPP distributions for the BSs of two tiers, followed by realization of user distribution and the association process. After that, outage probability and rate coverage are calculated based on the cumulative interference. The parameters used for the analysis and simulation are stated in Table 3.2. Monte Carlo simulations have been conducted to obtain the results, averaged over 10000 iterations, which are then compared with numerical evaluation of the derived expressions. Please note that comparisons between HD and FD systems had been carried out extensively in the literature [7, 64], and demonstrated FD superiority in cases of adequate SI cancellations, therefore, we will not incorporate those comparisons in

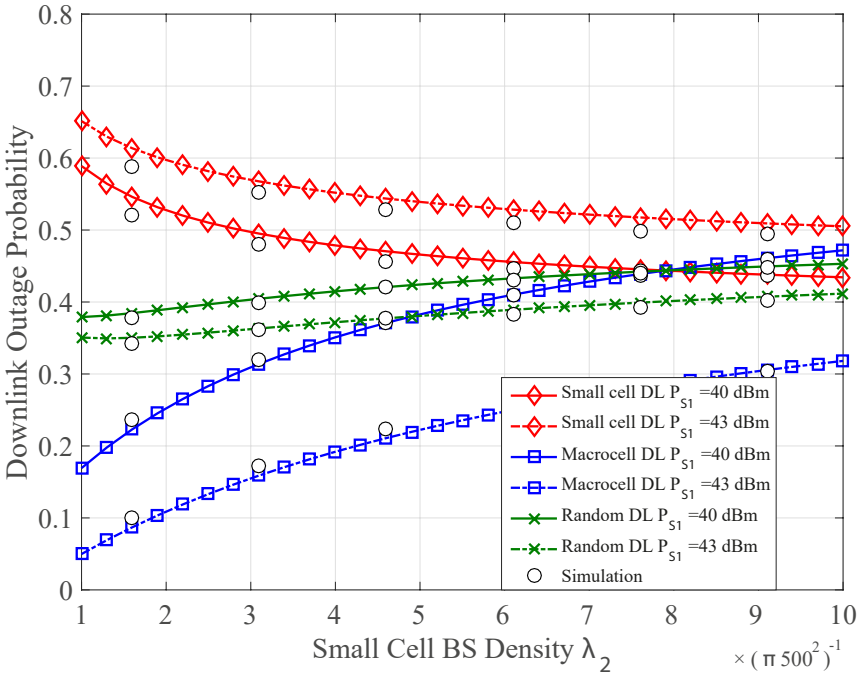

Figure 3.2: Outage probability of macrocell and small cell downlink as a function of small cell density λ_2.

this study.

Fig. 3.2 plots the outage probability of a typical DL user associated with macrocell BS, small cell BS, and random type of BS in the DL, as a function of small cell BSs density λ_2. We observe that the outage probability of macrocell DL user increases with increasing the small cell BS density. This results from the increase in aggregate interference from the small cell BSs, as shown in (3.4). Additionally, the outage probability of macrocell DL user decreases with increasing the transmit power at the macrocell BS, which is due to the increase in SINR at the typical downlink user associated with macrocell BS, as shown in (3.4). Interestingly, for the typical downlink user associated with small cell BS, the outage probability decreases with increasing the small cell BS density. This is because densification of tier 2 reduces the inter-link distances between the typical downlink user and the associated small cell BS, as shown in

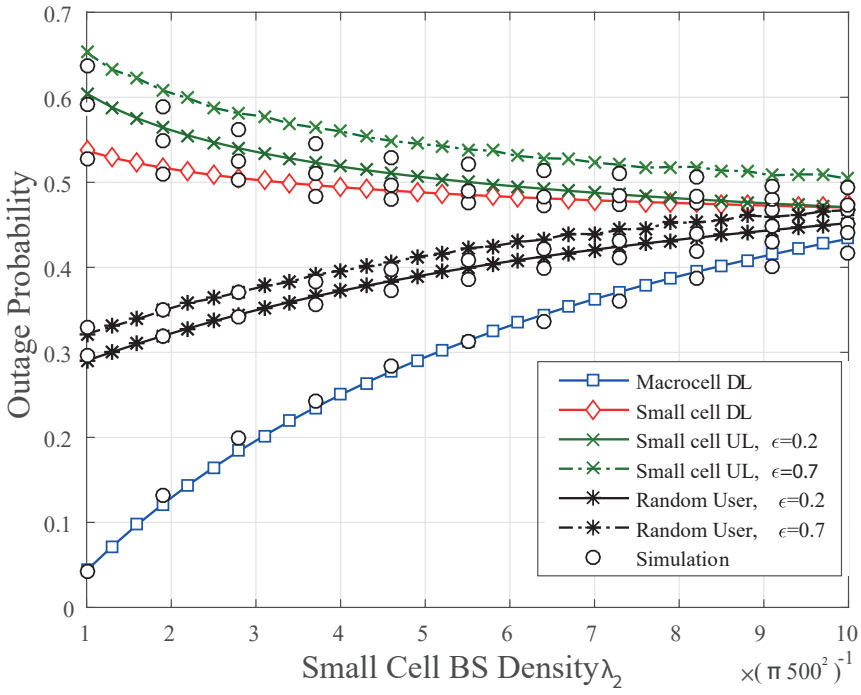

Figure 3.3: Outage probability as a function of small cell density λ_2.

(3.5). In addition, the outage probability of typical small cell DL user increase with increasing the transmit power at the macrocell BS, which is due to the increase in aggregate interference caused by macrocell BSs, as shown in (3.5). Finally, outage probability of a random DL user, which is defined as $\mathbb{O}_1^{DL}\mathcal{A}_1+\mathbb{O}_2^{DL}\mathcal{A}_2$, increases with both the increase of small cell density, and the decrease of transmit power of macrocell BS. This is because $\mathbb{O}_1^{DL}$ in the expression is lower than $\mathbb{O}_2^{DL}$, therefore the expression reflects such tendency. Note that the simulation results closely follow the analytical results, and therefore, validate the analytical modeling. Also note that when the density of small cells becomes very high, there will be a point where the interference originating from the small cells will eventually degrade the outage probability.

Fig. 3.3 plots the outage probability of macrocell DL user, small cell DL user, small cell UL BS, and a randomly located user versus the density of small cell BSs. In this figure, we focus on the impact of small

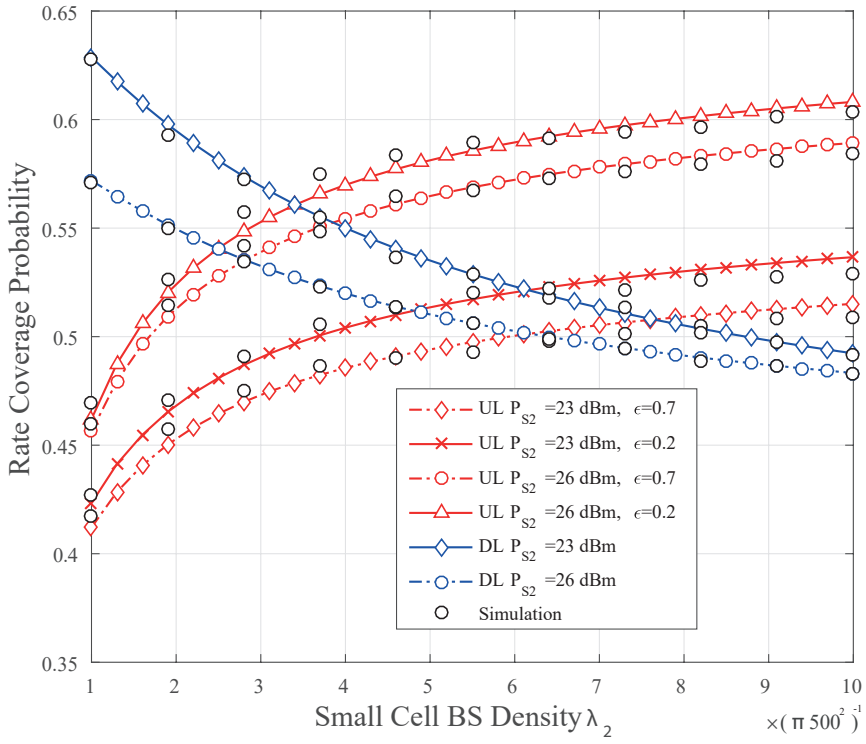

Figure 3.4: Rate coverage as a function of small cell density λ_2.

cell BSs density on the outage probability of a randomly located user. Interestingly, we observe that the outage probability of a randomly located user is not significantly affected by the increase in the small cell BS density. It suffers from slight increase that results from aggregate interference from the small cell BSs, as shown in (3.11). We also evaluate the impact of uplink power control factor, ϵ on outage. As shown by the results, a higher value of ϵ results in a higher outage probability, for small cell user in the uplink, due to reduced uplink transmit power as a consequence of more aggressive power control. The simulation results also closely follow the analytical results.

Fig. 3.4 plots rate coverage for a random DL user and UL small cell BS versus the small cell BSs density. We note that the rate coverage of a random DL user decrease as the density of small cell BSs increases. This is because of increase in aggregate interference caused by small cell

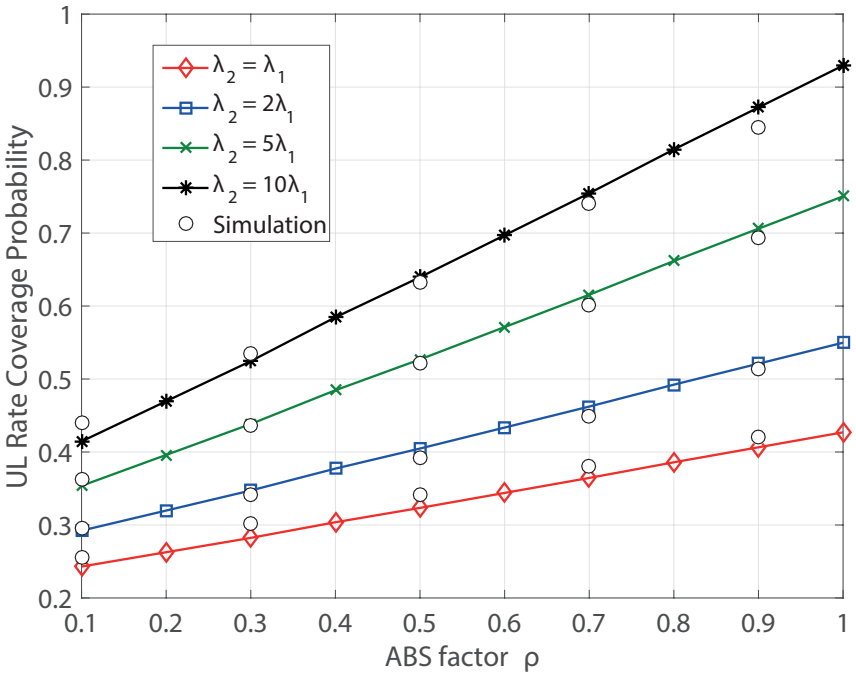

Figure 3.5: UL rate coverage probability as a function of ABS factor ρ.

BSs, as seen in (3.4). Similarly, the rate coverage of a random DL user decreases with increasing the transmission power of small cell BSs. On the contrary, rate coverage of an UL small cell BS increase with increase of small cell BSs density. This is due to the fact that densification reduces the inter-link distance between a user and it's associated BS, which can be verified by (3.7). Similarly, the rate coverage of an UL small cell BS increases with increasing the transmission power of small cell BSs due to higher SINR of small cell UL BS as can be verified by (3.7). We also evaluate the impact of uplink power control factor, ϵ on rate coverage. As shown by the results, a higher value of ϵ results in a lower rate coverage probability, for small cell user in the uplink, due to reduced uplink transmit power as a consequence of more aggressive power control.

Fig. 3.5 plots the rate coverage of UL small cell BSs as a function of the ABS factor ρ. We note that the rate coverage of UL small cell BSs increases as ρ increases. This is because of the aggregate interference

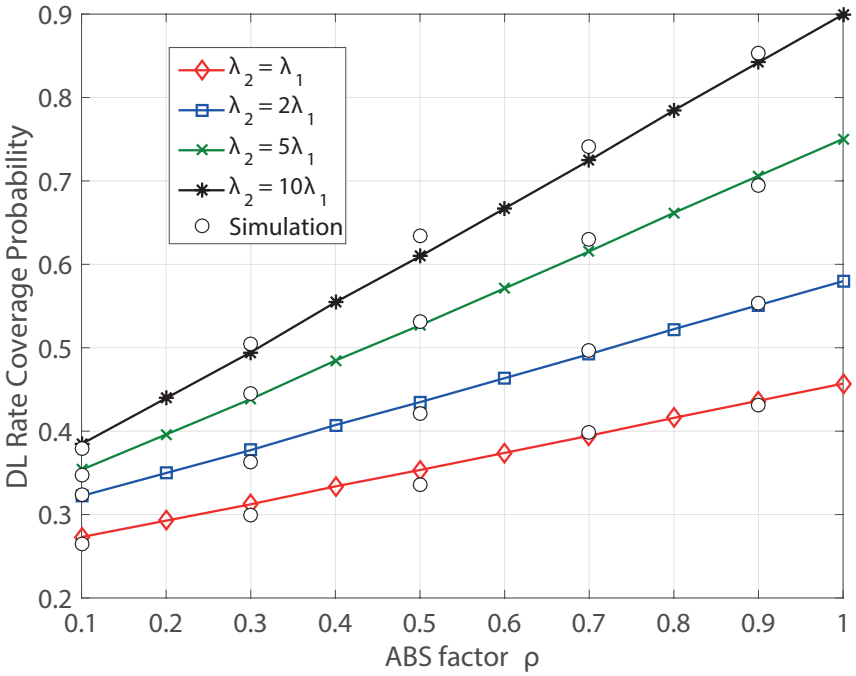

Figure 3.6: DL rate coverage probability as a function of ABS factor ρ.

caused by macrocell BSs, which can be seen in (3.7) and (3.8). Similarly, in Fig. 3.6, the rate coverage of random DL users increases with increasing ρ for the same reason, which can be seen in (3.5) and (3.6). Fig. 3.7 shows that the outage probability of a random user decreases as ρ increases. This is due to the fact that interference originated by macrocell BSs decreases with increasing ρ, as seen in (3.4) and (3.6). This trend advocate for the use of data/control separation, leaving data communications primarily for small cells, as it results in better performance.

Fig. 3.8 plots the relation between small cell UL rate coverage probability and the residual SI cancellation $RSI = P_{S_2}.10^{L_{dB}/10}$, where L_{dB} is the ratio of RSI after interference cancellation is applied to the transmission power at the receiver. We observe that outage probability of a randomly located user is initially high, especially when SI cancellation capability is low ($L_{dB} < -15$), then it decreases with increasing L_{dB}, until it nearly stabilise beyond ($L_{dB} > -37$). This is because the high

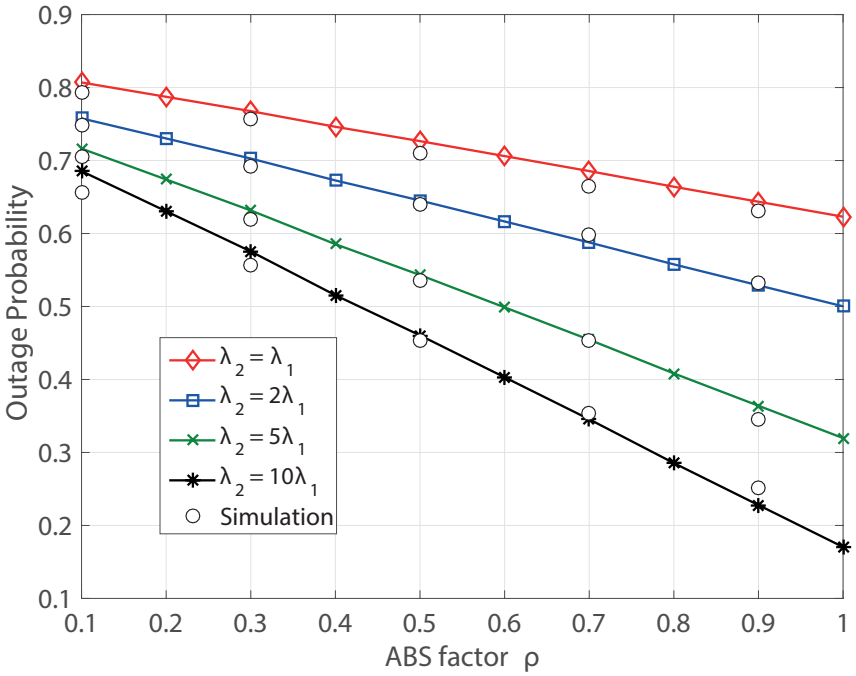

Figure 3.7: Outage probability in relation to ABS transmission factor ρ.

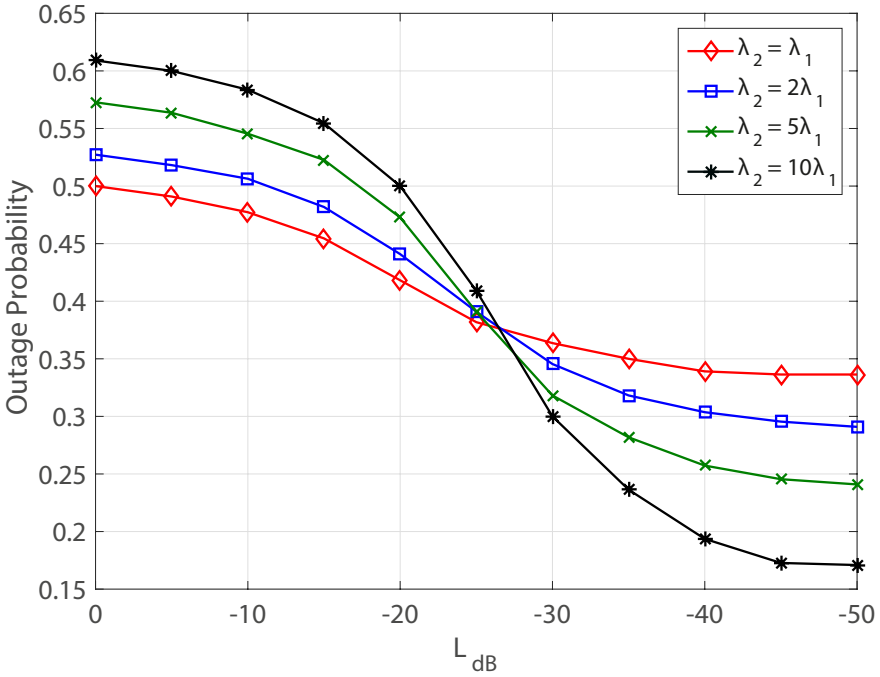

Figure 3.8: Outage probability as a function of the SI cancellation capability L_{dB}.

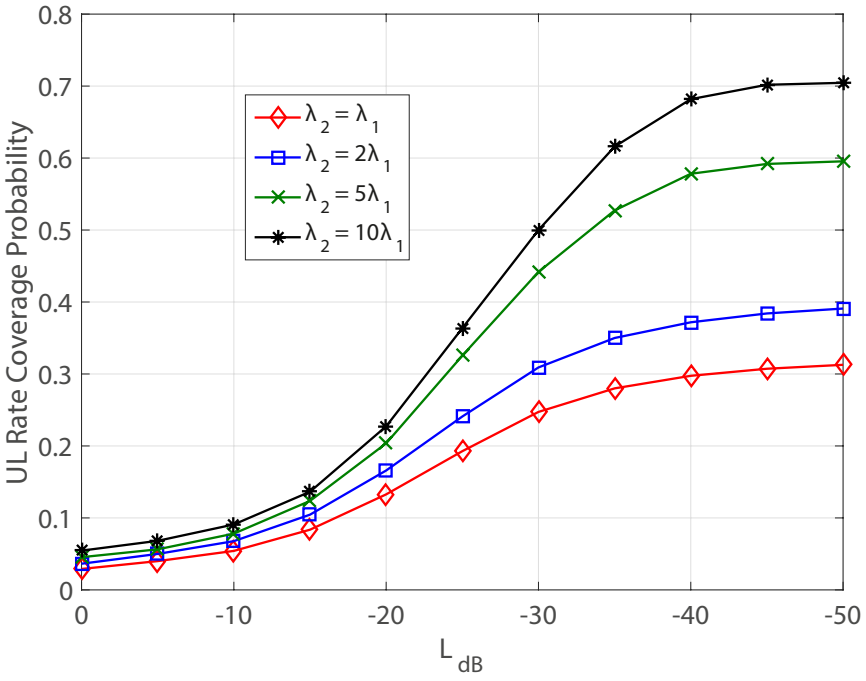

Figure 3.9: UL rate coverage probability as a function of the self-interference cancellation capability L_{dB}.

SI cancellation capabilities improve the performance of FD links as can be seen in (3.7). Additionally, we observe that the outage probability in high small cell densities is more sensitive to L_{dB} variations. This is due to increased FD links in higher small cell densities since only the small cell BSs operate in FD mode.

In Fig. 3.9, we plot the relation between small cell UL rate coverage probability and SI cancellation capability L_{dB}. Since only the small cell BSs operate in FD mode, SI only applies to those BSs. We note that the rate coverage increases with the increase of L_{dB}. This is because higher SI cancellation improves the performance of FD links, as can be seen in (3.7) and (3.8). Moreover, increasing the density of small cell BSs increases the rate coverage. This is due to the fact that more FD links exist in higher small cell densities.

3.7 Conclusions

Unprecedented technological developments like network densification and FD communications will be crucial in shaping 5G radio access networks for achieving the envisioned capacity objectives. Realizing the FD capability at small cells is particularly attractive due to simplicity, superior SI cancellation (compared to macrocells), and widespread deployment. In this chapter, we have investigated the performance of two-tier interference-coordinated HCNs with FD small cells. We have derived closed-form expressions for outage probability and rate coverage in two-tier HCNs with FD small cells explicitly accounting for interference coordination between macro and small cells. Performance evaluation investigates the impact of different network parameters on both outage and rate coverage probabilities. The results demonstrate that the outage probability and the rate coverage improves with higher ABS factor and better underlying SI cancellation capabilities of FD small cells.

Chapter 4

Energy-Efficient FD MAC Protocol for Distributed Wireless Networks

4.1 Introduction

Existing efforts towards full-duplex (FD) wireless communications have mainly focussed on investigating the Physical (PHY) layer aspects [91]. Although wireless full-duplexing is a physical layer mechanism, its implications go beyond physical layer throughput. Addressing FD in higher layers can lead to solving very challenging problems in wireless networks, including hidden terminals, fairness in wireless LANs, and end-to-end delay in multihop networks. Therefore, novel solutions and protocol enhancements are needed at higher layers to achieve the true benefits of FD technology.

4.2 Contribution

The main contribution of this chapter is to propose an FD-capable MAC protocol that aims at achieving energy efficiency, while particularly accounting for the peculiarities of FD environments such as bi-directional and uni-directional links (explained in Section 4.3). The protocol operation of [22] is adapted for the proposed energy saving technique. The proposed protocol, termed as Energy-FDM, particularly focuses on reducing the transmission power of data and acknowledgement (ACK) packets to achieve energy efficiency. The aims of the protocol can be summarized as follows

1. **Energy Efficiency:** Sending data using maximum transmission power can lead to unnecessary higher energy consumption. Energy-FDM is a protocol that aims at reducing the transmission power of data and acknowledgement (ACK), without compromising the reliability of transmission.

2. **Enabling Both Types of FD Links:** In FD wireless networks, link can be either bi-directional or uni-directionals, as illustrated in Fig. 4.1. Energy-FDM accounts for both types of links without additional protocol overheads.

3. **High Effective Throughput:** An important feature of FD technology is increasing the system throughput. Energy-FDM consumes lower energy without compromising the effective throughput. Additionally, Energy-FDM addresses the hidden node problem to further increase the effective throughput of the network.

4. **Backward Compatibility:** Energy-FDM enables the co-existence of FD and HD nodes by retaining the signalling associated with the

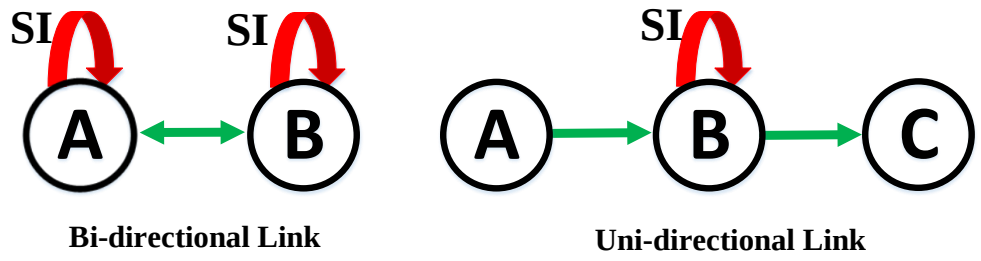

Figure 4.1: Two distinct types of FD links.

IEEE 802.11 DCF protocol and allowing nodes to choose the type of connection.

The proposed protocol is analysed through a stochastic geometry based approach for accurate and realistic performance evaluation.

4.3 System Model

We consider a Poisson distributed wireless network comprising both FD and HD nodes. For FD operation, we adopt a PHY layer model from [31] wherein, each node is equipped with a single shared antenna along with the proposed self-interference (SI) cancellation mechanism therein. We consider two types of FD wireless links. *Bi-directional links* (Bi-Links), where node A transmits to node B in the first transmission (FT) and node B transmits to node A in the second transmission (ST), with both FT and ST occurring simultaneously. In this case, both nodes suffer from SI and apply the necessary SI cancellation mechanism. *Uni-directional links* (Uni-Links), where node A transmits to B (FT) and B transmits to another node C (ST). In this case, only node B experiences SI.

Further, we define the following ranges for each node in the network, which are also illustrated in Fig. 4.2.

1. *Transmission Range:* In which any residing node can successfully decode the transmitted packets by a sender.

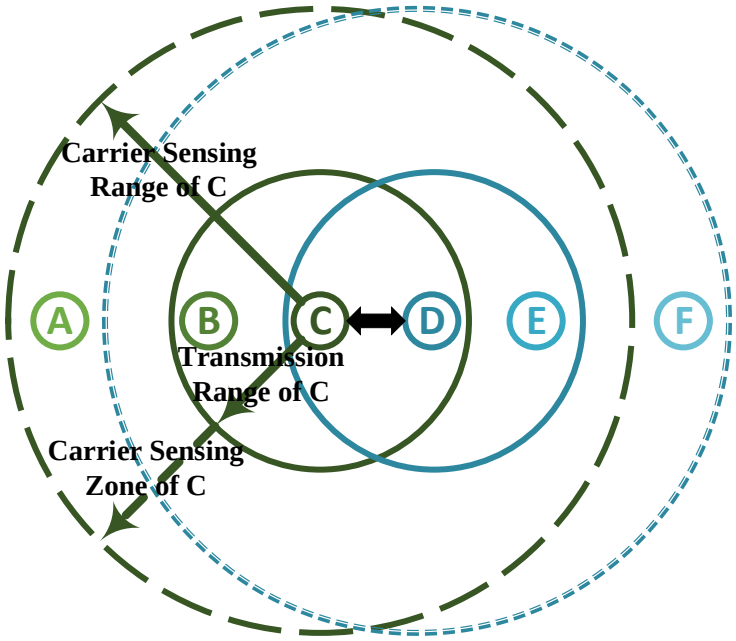

Figure 4.2: Range definitions in the underlying system model.

2. *Carrier Sensing Range:* In which residing nodes can sense the sender's transmission.

3. *Carrier Sensing Zone:* In which any residing node cannot successfully decode the transmitted packets by a sender node, and consequently sets its *Network Allocation Vector* (NAV) to *Extended Inter-Frame Spacing* (EIFS)[1]. The carrier sensing zone excludes the transmission range.

4.4 Energy-FDM Protocol

In our underlying system model, three distinct types of communications can occur:

1. FD bi-directional communication via Bi-links

2. FD uni-directional communication via Uni-links

[1]This is done in order to provide the intended receiver with an opportunity to return an acknowledgement (ACK) without interference.

3. Conventional HD communication

Consider that node A has data to send to node B. It takes a random back-off (BO) if the channel is sensed as busy. After the expiry of BO timer, if the channel is sensed as idle, it starts the transmission by sending a request-to-send (RTS) packet to node B with maximum power (P_{max}), in order to capture the channel and to make other nodes aware of an ongoing transmission. Note that this is the FT from node A which includes the source and destination addresses as well as the length of the transmission.

4.4.1 FD Bi-directional Communication

In case of FD bi-directional communication between nodes A and B, after receiving the RTS packet from A, node B waits for short inter-frame space (SIFS) duration before sending an FD clear-to-send (FD-CTS) packet to A. The FD-CTS packet includes the source and destination addresses along with the transmission durations of both FT and ST. Note that FD-CTS is also transmitted using P_{max} to capture the channel for ST. Additionally, node B also calculates P_{min}, which is defined as the minimum transmit power for successful data transmission such that

$$P_{min} = \frac{P_{max}}{P_{rx}} \times R_x^{thresh} \times c, \tag{4.1}$$

where P_{rx} is the received power, R_x^{thresh} is the minimum necessary received signal strength and c is a constant used for simulation purposes as [92].

Once node A receives the FD-CTS, it calculates P_{min} as well, and responds with another FD-CTS for synchronization with node B. After B receives FD-CTS from A, data transmission starts using P_{min} with

periodical increase to P_{max}, so that nodes in the sensing zone, which cannot decode the transmission and set their NAV to EIFS duration can sense the transmission. Note that the period between two successive power increase intervals must be less than the EIFS duration. According to the IEEE 802.11 standard [93], 15 μs is suitable for carrier sensing, and 2 μs is adequate to increase the power level from 10% to 90% and decrease it from 90% to 10%. Therefore, a duration of 20 μs is deemed adequate for transition of power level from P_{min} to P_{max} and vice versa, as shown in Fig. 4.3. Since EIFS is set to 364 μs in IEEE 802.11 standard, a node in Energy-FDM will transmit at P_{max} every 340 μs for a duration of 20 μs, and the cumulative transmission duration is less than the EIFS duration. Further, since the durations of FT and ST are known, the transmission will last for the longer duration, after which both nodes A and B will send an ACK. Note that the protocol operation inherently accounts for the necessary SIFS duration as shown in Fig. 4.3. Please note that those durations differ between standards, as a general notation EIFS duration can be calculated as the transmission time of Ack frame at lowest PHY mandatory rate + SIFS + DIFS.

4.4.2 FD Uni-directional Communication

The protocol operation in this case is illustrated in Fig. 4.3. If node B has packets to send to another node C, it waits for SIFS and then sends FD-CTS to both A and C using P_{max}, after which it calculates P_{min} using the received power from A. Next, node A calculates P_{min} and waits for a duration of 2 SIFS and an FD-CTS before initiating data transmission. When node C receives FD-CTS from B, it calculates P_{min} and waits for SIFS duration before sending FD-CTS back to node B. After that node B calculates P_{min} using the received power from node C and compares it

with the previously calculated P_{min} (from node A). Node B will use the higher P_{min} in order to maintain both FT and ST connections. The data transmission lasts for the longer duration of either FT or ST using P_{min} with periodic increase to P_{max}, as described earlier. After the completion of data transmission, node C sends ACK to node B, and B sends ACK to node A.

4.4.3 HD Communication

It is important to maintain backward compatibility with conventional HD nodes. If node B is an HD node, or does not have packets to send, it waits for SIFS duration and sends back a normal CTS to node A. The communication will proceed as HD based on the standard 802.11 DCF protocol [94].

The pseudo code of the protocol functionality is summarised in Algorithm 1.

4.4.4 Solving Hidden Nodes Problem

Refering to Fig. 4.2, consider that nodes C and D constitute a sender-receiver pair in HD mode. Node F, which resides in the carrier sensing range of D but not of node C, may act as a hidden node. In bi-directional transmission, both nodes transmit and receive simultaneously, and therefore the hidden node issue is implicitly resolved due to the FD nature of this transmission. In uni-directional transmission, hidden nodes may affect the receiver of ST. That is why Energy-FDM adopts RTS-CTS mechanism, and by sending FD-CTS using P_{max}, it ensures that nodes in the carrier sensing range of ST are aware of an ongoing transmission.

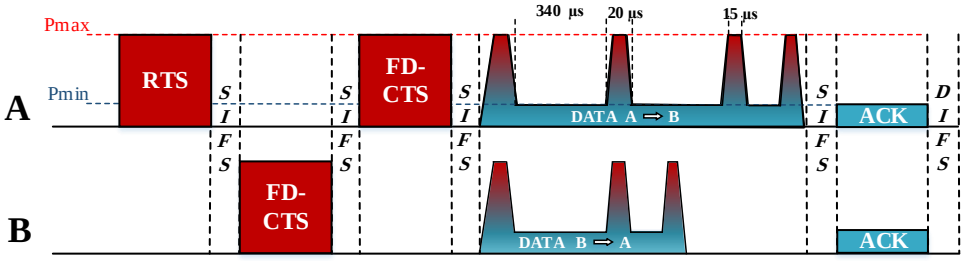

Bi-directional transmission

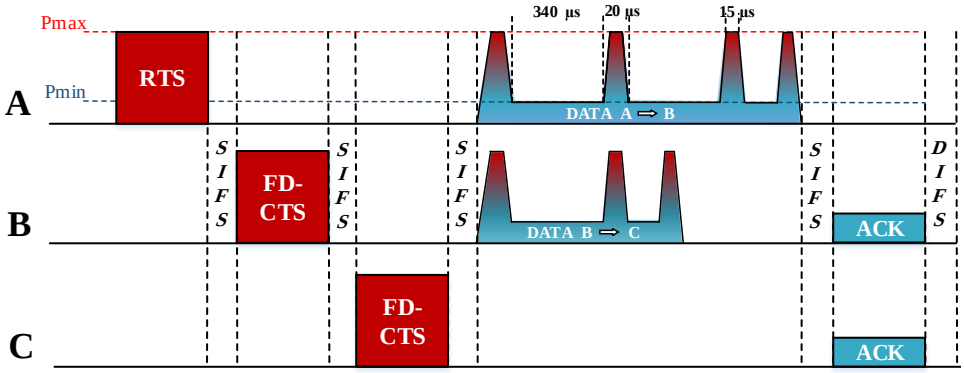

Uni-directional transmission

Figure 4.3: Example of the bi-directional and uni-directional transmission in Energy-FDM using 1 Mbps bandwidth.

Algorithm 1: *The proposed Power-FDM Protocol*

∗ **Initial state:** A has packets to send to B, channel is sensed idle and BO = 0.

• A Sends RTS to B using P_{max} and wait for response.

• B calc $P_{min} = \frac{P_{max}}{P_{received}} \times R_{x_{thresh}} \times c$

if *B has packets back to A (Bi-Link)* **then**

- B waits for SIFS time then send FD-CTS using P_{max}, and wait for another FD-CTS from A.
- After A receive FD-CTS from B. A calc P_{min}, wait for SIFS and send FD-CTS to B using P_{max}, then wait for SIFS time to start data transmission using P_{min} with alternating P_{max}.
- After B receive the second FD-CTS from A, it wait for SIFS time and then start data transmission using P_{min} with alternating P_{max}.
- Transmission will last for the longer period of $A \rightarrow B$ or $B \rightarrow A$
- After transmission is over, both A and B wait for SIFS time then send ACK using P_{min} to each other.

else if *B has packets to another node C (Uni-Link)* **then**

- B waits for SIFS time then send FD-CTS using P_{max} to both A and C
- A receive FD-CTS from B, calc P_{min} and wait for (2 SIFS + FD-CTS) time before starting transmission
- C also receive FD-CTS from B, calc P_{min}, wait for SIFS time and send FD-CTS to B using P_{max}, then wait for SIFS time before starting transmission.
- B receive FD-CTS from C, B calc new P_{min} using received power from C and use the higher P_{min}, then wait for SIFS to start transmission using P_{min} with alternating P_{max}.
- Transmission will last for the longer period of $A \rightarrow B$ or $B \rightarrow C$.
- Once transmission is done, B and C wait for SIFS, then C send ACK to B and B send ACK to A using P_{min}.

else

- B is HD OR does not have packets to send.
- B sends back normal CTS using P_{max}
- A calc P_{min} and start data transmission using it.
- Once received B sends back ACK using P_{min}.

4.5 Protocol Analysis

In this section, we develop an analytical model of the proposed protocol and derive expressions for throughput and energy consumption.

4.5.1 Spatial Throughput Analysis

We assume that nodes are distributed in an Euclidean plane $\mathbb{R}^2$ according to a homogeneous Poisson Point Process (HPPP) Φ with intensity λ. Node A located at x correctly receives and decodes packets transmitted from node B located at y if the received SINR (γ) is higher than a threshold β i.e.,

$$\gamma(A) = \frac{P_{rx}}{N_0 + I_x} > \beta, \tag{4.2}$$

where N_0 is the noise power, and I_x is the cumulative interference of all other transmitting nodes in the contention domain of node A.

To determine the subset of APs that transmit simultaneously, we adopt the modified Matérn model similar to [95], which captures essential features of CSMA based protocols while maintaining analytical tractability. Particularly, the model captures the fact that an AP refrains from transmitting if it senses the activity of another AP which has extracted a smaller back-off time. This model is suitable to describe the synchronized and slotted version of CSMA and hence complies with our protocol. In this model, each point x of Φ is attributed an independent mark t_x uniformly distributed in $[0, 1]$, representing back-off time. A node transmits if it does not sense the activity of any other node having smaller mark. The subset of neighboring nodes of x transmitting concurrently is given by

$$\mathcal{N}(x) = \{x \in \Phi : t_x < t_y, \forall y : P_{rx} > \beta\}. \tag{4.3}$$

The received power is given by $P_{rx} = P \cdot L(x,y) \cdot F(x,y)$, where P is the transmitted power (either P_{max} or P_{min}), $L(x,y)$ is the the path loss component, and $F(x,y)$ is a random variable accounting for the fading and shadowing. We adopt the notion of average spatial throughput from [95] and calculate for our scenario which depends on: (i) distance distribution between a pair of nodes, (ii) set of simultaneously transmitting nodes, and (iii) probability of successful transmission, and is given by

$$\tau_{FD} = \int_0^\infty \int_0^\infty (\alpha \mathbb{P}_{Bi} + (1-\alpha)\mathbb{P}_{Uni}) f_D(r,n) \mathrm{d}r\mathrm{d}n \tag{4.4}$$

where α is the fraction of Bi-links, r is the distance between sender and receiver nodes, $n = \mid \mathcal{N}(\cdot) \mid$, $\mathbb{P}_{Bi}$ and $\mathbb{P}_{Uni}$ respectively denote the probabilities of successful bi-directional and uni-directional transmissions, and $f_D(r,n)$ is the probability density function of the distance between the receiver and the neighbours in the contention domain, given by [96]

$$f_D(r,n) = \frac{(\pi\lambda r^2)^{n-1}}{(n-1)!} e^{-\pi\lambda r^2}. \tag{4.5}$$

Following the stochastic analysis of random networks in Section 3.2 of [97], we define the probability of successful transmission in our case as follows:

$$\begin{aligned} \mathbb{P} = & \left(\frac{(\mathcal{L}_{I_1})^{n-2}}{\left(1 + \Omega(\beta x^{\ell_1}, x) + B(1 - \frac{2}{\ell_1}, 1 + \frac{2}{\ell_1})\beta^{\frac{2}{\ell_1}}\right)} \right) \\ & \times \left(\frac{(\mathcal{L}_{I_2})^{n-2}}{\left(1 + \Omega(\beta y^{\ell_2}, y) + B(1 - \frac{2}{\ell_2}, 1 + \frac{2}{\ell_2})\beta^{\frac{2}{\ell_2}}\right)} \right) \end{aligned} \tag{4.6}$$

where $\mathcal{L}_{I_1}$ and $\mathcal{L}_{I_2}$ respectively denote the Laplace transforms of the interfering neighbours of FT and ST receivers, ℓ_1 and ℓ_2 respectively denote the path loss exponent between pair of FT and ST nodes, $B(\cdot,\cdot)$

is the Beta function, and $\Omega(s, X)$ is a function defined as

$$\Omega(s,X) = \frac{\mathcal{F}(1,1,1-\frac{2}{\ell},\frac{sX^{-\ell}}{1+sX^{-\ell}})}{1+sX^{-\ell}} - B(1-\frac{2}{\ell},1+\frac{2}{\ell})s^{\frac{2}{\ell}}X^{-2} - 1 \quad (4.7)$$

where $\mathcal{F}(\cdot,\cdot,\cdot,\cdot)$ is the Gaussian Hypergeometric function. Note that (4.6) is valid for both Bi-links and Uni-links.

Therefore, the average spatial throughput expression becomes

$$\begin{aligned}
\tau_{FD} =& \alpha \left(\frac{(\mathcal{L}_{I_1})^{n-2}}{\left(1+\Omega(\beta x^{\ell_1},x)+B(1-\frac{2}{\ell_1},1+\frac{2}{\ell_1})\beta^{\frac{2}{\ell_1}}\right)} \right) \\
&\times \left(\frac{(\mathcal{L}_{I_2})^{n-2}}{\left(1+\Omega(\beta y^{\ell_2},y)+B(1-\frac{2}{\ell_2},1+\frac{2}{\ell_2})\beta^{\frac{2}{\ell_2}}\right)} \right) \\
&+ (1-\alpha) \left(\frac{(\mathcal{L}_{I_1})^{n-2}}{\left(1+\Omega(\beta x^{\ell_1},x)+B(1-\frac{2}{\ell_1},1+\frac{2}{\ell_1})\beta^{\frac{2}{\ell_1}}\right)} \right) \\
&\times \left(\frac{(\mathcal{L}_{I_2})^{n-2}}{\left(1+\Omega(\beta y^{\ell_2},y)+B(1-\frac{2}{\ell_2},1+\frac{2}{\ell_2})\beta^{\frac{2}{\ell_2}}\right)} \right) \\
&\times \frac{(\pi\lambda r^2)^{n-1}}{(n-1)!} e^{-\pi\lambda r^2}. \qquad (4.8)
\end{aligned}$$

4.5.2 Energy Analysis

Owing to the presence of SI, it is important to consider FD efficiency [22] for a FD node, defined as the ratio of the effective received packet payload to the sent packet payload, and given by

$$\epsilon = \frac{\int_0^\infty \log_2(1+\kappa\gamma) f(\gamma) d\gamma}{\int_0^\infty \log_2(1+\gamma) f(\gamma) d\gamma}, \qquad (4.9)$$

where γ is the instantaneous received SINR at the FD node, $f(\gamma)$ is the probability density function of the channel and $\kappa \in [0,1]$ is the SI cancellation coefficient. When $\kappa \to 0$ the SI causes large interference on

the FD transmission, whereas when $\kappa \to 1$ the SI causes no interference. In bi-directional transmission, the FD efficiency is taken into account for both nodes as both operate in FD mode, while in uni-directional transmission, the efficiency is considered only for the FT receiver node as it is the only FD node. The effective packet payload δ_{FD} (in bits) is given by

$$\delta_{FD} = \begin{cases} \delta_{Bi} & = \epsilon(\delta_{FT} + \delta_{ST}) \\ \delta_{Uni} & = \epsilon\delta_{FT} + \delta_{ST} \end{cases}, \tag{4.10}$$

where δ_{Bi} and δ_{Uni} are the effective packet loads of the Bi-links and Uni-links respectively, δ_{FT} and δ_{ST} are the packet payload for the FT and ST respectively. For the sake of comparison, we define the effective packet payload of a HD link as $\delta_{HD} = \frac{\delta_{FT}+\delta_{ST}}{2}$.

Let, $E_{Bi} = E_A^{Bi} + E_B^{Bi}$ denote the average energy consumed during a successful FD bi-directional transmission, where E_A and E_B denote the energy consumed by nodes A and B respectively, such that

$$\begin{aligned} E_A^{Bi} =& T_{FDCTS} \cdot P_{on} + (T_{\delta_{FT}} - T_{IFT} + T_{ACK})P_{min} \\ &+ (T_{RTS} + T_{FDCTS} + T_{IFT})P_{max}, \end{aligned} \tag{4.11}$$

$$\begin{aligned} E_B^{Bi} =& (T_{RTS} + T_{FDCTS})P_{on} + (T_{FDCTS} + T_{IST})P_{max} \\ &+ (T_{\delta_{ST}} - T_{IST} + T_{ACK})P_{min}, \end{aligned} \tag{4.12}$$

where T_{RTS}, T_{FDCTS}, T_H and T_{ACK} denote the duration of RTS, FD-CTS, header (of both MAC and PHY) and ACK frames respectively, $SIFS$ and $DIFS$ denote the short and DCF inter-frame space duration (defined in the 802.11 DCF standard) respectively, $T_{\delta_{FT}}$ and $T_{\delta_{ST}}$ denote the duration of effective payload for FT and ST transmissions respec-

tively, P_{on} is the power consumed during the receive mode, and T_{IFT} and T_{IST} are the durations of power increase to P_{max} for the FT and ST respectively such that $T_{IFT} = 20 \cdot (\frac{\delta_{FT}}{EIFS} + 1)$ and $T_{IST} = 20 \cdot (\frac{\delta_{ST}}{EIFS} + 1)$. Note that the transmission duration (in μs) for c bits is calculated as $T_c = c/\mathcal{B}$, where $\mathcal{B}$ is the bandwidth.

Similarly, let $E_{Uni} = E_A^{Uni} + E_B^{Uni} + E_C^{Uni}$ denote the average energy consumed during a successful FD uni-directional transmission such that

$$\begin{aligned} E_A^{Uni} =& (T_{RTS} + T_{IFT})P_{max} + (2T_{FDCTS} + T_{ACK})P_{on} \\ &+ (T_{\delta_{FT}} - T_{IFT})P_{min}, \end{aligned} \tag{4.13}$$

$$\begin{aligned} E_B^{Uni} =& (T_{RTS} + T_{FDCTS})P_{rx} + (T_{FDCTS} + T_{IST})P_{max} \\ &+ (T_{\delta_{ST}} - T_{IST} + T_{ACK})P_{min}, \end{aligned} \tag{4.14}$$

$$\begin{aligned} E_C^{Uni} =& (T_{RTS} + T_{FDCTS} + T_{\delta_{ST}})P_{on} \\ &+ T_{FDCTS}P_{max} + T_{ACK}P_{min}. \end{aligned} \tag{4.15}$$

Therefore, the total energy consumption is given by $E = \alpha E_{Bi} + (1 - \alpha)E_{Uni}$.

4.6 Numerical Results

We assume Poisson distributed nodes in an area of 1500 m^2 and vary the density of nodes. Further, we assume 1 Mbps bandwidth with maximum transmit power of 24 dBm. The frame size (in bits) of different packets is set to 277 for RTS, 528 for FD-CTS, 240 for CTS, 240 for ACK, 128 for PHY header, 272 for MAC header, and 8184 for payload. Different inter-frame spacing durations (in μs) are set to as, 28 for SIFS, 128 for DIFS, 364 for EIFS. The slot duration is set to as 50 μs. Lastly, we assume $\alpha = 0.5$. We adopt the FD protocol RTS-FCTS [22] as the baseline as it

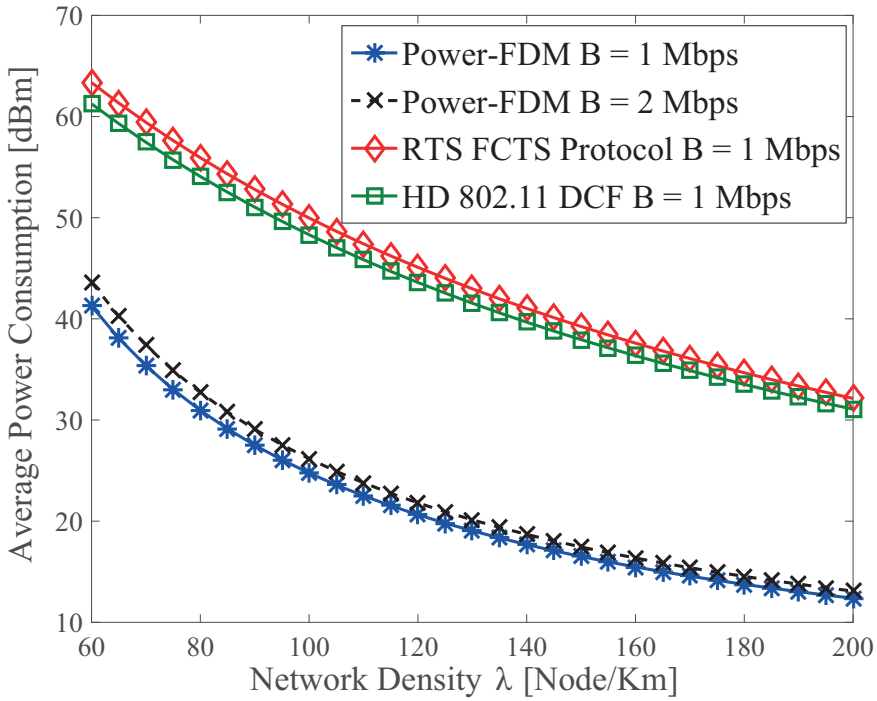

Figure 4.4: Average power consumption as a function of network density

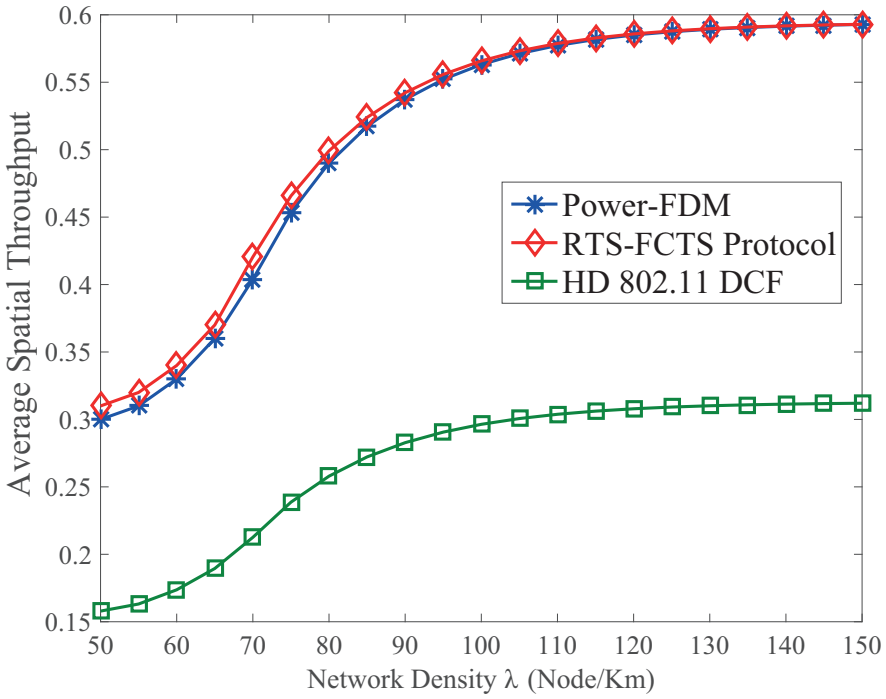

Figure 4.5: Average spatial throughput as a function of network density

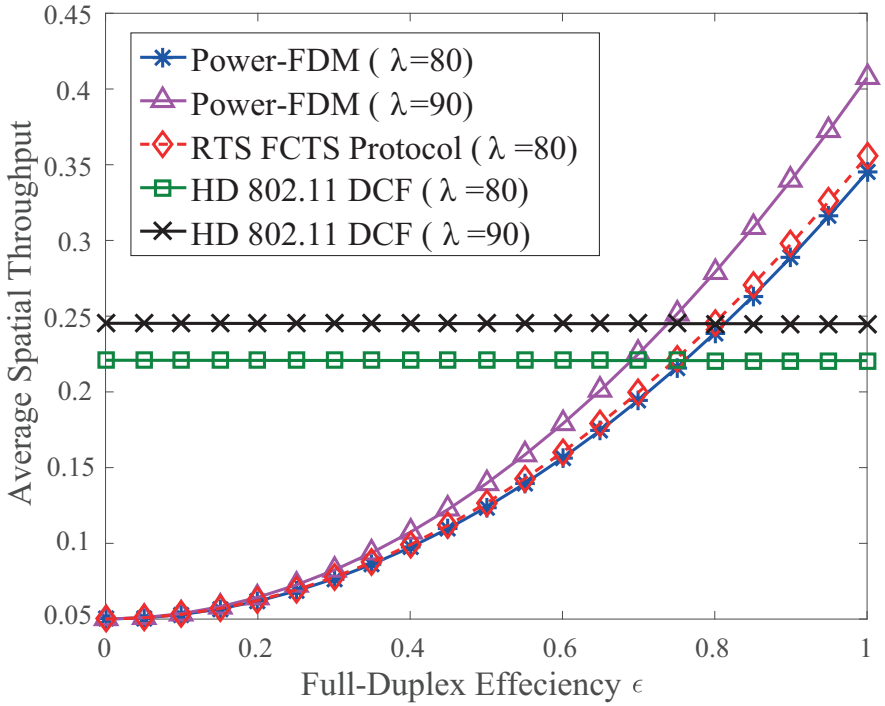

Figure 4.6: Average spatial throughput as a function of FD efficiency

uses similar control signals with maximum power. We also compare the performance with the standard IEEE 802.11 (HD) DCF protocol [94].

Figure 4.4 shows the energy consumption for different protocols. We note that the energy consumption reduces with the network density. This is because of overall reduced transmission power owing to shorter transmission links. Further, Energy-FDM outperforms the baselines protocols by consuming on average up to 47.2% and 44.8% lower energy compared to [22] and [94], respectively. The energy consumption increases with increase in bandwidth as the transmission duration of different messages as well as the inter-frame spacing durations decrease, as a result of which, the power must be increased more frequently during data transmission. Please note that the results do not account for the noise power and the circuit power in PHY layer, otherwise, the gap between the plots of power consumption where B = 1 Mbps and B = 2 Mbps will be bigger.

Figure 4.5 shows the average spatial throughput performance for

different protocols. We note that despite reducing the transmission power, Energy-FDM achieves similar throughput performance as [22] which transmits at maximum power. The throughput initially increases in low network density, where collision effects are not significant. After reaching the maximum value, it stops due to network saturation.

In FD networks, performance is heavily dependent on the SI cancellation. As shown by results in Fig. 4.6, the average spacial throughput increases when the FD efficiency (ϵ) increases. We note that it drops to the level of HD system when ϵ drops below 0.75. Therefore, SI must be dealt with properly to achieve the gain of FD technology at higher layers.

4.7 Concluding remarks

We have proposed Energy-FDM, which is an energy-efficient FD MAC protocol for distributed wireless networks. Energy-FDM achieves higher energy-efficiency without compromising the overall effective throughput. Moreover, it supports both Bi-links and Uni-links and is inherently backward compatible. Performance evaluation shows the achievable gains of Energy-FDM. Results also demonstrate that higher layer gains of FD technology heavily rely on SI cancellation mechanisms at the PHY layer. In the next chapter, a cross-layer FD routing protocol for distributed wireless networks is presented, adopting aspects from Energy-FDM as a MAC protocol.

Chapter 5

Cross-Layer Aided FD Routing Protocol for Distributed Wireless Networks

5.1 Introduction

FD technology not only offers the potential of doubling the capacity and the spectrum utilization, but also assists in solving some of the key problems in HD systems, such as the hidden node issues, loss of throughput due to high congestion rates, and large end-to-end delays [26]. Existing efforts towards FD communications have mainly focussed on investigating lower layers aspects [91]. However, these advancement necessitates novel solutions for protocol designs and enhancements at higher layers as well, to reap the actual benefits of FD technology. Research on FD routing protocols is still rather scarce, leaving room for taking further advantages of FD technology, which motivates this work.

On the other hand, energy saving in distributed wireless networks is of significant importance due to the limited battery supply of each node. The nodes continuously participate in constructing the network and act as relays for different and rapidly changing routes. In addition to continuous variation in the Channel State Information (CSI) caused by the instability of wireless channels, this leads to a large amount of control messages being exchanged across the network to maintain reliability, which potentially entails high energy consumption.

5.2 Contribution

The objective in this chapter is to design a cross-layer aided routing protocol for imperfect FD wireless networks, where the notion of imperfection implies that SI is not fully cancelled at the PHY layer. The proposed protocol, which is termed as X-FDR, is particularly designed for minimizing energy consumption and end-to-end latency in FD wireless networks. The key features of X-FDR can be summarized as follows

- X-FDR accounts for the residual self-interference (RSI) in the SINR expressions of the nodes, which is the interference caused by the imperfection of interference cancellation mechanisms.
- We adopt an energy-efficient collision-free MAC protocol (explained in Section 5.3.1), designed for FD capable network, which allows power control without causing hidden terminal problems. We also make further modifications on the adopted MAC protocol for compatibility. Additionally, X-FDR accounts for the MAC retransmission attempts to reconcile more realistic scenarios.
- In our protocol design, we use a novel energy cost as a metric, instead of hop counts.

- X-FDR makes use of the opportunities provided by FD technology, like the ability to sense the medium while transmitting, which provides immediate reaction towards channel errors. This consequently enables nodes to send a bundle of packets, sized by the minimum buffer size β_{min} of nodes on the selected route, and wait for an acknowledgement packet (ACK) for the last received packet only, instead of acknowledging the reception of each packet.

- X-FDR also employs immediate forwarding, where an FD node does not have to wait for the reception of the full packet before it starts forwarding. This feature reduces the end-to-end delay of the transmitting stream and increases network availability.

- We modify the route maintenance process to reduce the delays caused by new route discovery, by initiating route discovery at the node where the link broke, then resuming the transmission by the node that have received the full bundle of data.

The rest of the chapter is organized as follows. Section 5.3 provides the preliminaries, with the considered attributes from PHY and MAC layers. In Section 5.4, we present the routing protocol, with details on its route discovery, data transmission and route maintenance mechanisms. This is followed by the protocol performance evaluation and simulation results in Section 5.5. Finally, the chapter is concluded in Section 5.6.

5.3 System Model

We consider a distributed network comprising N FD wireless nodes. Let, $\mathcal{R}$ denote the set of all possible routes in the network. A route $R \in \mathcal{R}$ represents an ordered set of nodes between a source node S and a destination node D, where node S is the first element in the set and node

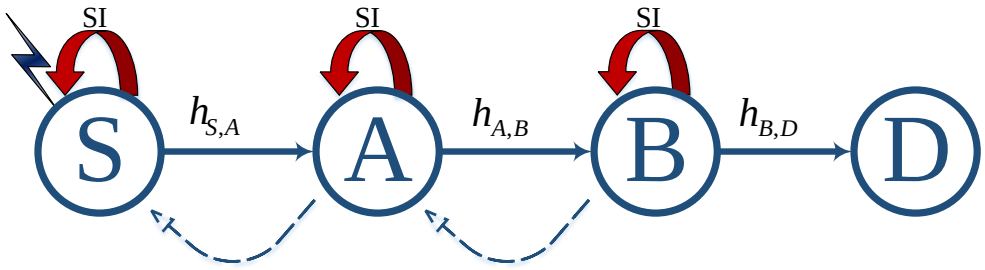

Figure 5.1: Example of a route $R = \{S, A, B, D\}$. Straight lines represent the intended transmission, while dotted lines represent neighbouring interference, and the red semi-circled arrows represent SI.

D is the last. Route $R \in \mathcal{R}$ is not obliged to include all N elements in the route. The order of R represent the transmission order, meaning that node (i) in R transmits to node $(i+1)$, while node $(i-1)$ transmits to node (i) simultaneously. For example, $R = \{S, A, B, D\}$ in Fig. 5.1 demonstrates a route of four nodes, where the source node S transmits to node A, which forwards to node B, which finally forwards to the destination node D.

Nodes in R are k hops away from each other when there are k elements between them, where adjacent elements in R have one hop away from each other. For example, in Fig. 5.1, the route $R = \{S, A, B, D\}$ involves 4 nodes, where node A is one hop from S and two hops from D. Therefore, hops are only defined in terms of routes, for example if the considered route was found to be $R = \{S, A, D\}$, then A and D would be one hop away from each other, regardless of B being physically located between A and D.

We assume that FD wireless nodes employ necessary SI cancellation techniques at the PHY layer. Since SI cancellation techniques are not perfect in practice, a node experiences RSI. We use an experimentally characterized model [27] for RSI, based on which, the power of the RSI

signal is given by

$$RSI = \frac{P_t^{(1-\rho)}}{\Delta \cdot \chi^{\rho}}, \tag{5.1}$$

where P_t is the transmit power, Δ is the interference suppression factor, χ depends on the SI cancellation technique, and ρ denotes the SI cancellation capability. Note that $\rho = \infty$ denotes perfect SI cancellation, resulting in zero RSI. Moreover, $\rho = 0$ implies a constant reduction in transmission power. Realistically, $0 < |\rho| < 1$; with $\rho = 1$ implying a constant power for RSI similar to noise.

Without loss of generality, we assume that the received signal power at a node j, based on a transmission from a node i) at maximum transmit power P_{max} is given by

$$P_r = \frac{P_{max}}{d_{i,j}^{-\alpha}} \times c, \tag{5.2}$$

such that $d_{i,j}$ denotes the distance, α denotes the path loss exponent, and c is a constant. We assume that nodes in the network employ a power control mechanism based on the received signal strength, nodes can estimate the distance between each other using (5.2), and the controlled power level P_{ctrl} is determined by

$$P_{ctrl} = \frac{P_{max}}{P_r} \times \zeta^{th} \times c', \tag{5.3}$$

where ζ^{th} denotes the minimum required received signal strength and $\hat{c}$ is a constant [92]. . In the considered distributed network, the required signal-to-noise-ratio (SINR) of a node i with SI cancellation enabled, for a successful packet decode, with distance d from its intended transmitter node j, can be expressed as

$$SINR_i = \frac{P_j |h_{i,j}|^2 {d_{i,j}}^{-\alpha}}{RSI + I_x + N_0} > \tau, \tag{5.4}$$

where τ is the SINR threshold, P_j denotes the transmitting power of node j, may it be P_{max} or P_{ctrl}, $h_{i,j}$ denote the small scale fading channel coefficient between i and j, α denotes the path loss exponent, and N_0 is the thermal noise. Moreover, I_x is the cumulative interference caused by x neighbouring transmitters, and is given as

$$I_x = \sum_{x \in N \setminus j} P_x |h_{x,i}|^2 {d_{x,i}}^{-\alpha} \tag{5.5}$$

where P_x is the transmitting power of an interfering node x, $h_{x,i}$ is the small scale fading channel coefficient between nodes x and i, and $d_{x,i}$ is the distance between x and i.

5.3.1 MAC Layer Design for X-FDR

This section presents the MAC layer design for X-FDR. In X-FDR, we adopt the modified version of our recently proposed MAC protocol [11] for distributed wireless networks. The MAC protocol in [11] enables both bi-directional FD transmissions and uni-directional FD transmissions. The former enables simultaneous two-way transfer of two distinct data streams between a pair of nodes, whereas, the latter involves three nodes and same data stream is forwarded from one node to another via an intermediate relay node. In X-FDR, we focus only on uni-directional FD transmission. We also omit the MAC layer ACK procedure.

We explain the protocol operation with the aid of Fig. 5.2. We define the following ranges for each node in the network, which are illustrated in Fig. 5.2.

1. *Transmission Range:* In which any residing node can successfully decode the transmitted packets by a sender.

2. *Carrier Sensing Range:* In which residing nodes can sense the

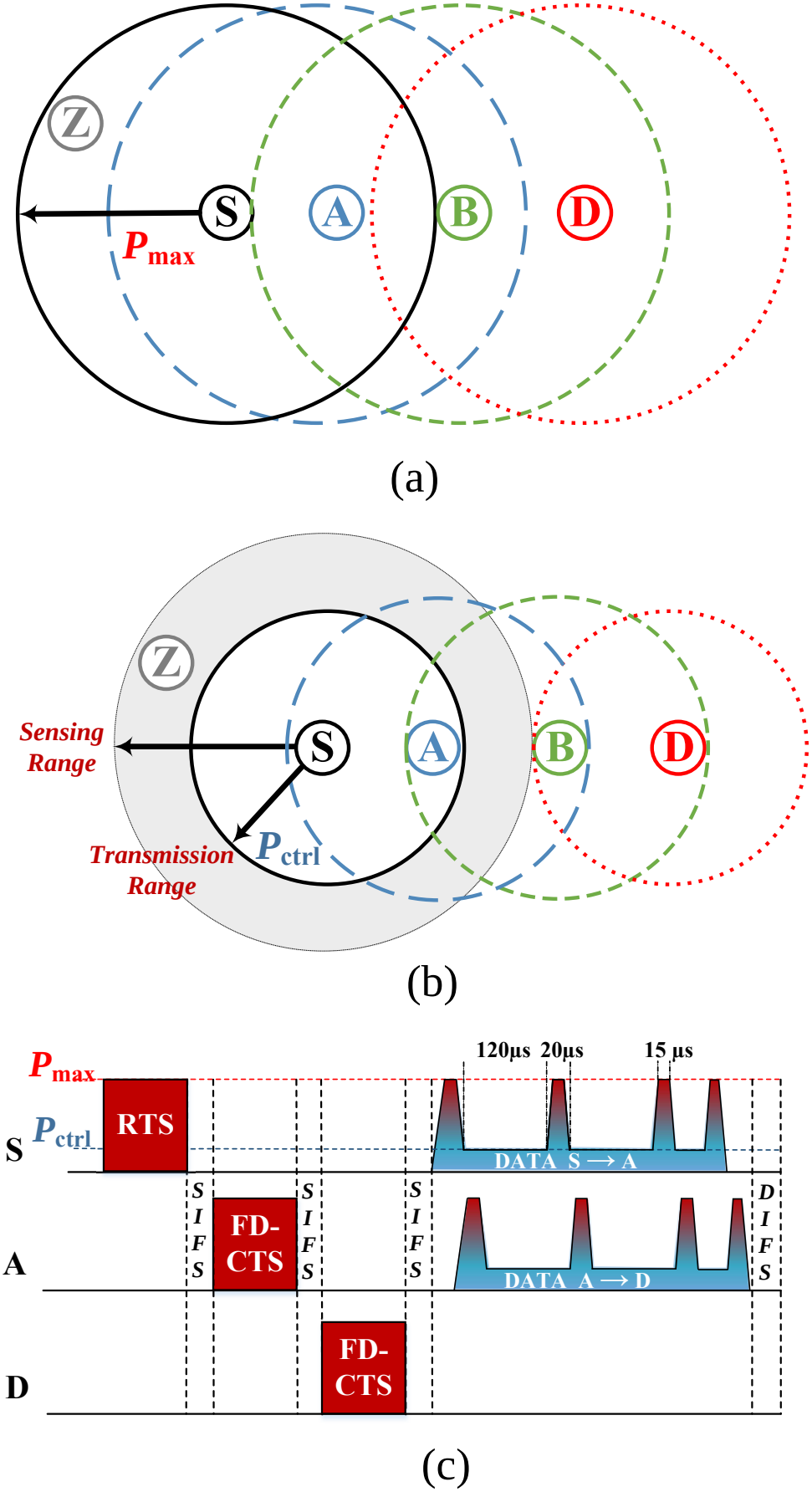

Figure 5.2: (a) Ranges of nodes transmitting control signals using P_{max}; (b) ranges of nodes after application of power control; (c) illustration of a uni-directional FD transmission at the MAC layer.

sender's transmission.

3. *Carrier Sensing Zone:* Illustrated in Fig. 5.2b as the grey area, where nodes residing in this range cannot successfully decode the transmitted packets by the sender.

Let $N = \{S, A, B, D\}$ be a set of nodes involved in the intended transmission, where S is the source node and D is the destination node. After sensing the spectrum idle, node S starts the transmission by sending a request-to-send (RTS) packet to node A using P_{max}. After receiving the RTS packet from S, node A waits for short inter-frame space (SIFS) duration before sending an FD clear-to-send (FD-CTS) packet [11] to both S and B. The FD-CTS packet includes the source and next hop addresses along with the transmission duration. Note that FD-CTS is also transmitted using P_{max} to capture the channel for forwarding. Using the received RTS from S, node A calculates P_{ctrl} following (5.3). Node S calculates its P_{ctrl} as well using the FD-CTS received from node A. Further, when node B receives the FD-CTS from node A, it replies with FD-CTS as well, and calculates its P_{ctrl} based on the received power from A. After that, node A recalculates P_{ctrl} based on the received FD-CTS from B and compares it with the previously calculated P_{ctrl}, where the higher P_{ctrl} is chosen to maintain connection with both S and B. Similarly, the rest of the relaying nodes attempt to acquire the channel until the intended destination is reached.

During data transmission, nodes use P_{ctrl} with periodical increase to P_{max}, so that nodes in the carrier sensing zone, which cannot successfully decode the transmission and set their Network Allocation Vector (NAV) to Extended InterFrame Space (EIFS) duration can sense the transmission. Note that the period between two successive power increase inter-

vals must be less than the EIFS duration[1]. These periodic increments preserve the channel, and ensure that nodes in the carrier sensing zone will not attempt to initiate a transmission.

5.3.2 Hidden Terminal Problem

Referring to Fig. 5.2b, consider that nodes S and A constitute a sender-receiver pair in HD mode. Node Z, which resides in the carrier sensing range of S but not of node A, may act as a hidden node. In FD transmission, hidden nodes may affect the reception of control signals at node S. Therefore, in the proposed protocol we adopt RTS-CTS handshake mechanism. Moreover, by sending FD-CTS using P_{max}, the protocol ensures that nodes in the carrier sensing ranges are aware of an ongoing transmission. After power control is applied for data transmission, node Z can again create a hidden node problem, which is why the periodic increments from P_{ctrl} to P_{max} are required.

5.4 X-FDR: Protocol Operation

In this section, we present the Energy-efficient Full-Duplex Routing Protocol X-FDR designed for distributed multi-hop wireless networks. Unlike conventional Ad-Hoc On-demand Distance Vector (AODV) routing protocol [98], where the route cost relies mainly on hop count, X-FDR uses energy consumption as a metric for route cost estimation. In the following, we introduce the new cost estimation metric, followed by the operation explanation of the presented protocol.

[1]According to the IEEE 802.11n standard [**?**], 15 μs is suitable for carrier sensing, and 2 μs is adequate to increase/decrease the power level from/to 10% to/from 90%. Therefore, a duration of 20 μs is deemed adequate for transition of power level from P_{ctrl} to P_{max} and vice versa. Since EIFS is set to 120 μs, nodes will transmit at P_{max} every 120 μs for a duration of 20 μs, and the cumulative transmission duration is less than the EIFS duration.

5.4.1 Route Cost Estimation

X-FDR is a cross-layer design routing protocol, which estimates SINR at the physical layer, determines the power levels at the MAC layer, accounts for the number of MAC retransmission attempts, then calculates the energy consumption of a route for the route selection process.

Nodes in the network initiate connections using RTS/FD-CTS messages with maximum power level P_{max}, in order to restrain other nodes residing in the sensing range from initiating an interfering transmission. Once the data transmission take place using controlled power level P_{ctrl}, a periodic increase of power to P_{max} takes place to stop potential interference and eliminate the problem of hidden nodes; therefore, the metric for route cost shall account for different power levels.

In route $R = \{S, A, B, D\}$, the cost of energy $\rho_{(S,A)}$ for sending data from node S to node A can be estimated as

$$\rho_{(S,A)} = N_r(E_{data} + E_{ctrl} + E_{on}) \tag{5.6}$$

where N_r is the the number of retransmission attempts given as $\frac{1}{\mathbb{P}_f}$, where $\mathbb{P}_f$ denotes the probability of occurring a transmission failure [99]. E_{data}, E_{ctrl} and E_{on} denotes the energy consumed during data transmission, control signals transmission and the energy consumed when the receiver is turned on, respectively. E_{data} can be expressed as

$$E_{data} = P_{ctrl_S}(\frac{\beta_{min}}{r} - T_{inc}) + P_{max}T_{inc} \tag{5.7}$$

where P_{ctrl_S} and P_{max} are the controlled power of node S and the maximum transmitting power respectively. β_{min} is the minimum buffer size (explained in Section 5.4.2), and r is the data rate. Moreover, T_{inc} is the

time of the periodic increases in power levels from P_{ctrl} to P_{max}, then back to P_{ctrl}. E_{ctrl} can be expressed as

$$E_{ctrl} = P_{max}(T_{RTS} + T_{FD-CTS}) \tag{5.8}$$

where T_{RTS} and T_{FD-CTS} donate the duration of sending RTS and FD-CTS packets respectively. Assume that there exists a route i where $\mathcal{R}_i = n_o \rightarrow n_1 \rightarrow ... \rightarrow n_k$ from the source node S to the destination D, where, without loss of generality, $S = n_0$ and $D = n_k$. Therefore, the total cost, $\bar{\rho_i}$, consumed along the route $\mathcal{R}_i$ can be presented as

$$\bar{\rho_i} = \sum_{j=0}^{k-1} \rho_{(j,j+1)}(P_j) \tag{5.9}$$

where P_j is the power level used by n_j to communicate with n_{j+l}, and $\rho_{(j,j+1)}(P_j)$ is the relaying cost between nodes n_j and n_{j+l}. Assuming that there are x routes from S to D, the minimum energy consumption route R_{min} chosen by destination node D would be

$$R_{min} = \arg\min(\bar{\rho_i}), i = 1, 2, \ldots, x. \tag{5.10}$$

5.4.2 Route Discovery

The first stage of X-FDR is route discovery. When a source node S requires a route to destination node D, it broadcasts a Route REQuest message (RREQ). Once neighbouring nodes receive RREQ, they calculate the energy cost, ρ, add it to RREQ and broadcast it to the neighboring nodes. After that the neighboring nodes calculate the new ρ, add it to the previous cost received in RREQ, and broadcast it further until it reaches the destination D. The destination node sets up a timer to allow several RREQ messages to arrive from different routes. After

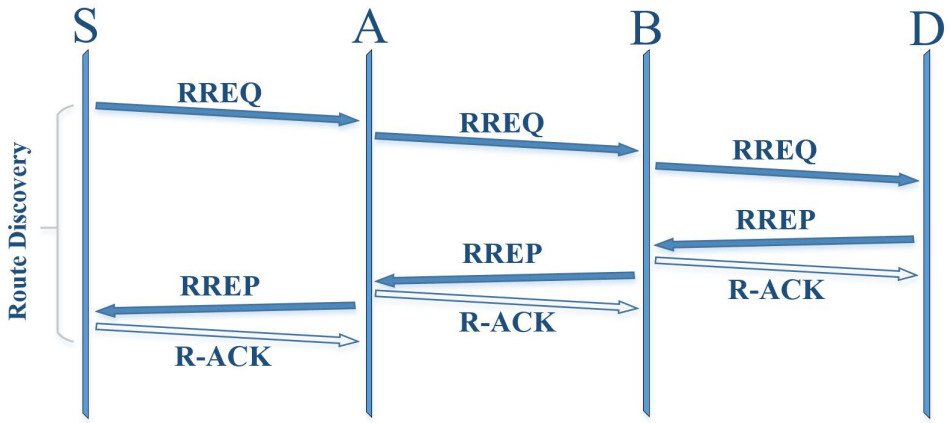

Figure 5.3: Example of route discovery process in X-FDR.

the timer expires, node D chooses the route R_{min} with minimum energy consumption and replies with a Route REPly (RREP) message via R_{min}. The routing table of each node is refreshed, whenever it receives RREQ/RREP messages. Each node maintains a received RREQ table and compares the new RREQ messages in order to eliminate the duplicate RREQ messages. Additionally, a Route-ACKnowledgement (R-ACK) packet is used by the nodes receiving RREP, in order to confirm successful reception of the RREP packet and establishment of the route. Fig. 5.3 demonstrates an example of route discovery performed by node S, where R_{min} is found to be $\{S, A, B, D\}$.

Instead of sending packets sequentially and wait for acknowledgement packets (ACKs) for each data packet. X-FD sends a collection of data packets termed as bundles of data, such that the number of packets in each bundle is determined by the minimum buffer size, β_{min}, of the nodes in the route R. For example, let β_S denote the buffer size (in terms of the number of packets) of node S. Further, node S encapsulates $\beta_{min} = \beta_S$ within RREQ and broadcasts it. When a neighboring node A receives RREQ, it compares β_{min} with its own buffer size (i.e., β_A). If $\beta_A < \beta_{min}$, node A updates $\beta_{min} = \beta_A$ in RREQ and broadcasts it forward. However, if $\beta_A > \beta_{min}$, node A keeps the buffer size as it is and forwards RREQ.

When D receives RREQ, it compares its buffer size with the received β_{min}, and sends the lowest of the two within RREP, which informs node S with the minimum buffer size to be used for data transmission. Note that if a node in the route does not have a buffer enabled, β_{min} will be set to 1, which represents the worst case scenario, nonetheless, this is not a significant issue since the main objective is to find the minimum energy consumption route, and β_{min} is involved in that calculation in Eq. (5.7). The process of route discovery has been summarized as Algorithm 2.

Algorithm 2: X-FDR route discovery process

Input: Source: S, Destination: D, Nodes: N, P_{max}
Output: Route: $\mathcal{R}_{min}$
while $S \rightarrow D$ **do**
  Node S broadcast RREQ packet
end
for *each node* $i \in N \setminus \{S, D\}$ **do**
  if *Node i recieves RREQ* **then**
    i calculates and update the cost ρ_i
    i updates buffer size β_{min}
    i broadcasts updated RREQ
  end
end
if *Node D recieves first RREQ packet* **then**
  set a timer t_{max}
  if $t \leq t_{max}$ **then**
  continue receiving RREQ packets.
  else stop receiving RREQ packets.
  compare the received RREQ packets and select the route $\mathcal{R}_{min}$ with minimum energy consumption according to Eq. (5.10)
end
return RREP packet with $\mathcal{R}_{min}$ and β_{min}.

5.4.3 Data Transmission

When node S receives the RREP message as a result of route discovery process, it becomes aware of the most energy-efficient route to the destination D. After the route discovery process, node S starts transmitting a bundle of data packets to next hop (node A), where the number of packet

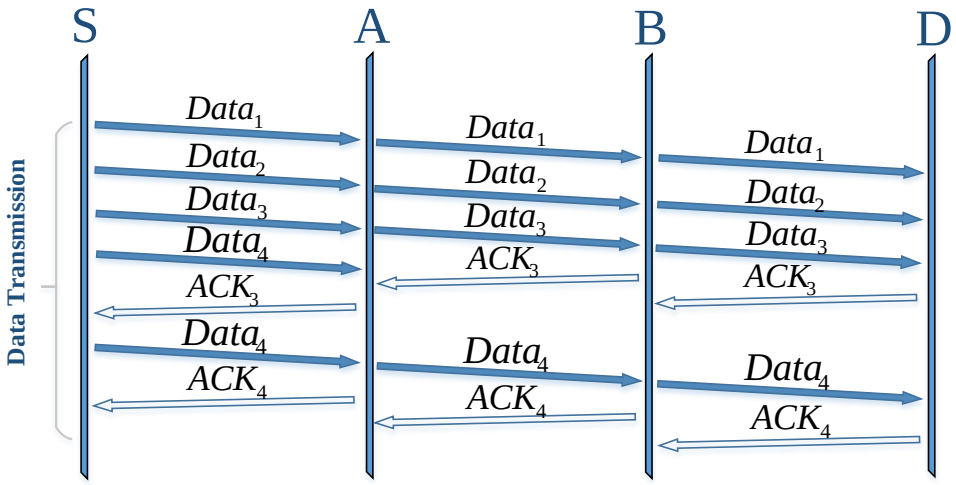

Figure 5.4: Example of data transmission in X-FDR.

in each bundle is given by β_{min} of the route. In conventional HD communications, when node S sends a bundle of data, it will not be notified of transmission errors, e.g., by receiving a Route ERRor (RERR) message, until after the entire bundle is transmitted. This incurs significant waste of time and resources. However, using continuous sensing offered by FD technology, node S can sense a problem in the transmission as soon as it occurs, which leads to immediate termination of the transmission. Hence, node S continuously senses the packets forwarded by node A and stops transmitting immediately if it receives RERR message.

Since node A is FD-capable, it can employ *immediate forwarding*, wherein it does not have to wait for the entire packet to be received before forwarding. Once node A receives all the packets, determined by β_{min}, it replies with an ACK to acknowledge the reception of the last packet. If a packet is dropped while the route is not deemed faulty, node S gets notified by the ACK packet sent by A, and it retransmits the lost packet. The same process is repeated at each hop until the destination is reached. Note that each node in the route only notifies the previous hop with an ACK. This is because data is assumed to be buffered by the previous node in the route as β_{min} is known to all nodes. Therefore, if a

node did not receive all the packets, it would request these from previous nodes using ACK.

For instance, assume that $\beta_{min} = 4$, and consider the scenario demonstrated in Fig. 5.4. Node S transmits data packets 1 through 4 while continuously sensing the signal transmitted by A. Node A starts forwarding immediately; however it only receives 3 packets. Therefore, it sends an ACK for data packet 3, which notifies S that it needs to retransmit data packet 4. Note that if the buffer size of node S is larger than the amount of data packets that needs to be sent, it will include an end-of-queue (EQ) notification message with the last packet, in order to avoid an unnecessary retransmission.

5.4.4 Route Maintenance

The process of route maintenance is depicted in Fig. 5.5, where the transmission of packets 1 to 3 from source S to destination D is exemplified. First, node S transmits the bundle of packets to node A. Node A receives the packets successfully and responds with an ACK packet to the source S to confirm the successful reception. As node A receives the packets, it starts forwarding them to node B. However, node B fails to receive the data packet 3 successfully, despite maximum number of retransmission attempts by node A due to a link error. Once the pre-set timer expires at node A without receiving any ACK from node B, it infers that the link $A-B$ is broken and sends an RERR message to its previous hop, which is node S in this case. The RERR message informs node S of a link failure and a new route discovery process. Node S updates its routing table and marks link $A-B$ as broken, and then acknowledges the RERR of node A. Since the route error occurred at node A, it initiates a new route discovery process by broadcasting a RREQ message. Intermediate

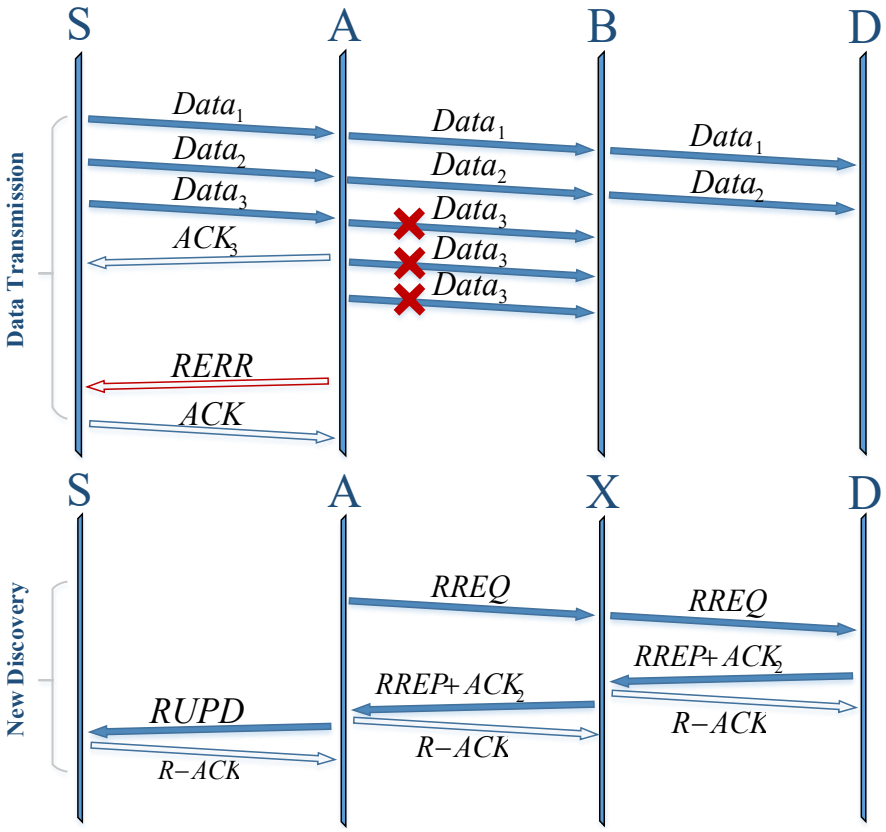

Figure 5.5: Example of route maintenance process in X-FDR.

nodes follow the same procedure as described earlier for route discovery. When the destination node D receives RREQ from node A, prior to the full reception of packets in the same bundle of β_{min}, it knows that the request is to complete the same data stream, and replies with RREP, piggybacked with an ACK packet to inform node A about the last packet node D had received. After receiving the RREP message, node A sends a Route UPDate (RUPD) message, with the new β_{min}, to the previous hop i.e., node S, to inform it of a new route. Finally, node A starts new data transmission to destination D from data packet 3 onwards. If node S has new bundle of data to send, it will use the updated route towards node D, starting the transmission after sensing the last packet sent by node A. The process of route maintenance is summarized in Algorithm 3.

Algorithm 3: Route Maintenance Process in X-FDR

Input: Source: S, Destination: D, Nodes: N, R_{min}
Output: New Route: Updated R_{min}
while $S \rightarrow D$ **do**
  Nodes forward incoming packets
  for *each node* $i \in \{R_{min} \setminus D\}$ **do**
    i transmits packets to $i+1$
    i sets timer t_{ACK}
    if *i receives ACK_z while $t_{ACK} \neq 0$* **then**
    i forwards packets $z+1$
    else i marks link $i \rightarrow (i+1)$ as broken
    Send RERR to node $i-1$
    Nodes $i-(x+1)$, $x \in \{0, 1, \cdots, \text{hops to } S\}$ traverse RERR back to S
    i broadcasts RREQ
    if *D receives RREQ for the same stream* **then**
      set a timer t_{max}
      if $t \leq t_{max}$ **then**
      continue receiving RREQ packets
      else stop receiving RREQ packets;
      compare received RREQ packets and select R_{min}
      return RREP packet with R_{min} and β_{min}.
      if *i receives new RREP* **then**
        Update R_{min}
        Send RUPD to node $i-1$
        Nodes $i-(x+1)$, $x \in \{0, 1, \cdots, \text{hops to } S\}$ update R_{min} and send RUPD back to S
        Closest node to D with full β_{min} received will resume transmission
      end
    end
  end
end

5.5 Performance Evaluation

In this section, we conduct a performance evaluation of X-FDR. We have implemented X-FDR in OPNET. Before we program the routing protocol, we made the necessary changes on the OPNET node model *manet_station_adv.nd*, to allow simultaneous transmission and reception using *wlan_port_rx* and *wlan_port_tx* blocks in addition to *wireless_lan_mac* block. The first step in creating a new protocol on OPNET is to develop a representation of the intended protocol, in OPNET this is called the model-specification, to modify or create a new model, the model-specification editors is used, which is organized in a hierarchical way, specifically, network as higher layer, node, and process and external system modeling environments as lower layer. X-FDR is designed in OPNET as one of the MANET protocols. First, we start by registering X-FDR through the *ip_higher_layer_proto_reg_sup.h* header file. Then we modify the *manet_mgr_routing_protocol_determine* and *manet_mgr_routing_process_create* functions in *manet_mgr.pr* process model, in order to allow the network nodes to configure X-FDR on their interfaces. Further, we add X-FDR as a child process to *manet_mgr.pr* process model. Then we define the new X-FDR parameters as a new group under the ad-hoc Routing Parameters group in *manet_mgr.pr* model attributes. For X-FDR, we need to modify some control packets and add some new ones using the packet format editor, like RREQ, RUPD etc. Then we define the finite state machine for X-FDR with the required transitions, addressing how the protocol behave sequentially. The main work is then done in *xfdr.pr* process model, where X-FDR functionality is defined by a finite state machine. The finite state machine initializes the required state variables and deploy the different stages of the protocol. We assume that nodes are randomly distributed in an area of 500 m2. The buffer size is as-

Table 5.1: Parametric Values (unless otherwise specified)

Parameter	Value
Maximum transmit power	23 dBm (200 mW)
Channel bandwidth	2 MHz
Path loss exponent	4
Noise power	-174 dBm/Hz
Application	File Transfer Protocol (FTP)
Packet size	1 kB
RSI parameter	$\chi = 13$ dB

sumed to be fixed and set to 10 kB. The simulation results are averaged over 10 iterations. In each iteration, source and destination nodes are randomly selected. Other simulation parameters are given in Table 5.1. For performance comparison, we select two different baseline protocols: AODV and FD version of AODV, termed as FD-AODV, wherein nodes employ immediate forwarding and acknowledge each packet. Moreover, both AODV and FD-AODV do not employ power control.

Fig. 5.6 shows the average power consumption of routes from source to designation nodes selected by different protocols. First, we note that the power consumption increases with the number of nodes in the network. This is due to inclusion of more nodes in the routes selected by different protocols. Second, we note that X-FDR outperforms both baseline protocols by performing up to 40% and 50% better than AODV and FD-AODV protocols, respectively. The performance gain of X-FDR in terms of energy-efficiency is primarily due to the use of power control at the MAC layer, which limits the effect of interference, and the adoption of energy-based routing cost metric. Third, we note that SI cancellation plays an important role in power consumption. A higher SI cancellation capability, corresponding to higher values of Δ and ρ, reduces the

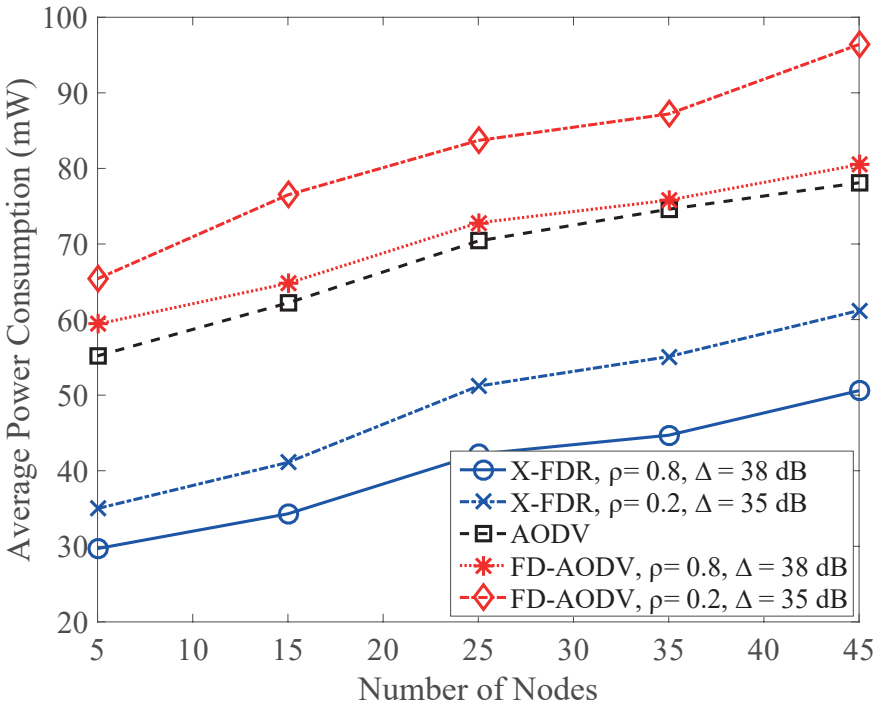

Figure 5.6: Power consumption as a function of network density.

power consumption due to less number of transmission failures due to interference.

Fig. 5.7 plots the relation between average power consumption of routes selected by AODV, FD-AODV and X-FDR, from source S to destination D with fixed distance between them, while keeping the number of nodes fixed to 25 and 35 nodes. We observe an increase in power consumption with the increase in distance between source and destination. This is because longer routes necessitates the involvement of more nodes, which increases the average power consumption. We observe that X-FDR consumes less power than the compared AODV and FD-AODV by up to 70% and 74% respectively when the network comprises of 35 nodes. This is because of he power control adopted by X-FDR and its the power consumption metric. Therefore, we can conclude that the difference in power consumption increases with the increase of distance and number of nodes in the network, making X-FDR an ideal candidate for longer

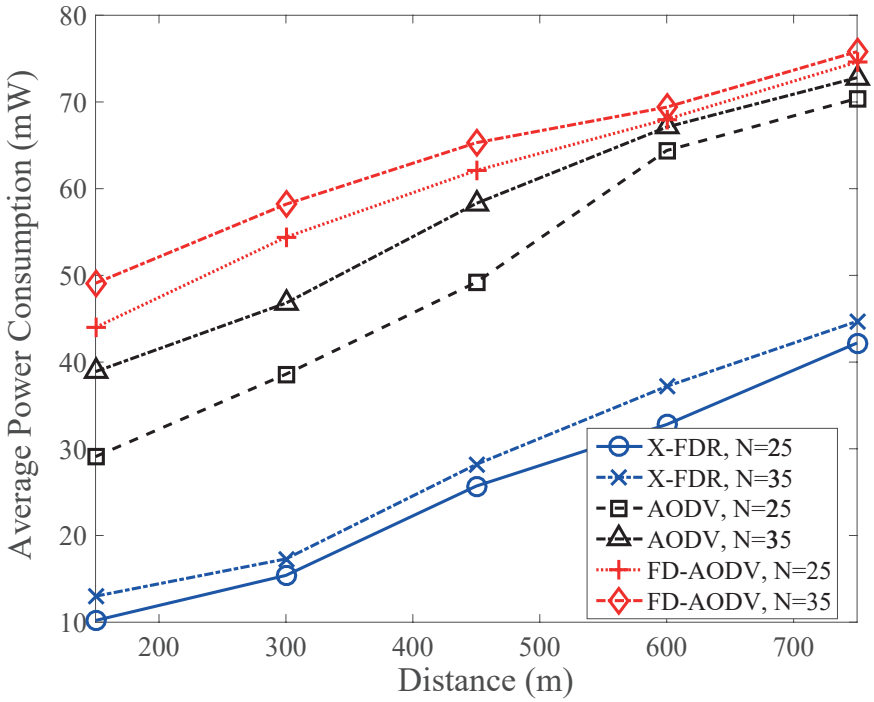

Figure 5.7: Power consumption as a function of distance between source and destination.

routes and networks with higher densities.

Fig. 5.8 shows network throughput against the number of network nodes. We note that X-FDR outperforms AODV by performing up to 50.2% and 21.2% better under high and low SI cancellation scenarios, respectively. This is primarily due to the FD features of X-FDR. Further, X-FDR achieves nearly 8.6% lower throughput than FD-AODV under high SI cancellation scenario. This can be attributed to the employment of power control in X-FDR as there is an inherent trade-off between power and throughput. Note that the presence of SI, due to low SI cancellation capability, can degrade the performance of FD-AODV to the extent that it achieves lower throughput than AODV. Such performance degradation is also visible in case of X-FDR.

Fig. 5.9 plots the average end-to-end delay against the number of network nodes. We note that X-FDR outperforms AODV by achieving up

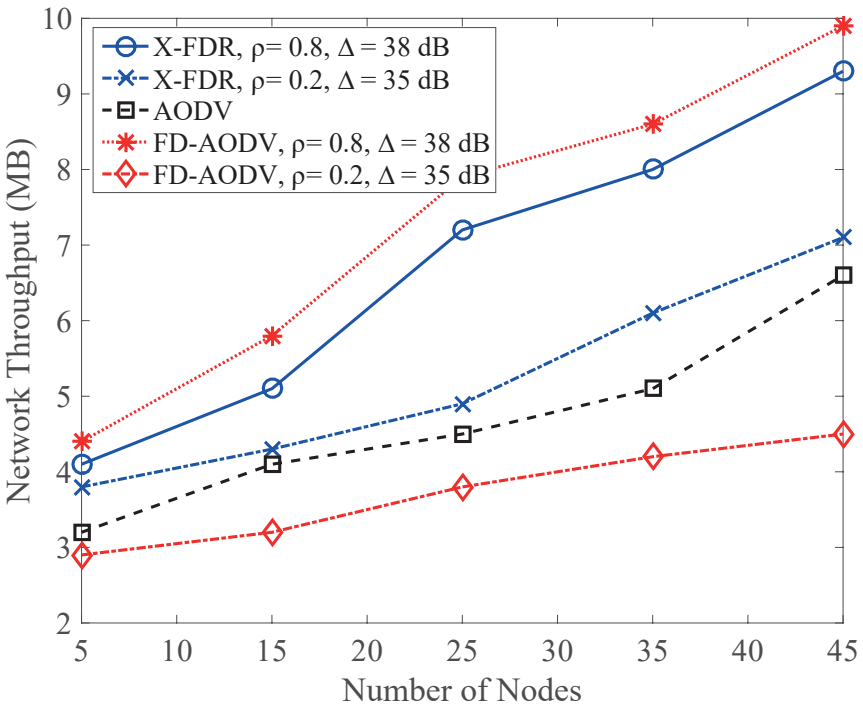

Figure 5.8: Network throughout as a function of network density.

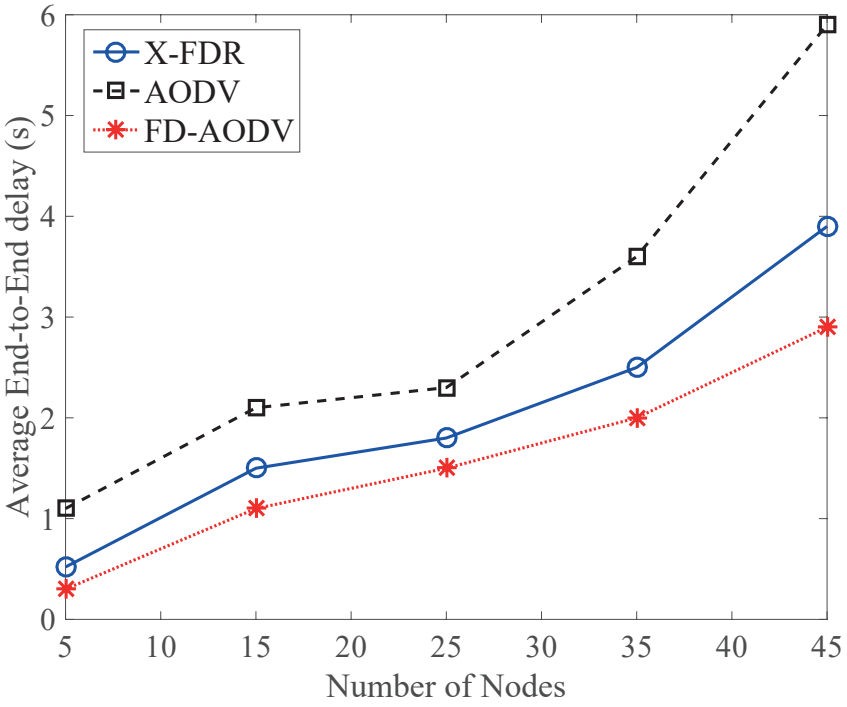

Figure 5.9: End-to-end delay a function of network density.

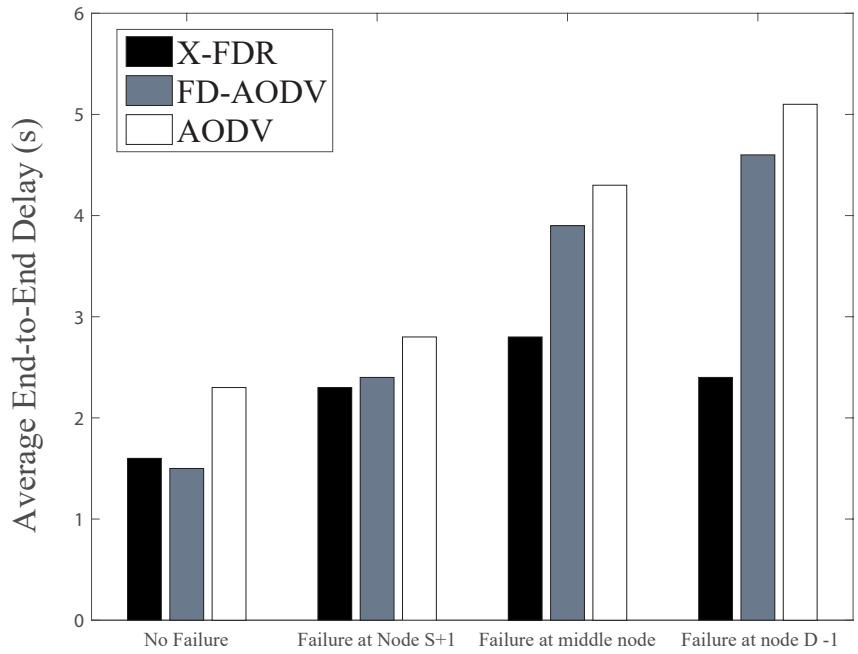

Figure 5.10: End-to-end delay as a function of network density, with nodes failures.

to 33% lower delay, due to the use of immediate forwarding, continuous sensing and bundle transmission mode. On the other hand, FD-AODV outperforms X-FDR by achieving up to 12% lower delay. This is due to the fact that X-FDR incurs higher hop count. Although both AODV and FD-AODV incur similar hop count, the latter achieves lower delay due to immediate forwarding feature. It is important to mention here that the results in Fig. 5.9 correspond to the scenario when the route does not suffer any failures along its path. In order to capture the impact of route maintenance, we deliberately mark nodes to fail (an option provided by OPNET) across the route during transmission process and evaluate end-to-end delay in Fig. 5.10. Initially, we fail the first node after the source, then a node at the middle of the route, and finally, a node right before the destination for worst case scenario. As shown by the results, X-FDR outperforms both AODV and FD-AODV by performing up to 39% and

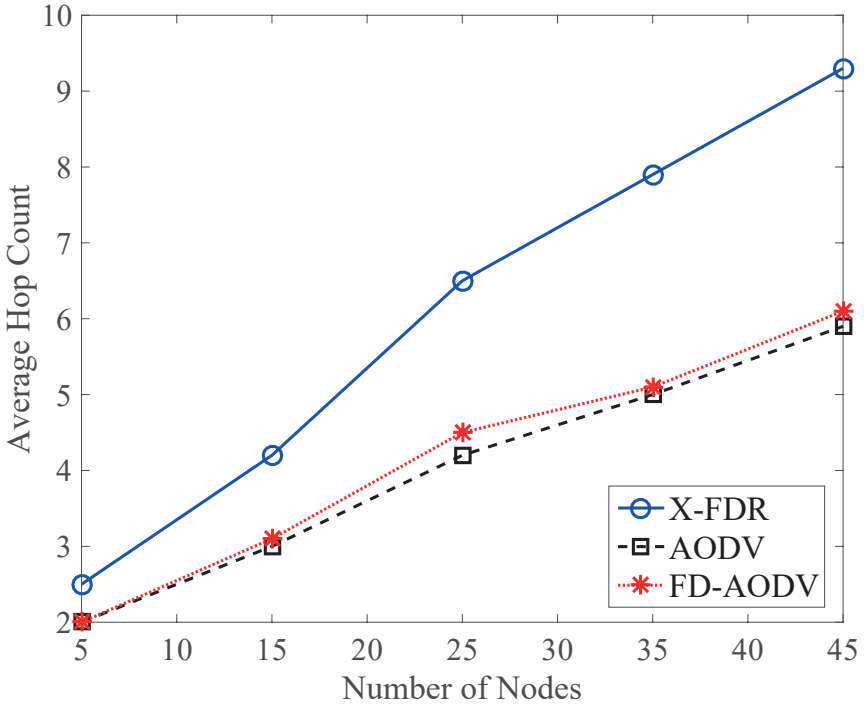

Figure 5.11: Average hop count as a function of network density.

34% better than the former and the latter, respectively. The performance gain is due to the proposed route maintenance procedure that initiates a route discovery process at the last buffered node instead of starting new route discovery process by the source.

Fig. 5.11 plots the average hop count between randomly located source and destination nodes, as a function of number of nodes in the network. The average hop count increases with the number of network nodes as more nodes are involved in the selected routes. We note that X-FDR has higher average hop count than the baseline protocols. This is because both AODV and FD-AODV use hop count as the routing metric. However, X-FDR focuses on routes with minimal energy consumption, and therefore, it incurs higher hop count.

Fig. 5.12 plots the average hop count between the source S and destination D located at a fixed distance from each other, as a function of that distance. We observe how the average hop count increases with

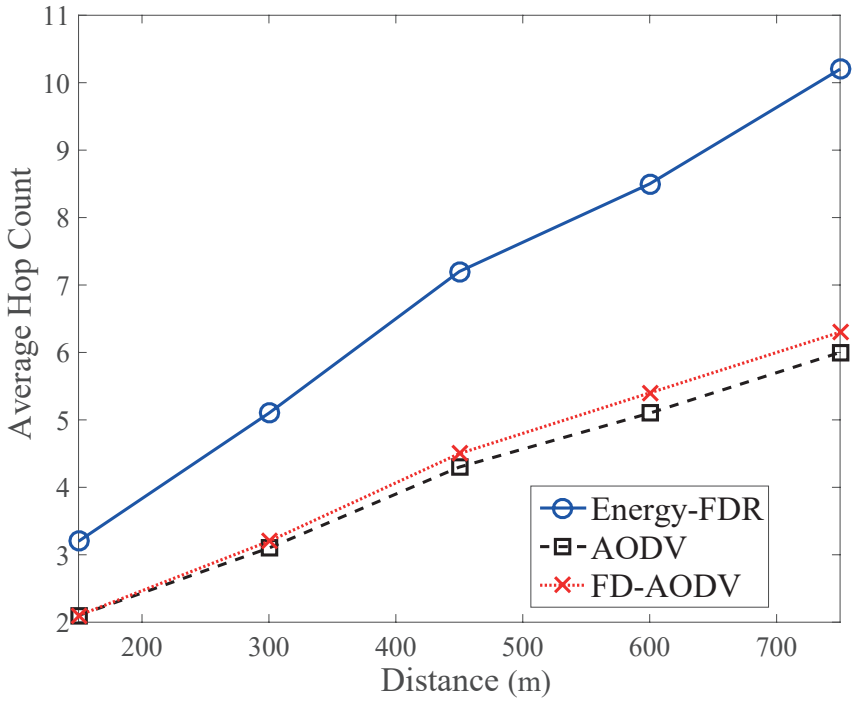

Figure 5.12: Average hop count as a function of distance between source and destination.

the increase of distance between S and D. X-FDR involves more nodes in its route than the compared counterparts do. This is because X-FDR uses power control and selects routes using power consumption metric, while both AODV and FD-AODV transmits with maximum power and use hop count as a metric.

Finally, Fig. 5.13 shows the average number of MAC layer retransmission attempts against the number of network nodes. The average number of retransmissions increase with the number of network nodes due to higher probability of failures as a result of higher inter-node interference. We note that X-FDR incurs the lowest number of retransmissions than both AODV and FD-AODV. This is primarily due to an optimized MAC protocol that minimizes collisions due to hidden node problem while using power control.

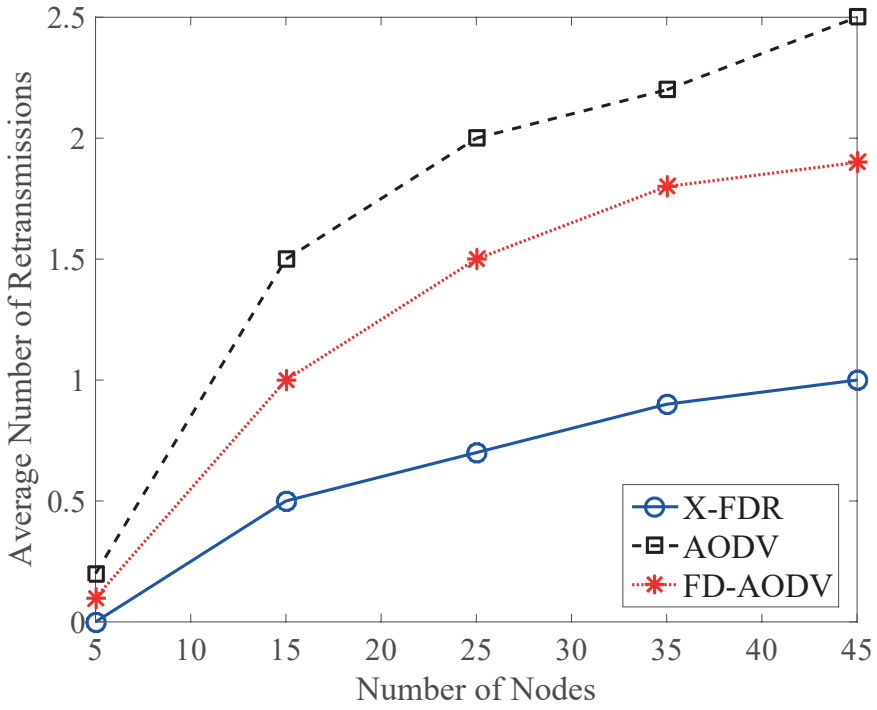

Figure 5.13: Average number of retransmissions as a function of network density.

5.6 Concluding Remarks

FD technology has the potential to play an important role in realizing the capacity objectives of future wireless networks. Realizing the FD capability at higher layers of the protocol stack is particularly attractive to reap the full potential of FD technology. In this chapter, we have designed a cross-layer routing protocol, termed as X-FDR, for multi-hop FD wireless networks with imperfect SI cancellation. X-FDR accounts for RSI at the PHY layer, adopts an optimized MAC protocol with power control feature, and exploits the opportunities provided by FD technology a the network layer. Performance evaluation demonstrates that X-FDR outperforms baseline protocols in terms of power consumption without a significant compromise on network throughput. Besides, it achieves lower end-to-end delay in the presence of route failures. Hence, X-FDR

provides a viable solution for multi-hop FD wireless networks.

Chapter 6

Summary, Concluding Remarks and Future Work

6.1 Summary

Full Duplex technology has recently drawn significant interests in both academic and industrial communities, considering it as a potential candidate towards realizing the capacity objectives of future wireless networks. It presents numerous attractive features like reducing the feedback delay, decreasing the end-to-end delay, enhancing network secrecy and improving the efficiency of network protocols. This study was set out to explore different aspects of FD technology and the impact of its application on different layers of the protocol stack.

Additionally, with growing tendency towards network densification, small cells are expected to play a key role in realizing the envisioned capacity objectives of emerging 5G cellular networks. From a practical perspective, small cells provide an ideal platform for deploying FD technology in cellular networks due to its lower powered nature, and lower cost of deployment compared to its macrocell counterparts. Motivated by these

developments, we analyzed a two-tier heterogeneous cellular networks (HCNs) wherein the first tier comprises half-duplex (HD) macro base stations (BSs) and the second tier consists of FD small cells. Through a stochastic geometry approach, we characterized and derive the closed-form expressions for the outage probability and the rate coverage. Our analysis explicitly accounts for the spatial density, the SI cancellation capabilities, and the interference coordination based on enhanced inter-cell interference coordination (eICIC) techniques. Performance evaluation investigates the impact of different parameters on the outage probability and the rate coverage in various scenarios.

Furthermore, moving higher up in the protocol stack towards MAC layer, we presented an energy-efficient medium access control (MAC) protocol for distributed full-duplex (FD) wireless network, termed as Energy-FDM. The key aspects of the Energy-FDM include energy-efficiency, co-existence of distinct types of FD links, throughput improvement, and backward comparability with conventional half-duplex (HD) nodes. Performance evaluation demonstrates the effectiveness of proposed protocol as a viable solution for full-duplex wireless networks.

After exploration on FD-enabled MAC layer, we present a cross layer aided routing protocol, termed as X-FDR, for distributed multi-hop FD wireless networks. X-FDR exploits a Physical (PHY) layer model capturing imperfection of SI cancellation. At the medium access control (MAC) layer, X-FDR adopts an optimized MAC protocol which implements a power control mechanism without creating the hidden terminal problem. X-FDR exploits the unique characteristics of FD technology at the network layer to construct energy-efficient and low end-to-end latency routes in the network. Performance evaluation demonstrates the effectiveness of X-FDR in achieving the gains of FD at higher layers of

the protocol stack.

6.2 Conclusions

The following conclusions can be drawn based on the overall picture of the research carried out in this thesis.

- The deployment of FD small cells could significantly improve the network performance, increase the capacity and coverage of the network, impose a cost-effective and easily deployable solution, in addition to the advantage of maintaining the conventional HD macrocells unmodified, which significantly decrease the time of FD technology deployment.

- The performance of multi-tier HetNets degrades if tiers comprises of hybrid-duplex base stations, for example, if the network comprises HD and FD small cells, it will perform worse than using FD only small cells and HD macrocells.

- The performance improvement of the two-tier HetNets with FD small cells, relies heavily on the network density, the Almost-Blank-Subframes (ABS) ratio of the enhanced inter-cell interference coordination method, and the self-interference cancellation scheme.

- Existing efforts towards FD communications have mainly investigated Physical (PHY) layer aspects; however, in order to reap the maximum benefits of FD technology, optimizations and novel solutions are required at different layers of the protocol stack.

- Deployment of power control in the MAC layer can lead to hidden nodes problems and fairness issues in the network, unless addressed properly by a scheme that prevent these issues from emerging.

- In the proposed Energy-FDM protocol, the periodic transmission power increase was proposed to solve the hidden nodes problems, while decreasing the transmission power of the data.

- With the proposal of using FD small cells while maintaining the HD macrocells unmodified, it is important to ensure that the proposed FD protocols are backward compatible with conventional HD nodes.

- Adopting FD features, like immediate forwarding and continuous sensing can significantly improve the performance of routing protocols, increasing the average throughput of the networking and decreasing the end-to-end latency.

- Due to energy limitations in wireless nodes and their dependencies on batteries, in addition to the additional processing requirements as some FD features can be energy consuming, it is significantly important to design and deploy protocols that aims to reduce energy consumption at MAC and network layers. Which is the basic purpose of the proposed protocol X-FDR.

- Choosing the proper SI cancellation mechanism plays a significant role in the network performance in all layers, therefore, a proper combination between digital and analogue SI cancellation schemes must be considered to maximize the benefits of FD technology and the performance of FD-enabled nodes.

6.3 Future Work

The Full-Duplex technology is rapidly emerging and have attracted a lot of academic and industrial attention. There are many aspects to needs

to be explored to have a wider comprehension of the technology and its applications.

Research on FD have mainly targeted PHY layer, however there are still many aspects that needs further investigation to complete the vision of FD technology. In Chapter 3, we have derived the outage and rate coverage probabilities for HetNets comprising FD small cells, based on the conclusion that the network perform better when tiers operate in a distinct duplex mode rather than hybrid mode. It would be interesting to investigate more network metrics like energy consumption or latency, as well as investigating energy harvesting in FD environment, also different system models and BSs/users distribution tools can be investigated. Additionally, emerging technologies can be investigated within the considered system model, like Massive MIMO and device-to-device pairs. Moreover, different inter-cell interference coordination schemes can be investigated to study the impact of those schemes on the FD-enabled network.

Another interesting research direction of FD could be to investigate the Cognitive Radio (CR) networks. Issues like how the secondary users (SU) can consider multiple primary users (PU) and SUs. FD SUs can negotiate together in the control phase to determine the final decision given that both nodes may have different traffic flows. Also, SUs can jointly control their power levels to guarantee the quality of service of multiple PUs.

An interesting and rather important research direction of FD would be to investigate security in FD PHY layer. An eavesdropper with FD transmission capability knows the strategies of FD nodes employed at the destination, and performs similar FD operation. Additionally, FD eavesdropped can perform the man in the middle attack in distributed

wireless networks with almost no delay.

In Chapter 4, an energy-efficient MAC protocol termed as Energy-FDR was proposed, in that protocol, nodes were assumed to work in either HD or FD modes, it would be interesting to investigate a selection process between FD and HD modes for nodes that are capable of operating in both modes, where in certain scenarios and conditions, HD mode transmission may outperform the FD transmission when for example interference is overwhelming, also further investigation towards different network parameters can be investigated.

We have proposed in Chapter 5 a cross-layer aided FD routing protocol that aims at minimizing energy consumption and network latency termed as X-FDR. Our protocol uses energy consumption as a metric to determine the route with lowest energy cost, it would be interesting to allow the protocol to choose between different cost metrics to meet certain quality of service levels, like choosing routes with highest throughput, or lowest delay, also network coding can be investigated on TCP to keep the window open. Furthermore, different mobility trajectories can be investigated, and it might be of interest to investigate the ability to switch between traditional and opportunistic routing based on network topology and conditions.

Appendix A

Proof of Theorem 1.

From (3.10), the outage probability $\mathbb{O}_1^{DL}$ is given as

$$\begin{aligned}\mathbb{O}_1^{DL} =&\mathbb{E}\Big[\mathbb{P}\left[SINR_{u_1}^{DL} < \tau_1\right]\Big] \\ =&1 - \int_0^\infty \mathbb{P}\left[SINR_{u_1}^{DL} > \tau_1\right] f_{R_{S_1^*,u_1^0}}(r)dr \\ =&1 - \frac{2\pi\lambda_{S_1}}{\mathcal{A}_{S_1}} \int_0^\infty \mathbb{P}\left[SINR_{u_1}^{DL} > \tau_1\right] r \exp\Big\{-\pi \sum_{j=1}^{2} \lambda_j (\frac{P_{S_j}}{P_{S_1}})^{\zeta_1} r^{\zeta_1}\Big\} dr,\end{aligned} \tag{A.1}$$

where $\zeta_1 = \frac{2}{\alpha_j/\alpha_1}$.

By setting $Q_1 = I_{u_2}^{UL} + I_{S_2} + I_{S_1}^{DL} + N_0$, We rewrite $SINR_{u_1}^{DL}$ as $\frac{h_{S_1^*,u_1}}{{P_{S_1}}^{-1} r^{\alpha_1} Q_1}$. Therefore,

$$\begin{aligned}&\mathbb{P}\left[SINR_{u_1}^{DL} > \tau_1\right] = \mathbb{P}\left[h_{S_1,u_1} > {P_{S_1}}^{-1} r^{\alpha_1} \tau_1 Q_1\right] \\ &= \int_0^\infty \exp\{-{r_{S_1^*,u_1^0}}^{\alpha_{S_1^*,u_1^0}} {P_{S_1}}^{-1} \tau_1 q_1\} f_{Q_1}(q_1) dq_1 \\ &= \mathbb{E}_{Q_1}\left[\exp\{-r^{\alpha_1} {P_{S_1}}^{-1} \tau_1 q_1\}\right] \\ &= \exp\left\{-r^{\alpha_1} {P_{S_1}}^{-1} N_0 \tau_1\right\} \mathcal{L}_{I_{u_2}^{UL}}(r^{\alpha_1} {P_{S_1}}^{-1} \tau_1) \mathcal{L}_{I_{S_2}}(r^{\alpha_1} {P_{S_1}}^{-1} \tau_1) \mathcal{L}_{I_{u_1}^{DL}}(r^{\alpha_1} {P_{S_1}}^{-1} \tau_1).\end{aligned} \tag{A.2}$$

Starting with the Laplace transform of the interference originated from small cell UL users on the macrocell DL user, presented in (A.2), we have

$$\begin{aligned}
&\mathcal{L}_{I_{u_2}^{UL}}(r^{\alpha_1}{P_{S_1}}^{-1}\tau_1) = \mathbb{E}_{I_{u_2}^{UL}}\left[\exp\left\{-r^{\alpha_1}{P_{S_1}}^{-1}\tau_1 I_{u_2}^{UL}\right\}\right] \\
&= \mathbb{E}_{\Phi_{U_2}}\Big[\exp\Big\{-r^{\alpha_1}\frac{P_{u_2}}{P_{S_1}}\tau_1 \sum_{u_2\in\Phi_{U_2}} \mathrm{h}_{u_2,u_1^0} {R_{u_2,u_1^0}}^{-\alpha_2}\Big\}\Big] \\
&\underset{=}{\text{(b)}} \exp\Big\{-2\pi\lambda_{u_2}\int_0^\infty 1-\mathcal{L}_{h_{S_1,u_1}}\Big(r^{\alpha_1}\frac{P_{u_2}}{P_{S_1}}\tau_1 x^{-\alpha_2}\Big)xdx\Big\} \\
&= \exp\Big\{-2\pi\lambda_{S_1}\int_0^\infty\Big(1-\frac{1}{1+r^{\alpha_1}\frac{P_{S_1}}{P_{S_1^*}}\tau_1 x^{-\alpha_1}}\Big)xdx\Big\} \\
&= \exp\Big\{-2\pi\lambda_{u_2}\int_0^\infty \frac{x}{1+\Big(r^{\alpha_1}\frac{P_{u_2}}{P_{S_1}}\tau_1\Big)^{-1}x^{\alpha_2}}dx\Big\}. \qquad \text{(A.3)}
\end{aligned}$$

where (b) is provided in [100]. Note that the integration limits in (A.3) are from 0 to ∞ since the small cell UL users can be at any distance from the DL macrocell users. Now, with a change of variables

$v_1 = (r^{\alpha_1}\frac{P_{u_2}}{P_{S_1}}\tau_1)^{-2/\alpha_2}x^2$, We express

$$\mathcal{L}_{I_{u_2}^{UL}}(r^{\alpha_1}{P_{S_1}}^{-1}\tau_1) = \exp\Big\{-\pi\lambda_{u_2}\Big(\frac{P_{u_2}}{P_{S_1}}\Big)^{2/\alpha_2} Z_1(\tau_1,\alpha_2) r^{\frac{2}{\alpha_2/\alpha_1}}\Big\}, \qquad \text{(A.4)}$$

where

$$\begin{aligned}
Z_1(\tau_1,\alpha_2) &= \tau_1^{2/\alpha_2}\int_{x_1}^\infty \frac{1}{1+v_1^{\alpha_2/2}}dv_1 \\
&= \frac{2\tau_1}{\alpha_2-2}{}_2F_1[1,1-2/\alpha_2;2-2/\alpha_2;-\tau_1]. \qquad \text{(A.5)}
\end{aligned}$$

In (A.5), ${}_2F_1[\cdot]$ denote the Gauss hypergeometric function and $x_1 = (1/\tau_1)^{2/\alpha_2}$. The expression holds for $\alpha_2 > 2$.

Similarly, we can derive the Laplace transform for the interference

from small cells BSs expressed in (A.2), as

$$\mathcal{L}_{I_{S_2}}(r^{\alpha_1}{P_{S_1}}^{-1}\tau_1) = \exp\Big\{ - \pi\lambda_{S_2}(P_{S_2}/P_{S_1})^{2/\alpha_2} \times \frac{2\tau_1}{\alpha_2 - 2}{}_2F_1[1, 1 - 2/\alpha_2; 2 - 2/\alpha_2; -\tau_1]\Big\}, \tag{A.6}$$

for $\alpha_2 > 2$. We finally derive the Laplace transform for the interference originated from macrocell BSs expressed in (A.2) using similar approach, as

$$\mathcal{L}_{I^{DL}_{S_1}}(r^{\alpha_1}{P_{S_1}}^{-1}\tau_1) = \exp\Big\{ - \pi\lambda_{S_1}\big(P_{S_1}/P_{S_1^*}\big)^{2/\alpha_1} \times \frac{2\tau_1}{\alpha_1 - 2}{}_2F_1[1, 1 - 2/\alpha_1, -\tau_1]\Big\}, \tag{A.7}$$

for $\alpha_1 > 2$. Now, plugging (A.4), (A.6) and (A.7) into $\mathbb{P}[SINR^{DL}_{u_1} > \tau_1]$ we obtain

$$\mathbb{P}[SINR^{DL}_{u_1} > \tau_1] = \exp\Big\{ - r^{\alpha_1}{P_{S_1}}^{-1}N_0\tau_1 - \pi\Big(\Big(\Psi_1 r^{\frac{2}{\alpha_2/\alpha_1}}\Big) + \Big(\Psi_2 r^{\frac{2}{\alpha_2/\alpha_1}}\Big) + \Big(\Psi_3 r^2\Big)\Big)\Big\}. \tag{A.8}$$

given

$$\begin{aligned}
\Psi_1 =& \lambda_{u_2}\left(\frac{P_{u_2}}{P_{S_1}}\right)^{2/\alpha_2}\frac{2\tau_1}{\alpha_2 - 2}{}_2F_1[1, 1 - 2/\alpha_2; 2 - 2/\alpha_2; -\tau_1],\\
\Psi_2 =& \lambda_{S_2}\left(\frac{P_{S_2}}{P_{S_1}}\right)^{2/\alpha_2}\frac{2\tau_1}{\alpha_2 - 2}{}_2F_1[1, 1 - 2/\alpha_2; 2 - 2/\alpha_2; -\tau_1],\\
\Psi_3 =& \lambda_{S_1}\left(\frac{P_{S_1}}{P_{S_1^*}}\right)^{2/\alpha_1}\frac{2\tau_1}{\alpha_1 - 2}{}_2F_1[1, 1 - 2/\alpha_1; 2 - 2/\alpha_2; -\tau_1],
\end{aligned}$$

where $\alpha_j > 2$. Therefore, the final expression for a randomly located macrocell DL user is given by (3.13).

Appendix B

Proof of Theorem 2.

From (3.10), the outage probability $\mathbb{O}_2^{DL}$, considering the adapted eICIC mechanism is given by

$$\mathbb{O}_2^{DL} =(1-\rho)\mathbb{E}\Big[\mathbb{P}\left[SINR_{u_2}^{DL} < \tau_2\right]\Big] + \rho\mathbb{E}\Big[\mathbb{P}\left[SINR_{u_2}^{DL\_ABS} < \tau_2\right]\Big], \tag{B.1}$$

where ρ is the ABS transmission ratio.

Starting by the first term of (B.1), we have

$$\begin{aligned}
&(1-\rho)\mathbb{E}\left[\mathbb{P}\left[SINR_{u_2}^{DL} > \tau_2\right]\right] \\
&= 1 - \Big((1-\rho)\int_0^{\infty} \mathbb{P}\left[SINR_{u_2}^{DL} > \tau_2\right] f_{R_{S_2^*,u_2^0}}(r)dr\Big) \\
&= 1 - \frac{2\pi(1-\rho)\lambda_{S_2}}{\mathcal{A}_{S_2}} \int_0^{\infty} \mathbb{P}\left[SINR_{u_2}^{DL} > \tau_2\right] r \\
&\quad \times \exp\Big\{-\pi \sum_{j=1}^{2} \lambda_j \big(\frac{P_j}{P_{S_2}}\big)^{\zeta_2} r^{\zeta_2}\Big\} dr,
\end{aligned} \tag{B.2}$$

where $\zeta_2 = \frac{2}{\alpha_j/\alpha_2}$.

By setting $Q_2 = I_{u_2}^{UL} + I_{S_2} + I_{S_1}^{DL} + N_0$, we get

$$\begin{aligned}
\mathbb{P}\left[SINR_{u_2}^{DL} > \tau_2\right] &= \mathbb{P}\left[h_{S_2,u_2} > {P_{S_2}}^{-1} r^{\alpha_2} \tau_2 Q_2\right] \\
&= \int_0^\infty \exp\{-r^{\alpha_2} {P_{S_2}}^{-1} \tau_2 q\} f_{Q_2}(q) dq \\
&= \mathbb{E}_{Q_2}\left[\exp\{-r^{\alpha_2} {P_{S_2}}^{-1} \tau_2 q\}\right] \\
&= \exp\left\{-r^{\alpha_2} {P_{S_2}}^{-1} N_0 \tau_2\right\} \mathcal{L}_{I_{u_2}^{UL}}(r^{\alpha_2} {P_{S_2}}^{-1} \tau_2) \\
&\quad \times \mathcal{L}_{I_{S_2}}(r^2 {P_{S_2}}^{-1} \tau_2) \mathcal{L}_{I_{S_1}^{DL}}(r^{\alpha_2} {P_{S_2}}^{-1} \tau_2). \qquad \text{(B.3)}
\end{aligned}$$

Following the approach presented in Appendix A, we can obtain the Laplace transforms in (B.3), starting with the Laplace transform of the interference originated from UL to DL small cell users as follows

$$\mathcal{L}_{I_{u_2}^{UL}}(r^{\alpha_2} {P_{S_2}}^{-1} \tau_2) = \exp\Big\{ - \pi r^2 \lambda_{u_2} \left(\frac{P_{u_2}}{P_{S_2}}\right)^{2/\alpha_2} Y_1(\tau_2, \alpha_2)\Big\} \qquad \text{(B.4)}$$

given

$$\begin{aligned}
Y_1(\tau_2, \alpha_2) &= \tau_2^{2/\alpha_2} \int_{{\tau_2}^{-(2/\alpha_2)}}^\infty \frac{1}{1 + y_1^{\alpha_2/2}} dy_1 \\
&= \frac{2\tau_2}{\alpha_2 - 2} {}_2F_1[1, 1 - \frac{2}{\alpha_2}; 2 - \frac{2}{\alpha_2}; -\tau_2], \qquad \text{(B.5)}
\end{aligned}$$

where $\alpha_2 > 2$, and $y_1 = (r^{\alpha_2} \frac{P_{S_2}}{P_{S_2^*}} \tau_2)^{-2/\alpha_2} r^2$.

Similarly, the second Laplace transform in (B.3) of the interference originated from small cell BS on DL small cell user is given as

$$\mathcal{L}_{I_{S_2}}(r^{\alpha_2} {P_{S_2}}^{-1} \tau_2) = \exp\Big\{ - \pi r^2 \lambda_{S_2} \left(\frac{P_{S_2}}{P_{S_2^*}}\right)^{2/\alpha_2} Y_1(\tau_2, \alpha_2)\Big\} \qquad \text{(B.6)}$$

The Laplace transform of the interference originated from macrocell

BS on DL small cell user is given as

$$\mathcal{L}_{I_{S_1}^{DL}}(r^{\alpha_2}{P_{S_2}}^{-1}\tau_2) = \exp\Big\{ -\pi\lambda_{S_1}\Big(\frac{P_{S_1}}{P_{S_2}}\Big)^{2/\alpha_1} Y_2(\tau_2,\alpha_1) r^{\frac{2}{\alpha_1/\alpha_2}}\Big\}, \quad \text{(B.7)}$$

given

$$\begin{aligned} Y_2(\tau_2,\alpha_1) &= \tau_2^{2/\alpha_1}\int_{{\tau_2}^{-(2/\alpha_1)}}^{\infty} \frac{1}{1+y_2^{\alpha_1/2}} dy_2 \\ &= \frac{2\tau_2}{\alpha_1-2}{}_2F_1[1,1-\frac{2}{\alpha_1};2-\frac{2}{\alpha_1};-\tau_2], \end{aligned} \quad \text{(B.8)}$$

where $\alpha_1 > 2$, and $y_2 = (r^{\alpha_2}\frac{P_{S_1}}{P_{S_2}}\tau_2)^{-2/\alpha_1} r^2$.

Plugging (B.4), (B.6) and (B.7) into $\mathbb{P}\left[SINR_{u_2}^{DL} > \tau_2\right]$ we obtain

$$\begin{aligned} \mathbb{P}\Big[SINR_{u_2}^{DL} > \tau_2\Big] = \exp\Big\{ &- r^{\alpha_2}{P_{S_2}}^{-1}N_0\tau_2 - \pi\Big((\eta_1 r^2) \\ &+ (\eta_2 r^{\frac{2}{\alpha_2/\alpha_1}}) + (\eta_3 r^{\frac{2}{\alpha_1/\alpha_2}})\Big)\Big\}, \end{aligned} \quad \text{(B.9)}$$

where

$$\begin{aligned} \eta_1 &= \lambda_{u_2}\left(\frac{P_{u_2}}{P_{S_2}}\right)^{2/\alpha_2} Y_1(\tau_2,\alpha_2) \\ \eta_2 &= \lambda_{S_2}\left(\frac{P_{S_2}}{P_{S_2^*}}\right)^{2/\alpha_2} Y_1(\tau_2,\alpha_2) \\ \eta_3 &= \lambda_{S_1}\left(\frac{P_{S_1}}{P_{S_2}}\right)^{2/\alpha_1} Y_2(\tau_2,\alpha_1). \end{aligned}$$

Similarly, the analysis of the second term in (B.1) of the outage probability during ABS subframes transmission is given as follows.

First, we consider the SINR expressed in (3.6) for the ABS subframes

transmission. By setting $Q_2^* = I_{u_2}^{UL} + I_{S_2} + N_0$, we have

$$\begin{aligned}
\mathbb{P}\left[SINR_{u_2}^{DL_ABS} > \tau_2\right] &= \mathbb{P}\left[h_{S_2,u_2} > {P_{S_2}}^{-1} r^{\alpha_2} \tau_2 Q_2^*\right] \\
&= \int_0^\infty \exp\{-r^{\alpha_2} {P_{S_2}}^{-1} \tau_2 q\} f_{Q_2^*}(q) dq \\
&= \mathbb{E}_{Q_2^*}\left[\exp\{-r^{\alpha_2} {P_{S_2}}^{-1} \tau_2 q\}\right] \\
&= \exp\left\{-r^{\alpha_2} {P_{S_2}}^{-1} N_0 \tau_2\right\} \mathcal{L}_{I_{u_2}^{UL}}(r^{\alpha_2} {P_{S_2}}^{-1} \tau_2) \\
&\quad \times \mathcal{L}_{I_{S_2}}(r^{\alpha_2} {P_{S_2}}^{-1} \tau_2). \qquad \text{(B.10)}
\end{aligned}$$

Since we have previously derived $\mathcal{L}_{I_{u_2}^{UL}}(r^{\alpha_2} {P_{S_2}}^{-1} \tau_2)$ and $\mathcal{L}_{I_{S_2}}(r^{\alpha_2} {P_{S_2}}^{-1} \tau_2)$, we can obtain the probability $\mathbb{P}\left[SINR_{u_2}^{DL\_ABS} > \tau_2\right]$ as

$$\mathbb{P}\left[SINR_{u_2}^{DL\_ABS} > \tau_2\right] = \exp\Big\{ - r^{\alpha_2} {P_{S_2}}^{-1} N_0 \tau_2 - \pi\Big((\eta_1 r^2) + (\eta_2 r^{\frac{2}{\alpha_2/\alpha_1}})\Big)\Big\}. \qquad \text{(B.11)}$$

Therefore, the final expression for the outage probability for a randomly located DL small cell user, considering eICIC is given in (3.15), accounting for (3.10).

Appendix C

Proof of Theorem 3.

From (3.10), The outage probability $\mathbb{O}_2^{UL}$ can be obtained by

$$\mathbb{O}_2^{UL} =(1-\rho)\mathbb{E}\Big[\mathbb{P}\left[SINR_{S_2}^{UL} < \tau_3\right]\Big] + \rho\mathbb{E}\Big[\mathbb{P}\left[SINR_{S_2}^{UL\_ABS} < \tau_3\right]\Big] \tag{C.1}$$

Starting by the first term of (C.1), we have

$$\begin{aligned}
&(1-\rho)\mathbb{E}\left[\mathbb{P}\left[SINR_{S_2}^{UL} > \tau_2\right]\right] \\
&= 1 - \Big((1-\rho)\int_0^{\infty} \mathbb{P}\left[SINR_{S_2}^{UL} > \tau_2\right] f_{R_{S_2,u_2^{UL}}}(r)dr\Big) \\
&= 1 - \Big(2\pi(1-\rho)\lambda_{S_2}\int_0^{\infty} \mathbb{P}\left[SINR_{S_2}^{UL} > \tau_2\right] r\exp\left\{-\pi\lambda_2 r^2\right\} dr\Big), \quad \text{(C.2)}
\end{aligned}$$

Following the same steps used in previous derivations, taking into account the power control factor ϵ, we obtain the final expression of the UL small cell outage probability as given in (3.17), accounting for (3.10).

References

[1] J. Gantz and D. Reinsel, "The digital universe in 2020: Big data, bigger digital shadows, and biggest growth in the far east," *IDC iView: IDC Analyze the future*, vol. 2007, no. 2012, pp. 1–16, Dec. 2012.

[2] D. Evans, "The internet of things: How the next evolution of the internet is changing everything," *Cisco Internet Business Solutions Group (IBSG). White paper*, vol. 1, pp. 1–11, Apr. 2011.

[3] T. Yucek and H. Arslan, "A survey of spectrum sensing algorithms for cognitive radio applications," *IEEE Commun. Surveys Tuts.*, vol. 11, no. 1, pp. 116–130, Mar. 2009.

[4] T. S. Rappaport, S. Sun, R. Mayzus, H. Zhao, Y. Azar, K. Wang, G. N. Wong, J. K. Schulz, M. Samimi, and F. Gutierrez, "Millimeter wave mobile communications for 5g cellular: It will work!" *IEEE access*, vol. 1, pp. 335–349, May 2013.

[5] A. Asadi, Q. Wang, and V. Mancuso, "A survey on device-to-device communication in cellular networks," *IEEE Commun. Surveys Tuts.*, vol. 16, no. 4, pp. 1801–1819, Apr. 2014.

[6] H. Ju, X. Shang, H. V. Poor, and D. Hong, "Bi-directional use of spatial resources and effects of spatial correlation," *IEEE Trans. Wireless Commun.*, vol. 10, no. 10, pp. 3368–3379, Nov. 2011.

[7] M. Al-Kadri, A. Aijaz, and A. Nallanathan, "Ergodic capacity of interference coordinated hetnet with full-duplex small cells," *EW*, pp. 1–6, May 2015.

[8] D. Kim, S. Park, H. Ju, and D. Hong, "Transmission Capacity of Full-Duplex-Based Two-Way Ad Hoc Networks With ARQ Protocol," *IEEE Trans. Veh. Technol*, vol. 63, no. 7, pp. 3167–3183, Sep. 2014.

[9] H. Ju, E. Oh, and D. Hong, "Catching resource-devouring worms in next-generation wireless relay systems: two-way relay and full-duplex relay," *IEEE Commun. Mag.*, vol. 47, no. 9, pp. 58–65, Oct. 2009.

[10] G. Zheng, I. Krikidis, J. Li, A. P. Petropulu, and B. Ottersten, "Improving physical layer secrecy using full-duplex jamming receivers," *IEEE Trans. Signal Process.*, vol. 61, no. 20, pp. 4962–4974, Jun. 2013.

[11] M. Al-Kadri, A. Aijaz, and A. Nallanathan, "An Energy-Efficient Full-Duplex MAC Protocol for Distributed Wireless Networks," *IEEE Wireless Commun. Lett.*, vol. 5, no. 1, pp. 44–47, Feb. 2016.

[12] E. Dahlman, S. Parkvall, and J. Skold, *4G: LTE/LTE-Advanced for Mobile Broadband*, 1st ed. Academic Press, 2011.

[13] M. Mouly, M.-B. Pautet, and T. Foreword By-Haug, *The GSM system for mobile communications*. Telecom publishing, 1992.

[14] V. K. Garg, *IS-95 CDMA and CDMA2000: Cellular/PCS systems implementation*. Pearson Education, 1999.

[15] T. Starr, J. M. Cioffi, and P. J. Silverman, *Understanding digital subscriber line technology*. Prentice Hall PTR, 1999.

[16] M. Gast, *802.11 wireless networks: the definitive guide*. " O'Reilly Media, Inc.", 2005.

[17] B. A. Miller and C. Bisdikian, *Bluetooth revealed: the insider's guide to an open specification for global wireless communication*. Prentice Hall PTR, 2001.

[18] H. Ju, X. Shang, H. V. Poor, and D. Hong, "Bi-directional use of spatial resources and effects of spatial correlation," *IEEE Trans. Wireless Commun.*, vol. 10, no. 10, pp. 3368–3379, 2011.

[19] H. Ju, D. Kim, H. V. Poor, and D. Hong, "Bi-directional beamforming and its capacity scaling in pairwise two-way communications," *IEEE Trans. Wireless Commun.*, vol. 11, no. 1, pp. 346–357, 2012.

[20] H. Ju, S. Lim, D. Kim, H. V. Poor, and D. Hong, "Full duplexity in beamforming-based multi-hop relay networks," *IEEE J. Sel. Areas Commun.*, vol. 30, no. 8, pp. 1554–1565, 2012.

[21] O. Cepheli, S. Tedik, and G. K. Kurt, "A high data rate wireless communication system with improved secrecy: Full duplex beamforming," *IEEE Commun. Lett.*, vol. 18, no. 6, pp. 1075–1078, 2014.

[22] W. Cheng, X. Zhang, and H. Zhang, "RTS/FCTS Mechanism Based Full-Duplex MAC Protocol for Wireless Networks," in *IEEE GC Wkshps*, 2013, pp. 5017–5022.

[23] A. Sabharwal, P. Schniter, D. Guo, D. W. Bliss, S. Rangarajan, and R. Wichman, "In-Band Full-Duplex Wireless: Challenges and Opportunities," *IEEE J. Sel. Areas Commun.*, vol. 32, no. 9, pp. 1637–1652, Sept 2014.

[24] M. Duarte, C. Dick, and A. Sabharwal, "Experiment-driven characterization of full-duplex wireless systems," *IEEE Trans. Wireless Commun*, vol. 11, no. 12, pp. 4296–4307, Dec. 2012.

[25] M. Duarte, A. Sabharwal, V. Aggarwal, R. Jana, K. Ramakrishnan, C. W. Rice, and N. Shankaranarayanan, "Design and characterization of a full-duplex multiantenna system for wifi networks," *IEEE Trans. Veh. Technol*, vol. 63, no. 3, pp. 1160–1177, Nov. 2014.

[26] J. I. Choi, M. Jain, K. Srinivasan, P. Levis, and S. Katti, "Achieving single channel, full duplex wireless communication," *ACM MobiCom*, pp. 1–12, Sep. 2010.

[27] M. Duarte, C. Dick, and A. Sabharwal, "Experiment-driven characterization of full-duplex wireless systems," *IEEE Trans. Wireless Commun.*, vol. 11, no. 12, pp. 4296–4307, May 2012.

[28] H. Ju, X. Shang, H. V. Poor, and D. Hong, "Rate improvement of beamforming systems via bi-directional use of spatial resources," in *IEEE GLOBECOM*, Dec. 2011, pp. 1–5.

[29] B. P. Day, A. R. Margetts, D. W. Bliss, and P. Schniter, "Full-duplex MIMO relaying: Achievable rates under limited dynamic range," *IEEE J. Sel. Areas Commun.*, vol. 30, no. 8, pp. 1541–1553, Sep. 2012.

[30] T. M. Kim, H. J. Yang, and A. J. Paulraj, "Distributed sum-rate optimization for full-duplex mimo system under limited dynamic range," *IEEE Signal Process. Lett.*, vol. 20, no. 6, pp. 555–558, Feb. 2013.

[31] D. Bharadia, E. McMilin, and S. Katti, "Full Duplex Radios," in *ACM SIGCOMM*, 2013, pp. 375–386.

[32] M. E. Knox, "Single antenna full duplex communications using a common carrier," in *IEEE WAMICON*, Apr. 2012, pp. 1–6.

[33] P. Lindberg and E. Ojefors, "A bandwidth enhancement technique for mobile handset antennas using wavetraps," *IEEE Trans. Antennas Propag*, vol. 54, no. 8, pp. 2226–2233, Aug. 2006.

[34] D. Sievenpiper, L. Zhang, R. F. J. Broas, N. G. Alexopolous, and E. Yablonovitch, "High-impedance electromagnetic surfaces with a forbidden frequency band," *IEEE Trans. Microw. Theory Techn.*, vol. 47, no. 11, pp. 2059–2074, Nov 1999.

[35] M. Duarte and A. Sabharwal, "Full-duplex wireless communications using off-the-shelf radios: Feasibility and first results," *in Proc. Signals, Syst. Comput. Conf. (ASILOMAR)*, pp. 1558–1562, Nov. 2010.

[36] E. Everett, A. Sahai, and A. Sabharwal, "Passive self-interference suppression for full-duplex infrastructure nodes," *IEEE Trans. Wireless Commun.*, vol. 13, no. 2, pp. 680–694, Feb. 2014.

[37] E. Aryafar, M. A. Khojastepour, K. Sundaresan, S. Rangarajan, and M. Chiang, "Midu: Enabling mimo full duplex," in *ACM Mobicom*, Aug. 2012, pp. 257–268.

[38] E. Everett, M. Duarte, C. Dick, and A. Sabharwal, "Empowering full-duplex wireless communication by exploiting directional diversity," in *IEEE ASILOMAR*, Nov. 2011, pp. 2002–2006.

[39] J. I. Choi, M. Jain, K. Srinivasan, P. Levis, and S. Katti, "Achieving Single Channel, Full Duplex Wireless Communication," ser. ACM MobiCom, 2010, pp. 1–12.

[40] D. Bharadia, E. McMilin, and S. Katti, "Full duplex radios," *SIGCOMM Comput. Commun. Rev.*, vol. 43, no. 4, pp. 375–386, Aug. 2013.

[41] M. Knox, "Single antenna full duplex communications using a common carrier," *IEEE WAMICON*, pp. 1–6, Apr. 2012.

[42] N. Phungamngern, P. Uthansakul, and M. Uthansakul, "Digital and rf interference cancellation for single-channel full-duplex transceiver using a single antenna," in *Int. Conf. ECTI-CON*, May 2013, pp. 1–5.

[43] B. Yang, Y. Dong, Z. Yu, and J. Zhou, "An rf self-interference cancellation circuit for the full-duplex wireless communications," in *IEEE ISAP*, vol. 02, Oct. 2013, pp. 1048–1051.

[44] S. W. Kim, Y. J. Chun, and S. Kim, "Co-channel interference cancellation using single radio frequency and baseband chain," *IEEE Trans. Commun.*, vol. 58, no. 7, pp. 2169–2175, Jul. 2010.

[45] M. Jain, J. I. Choi, T. Kim, D. Bharadia, S. Seth, K. Srinivasan, P. Levis, S. Katti, and P. Sinha, "Practical, real-time, full duplex wireless," *ACM MobiCom*, pp. 301–312, Nov. 2011.

[46] M. S. Rahman, Y. Li, and B. Vucetic, "An iterative zigzag decoding for combating collisions in wireless networks," *IEEE Commun. Lett.*, vol. 14, no. 3, pp. 242–244, Mar. 2010.

[47] D. Halperin, T. Anderson, and D. Wetherall, "Taking the sting out of carrier sense: Interference cancellation for wireless lans," *ACM MobiCom*, pp. 339–350, Sep. 2008.

[48] I. Krikidis and H. A. Suraweera, "Full-duplex cooperative diversity with alamouti space-time code," *IEEE Wireless Commun. Lett.*, vol. 2, no. 5, pp. 519–522, Oct. 2013.

[49] M. Heino, D. Korpi, T. Huusari, E. Antonio-Rodriguez, S. Venkatasubramanian, T. Riihonen, L. Anttila, C. Icheln, K. Haneda, R. Wichman, and M. Valkama, "Recent advances in antenna design and interference cancellation algorithms for in-band full duplex relays," *IEEE Commun. Mag.*, vol. 53, no. 5, pp. 91–101, May 2015.

[50] H. Q. Ngo, H. A. Suraweera, M. Matthaiou, and E. G. Larsson, "Multipair full-duplex relaying with massive arrays and linear processing," *IEEE J. Sel. Areas Commun.*, vol. 32, no. 9, pp. 1721–1737, Jun. 2014.

[51] T. Riihonen, S. Werner, and R. Wichman, "Optimized gain control for single-frequency relaying with loop interference," *IEEE Trans. Wireless Commun.*, vol. 8, no. 6, pp. 2801–2806, Jun. 2009.

[52] H. A. Suraweera, I. Krikidis, G. Zheng, C. Yuen, and P. J. Smith, "Low-complexity end-to-end performance optimization in mimo full-duplex relay systems," *IEEE Trans. Wireless Commun.*, vol. 13, no. 2, pp. 913–927, Feb. 2014.

[53] T. Riihonen, S. Werner, and R. Wichman, "Mitigation of loopback self-interference in full-duplex mimo relays," *IEEE Trans. Signal Process.*, vol. 59, no. 12, pp. 5983–5993, Dec. 2011.

[54] M. Win, P. Pinto, and L. Shepp, "A mathematical theory of network interference and its applications," *Proceedings of the IEEE*, vol. 97, no. 2, pp. 205–230, Feb. 2009.

[55] H. ElSawy, E. Hossain, and M. Haenggi, "Stochastic geometry for modeling, analysis, and design of multi-tier and cognitive cellular wireless networks: A survey," *Commun. Surveys Tuts.*, vol. 15, no. 3, pp. 996–1019, Jul. 2013.

[56] R. Heath, M. Kountouris, and T. Bai, "Modeling heterogeneous network interference using poisson point processes," *IEEE Trans. Signal Process.*, vol. 61, no. 16, pp. 4114–4126, Aug. 2013.

[57] U. Schilcher, S. Toumpis, M. Haenggi, A. Crismani, G. Brandner, and C. Bettstetter, "Interference functionals in poisson networks," *IEEE Trans. Inf. Theory*, vol. 62, no. 1, pp. 370–383, Jan. 2016.

[58] H. Dhillon, R. Ganti, F. Baccelli, and J. Andrews, "Modeling and analysis of K-tier downlink heterogeneous cellular networks," *IEEE J. Sel. Areas Commun.*, vol. 30, no. 3, pp. 550–560, Apr. 2012.

[59] T. Novlan, H. Dhillon, and J. Andrews, "Analytical modeling of uplink cellular networks," *IEEE Trans. Wireless Commun.*, vol. 12, no. 6, pp. 2669–2679, Jun. 2013.

[60] H. Dhillon, R. Ganti, and J. Andrews, "Load-aware modeling and analysis of heterogeneous cellular networks," *IEEE Trans. Wireless Commun.*, vol. 12, no. 4, pp. 1666–1677, Apr. 2013.

[61] Y. S. Soh, T. Quek, M. Kountouris, and H. Shin, "Energy efficient heterogeneous cellular networks," *IEEE J. Sel. Areas Commun.*, vol. 31, no. 5, pp. 840–850, May 2013.

[62] H.-S. Jo, Y. J. Sang, P. Xia, and J. Andrews, "Heterogeneous Cellular Networks with Flexible Cell Association: A Comprehensive Downlink SINR Analysis," *IEEE Trans. Wireless Commun.*, vol. 11, no. 10, Oct. 2012.

[63] D. Kim, H. Lee, and D. Hong, "A survey of in-band full-duplex transmission: From the perspective of phy and mac layers," *Commun. Surveys Tuts*, vol. 17, no. 4, pp. 2017–2046, Fourthquarter 2015.

[64] J. Lee and T. Quek, "Hybrid full-/half-duplex system analysis in heterogeneous wireless networks," *IEEE Trans. Wireless Commun*, vol. 14, no. 5, pp. 2883–2895, May 2015.

[65] H. Tabassum, A. H. Sakr, and E. Hossain, "Massive MIMO-Enabled Wireless Backhauls for Full-Duplex Small Cells," *IEEE GLOBECOM*, pp. 1–6, Dec. 2015.

[66] S. Han, C. Yang, and P. Chen, "Full duplex-assisted intercell interference cancellation in heterogeneous networks," *IEEE Trans. Commun.*, vol. 63, no. 12, pp. 5218–5234, Dec. 2015.

[67] A. AlAmmouri, H. ElSawy, and M. S. Alouini, "Flexible design for α-duplex communications in multi-tier cellular networks," *IEEE Trans. Commun.*, vol. 64, no. 8, pp. 3548–3562, Aug 2016.

[68] S. Goyal, C. Galiotto, N. Marchetti, and S. Panwar, "Throughput and coverage for a mixed full and half duplex small cell network," in *2016 IEEE ICC*, May 2016, pp. 1–7.

[69] X. Xie and X. Zhang, "Does Full-Duplex Double The Capacity of Wireless Networks?" in *IEEE INFOCOM*, 2014, pp. 253–261.

[70] S. Kim and W. E. Stark, "On The Performance of Full Duplex Wireless Networks," in *IEEE CONF CISS*, 2013, pp. 1–6.

[71] N. Singh, D. Gunawardena, A. Proutiere, B. Radunovic, H. V. Balan, and P. Key, "Efficient and Fair MAC for Wireless Networks With Self-Interference Cancellation," in *IEEE CONF WiOpt*, 2011, pp. 94–101.

[72] S. Goyal, P. Liu, O. Gurbuz, E. Erkip, and S. Panwar, "A Distributed MAC Protocol for Full Duplex Radio," in *IEEE ASILOMAR*, 2013, pp. 788–792.

[73] K. Tamaki, A. R. H., Y. Sugiyama, M. Bandai, S. Saruwatari, and T. Watanabe, "Full duplex media access control for wireless multihop networks," in *IEEE VTC Spring*, Jun. 2013, pp. 1–5.

[74] K. Miura and M. Bandai, "Node architecture and mac protocol for full duplex wireless and directional antennas," in *IEEE PIMRC*, Sep. 2012, pp. 369–374.

[75] Y. Sugiyama, K. Tamaki, S. Saruwatari, and T. Watanabe, "A wireless full-duplex and multi-hop network with collision avoidance using directional antennas," in *Seventh International Conference on Mobile Computing and Ubiquitous Networking (ICMU)*, Jan. 2014, pp. 38–43.

[76] X. Fang, D. Yang, and G. Xue, "Distributed algorithms for multipath routing in full-duplex wireless networks," *IEEE MASS*, pp. 102–111, Oct. 2011.

[77] K. Kato and M. Bandai, "Routing protocol for directional full-duplex wireless," *IEEE PIMRC*, pp. 3239–3243, Sep. 2013.

[78] D. Ramirez and B. Aazhang, "Optimal Routing and Power Allocation for Wireless Networks with Imperfect Full-Duplex Nodes," *IEEE Trans. Wireless Commun.*, vol. 12, no. 9, pp. 4692–4704, September 2013.

[79] B. Mahboobi and M. Ardebilipour, "Joint power allocation and routing in full-duplex relay network: An outage probability approach," *IEEE Commun. Lett.*, vol. 17, no. 8, pp. 1497–1500, Aug. 2013.

[80] J. G. Andrews, "Seven ways that hetnets are a cellular paradigm shift," *IEEE Commun. Mag*, vol. 51, no. 3, pp. 136–144, Mar. 2013.

[81] V. Chandrasekhar, J. Andrews, and A. Gatherer, "Femtocell networks: a survey," *IEEE Commun. Mag*, vol. 46, no. 9, pp. 59–67, Sep. 2008.

[82] R1-104968, "Summary of the Description of Candidate eICIC Solutions," 3GPP std., Madrid, Spain, Aug. 2010.

[83] C. Cox and E. Ackerman, "Demonstration of a single-aperture, full-duplex communication system," *IEEE RWS*, pp. 148–150, Jan. 2013.

[84] D. Ng, E. Lo, and R. Schober, "Dynamic Resource Allocation in MIMO-OFDMA Systems with Full-Duplex and Hybrid Relaying," *IEEE Trans. Commun.*, vol. 60, no. 5, pp. 1291–1304, May 2012.

[85] T. Riihonen, S. Werner, and R. Wichman, "Mitigation of Loopback Self-Interference in Full-Duplex MIMO Relays," *IEEE Trans. Signal Process.*, vol. 59, no. 12, pp. 5983–5993, Dec. 2011.

[86] D. Kim, H. Ju, S. Park, and D. Hong, "Effects of channel estimation error on full-duplex two-way networks," *IEEE Trans. Veh. Technol*, vol. 62, no. 9, pp. 4666–4672, Nov. 2013.

[87] T. Snow, C. Fulton, and W. J. Chappell, "Transmit–receive duplexing using digital beamforming system to cancel self-interference," *IEEE Trans. Microw. Theory Tech.*, vol. 59, no. 12, pp. 3494–3503, Dec. 2011.

[88] P. Lioliou, M. Viberg, M. Coldrey, and F. Athley, "Self-interference suppression in full-duplex MIMO relays," in *IEEE ASILOMAR*, Nov. 2010, pp. 658–662.

[89] T. D. Novlan, H. S. Dhillon, and J. G. Andrews, "Analytical modeling of uplink cellular networks," *IEEE Trans. Wireless Commun.*, vol. 12, no. 6, pp. 2669–2679, Jun. 2013.

[90] S. Singh, H. Dhillon, and J. Andrews, "Offloading in heterogeneous networks: Modeling, analysis, and design insights," *IEEE Trans. Wireless Commun*, vol. 12, no. 5, pp. 2484–2497, May 2013.

[91] D. Kim, H. Lee, and D. Hong, "A Survey of In-band Full-duplex Transmission: From the Perspective of PHY and MAC Layers," *IEEE Commun. Surveys Tuts.*, vol. 17, no. 4, pp. 2017–2046, 2015.

[92] E.-S. Jung and N. H. Vaidya, "A Power Control MAC Protocol for Ad hoc Networks," in *ACM MobiCom*, 2002, pp. 36–47.

[93] IEEE, "Wireless LAN Medium Access Control (MAC) and Physical Layer (PHY) Specifications," 1997.

[94] G. Bianchi, "Performance analysis of the IEEE 802.11 distributed coordination function," *IEEE J. Sel. Areas Commun.*, vol. 18, no. 3, pp. 535–547, 2000.

[95] G. Alfano, M. Garetto, and E. Leonardi, "New insights into the stochastic geometry analysis of dense csma networks," in *IEEE INFOCOM*, 2011, pp. 2642–2650.

[96] D. Moltchanov, "Distance distributions in random networks," *Ad Hoc Networks*, vol. 10, no. 6, pp. 1146–1166, 2012.

[97] T. Bourgeois and S. Shimamoto, "Stochastic analysis of random ad hoc networks with maximum entropy deployments," *IJWMC*, vol. 6, no. 3, p. 19, 2014.

[98] C. Perkins, E. Belding-Royer, and S. Das, "Ad hoc on-demand distance vector (AODV) routing," *No. RFC 3561*, Oct. 2003.

[99] K.-P. Shih, H.-C. Chen, C.-C. Li, and H.-I. Chen, "Cle2ar2: A cross-layer energy-efficient and reliable routing protocol for wireless ad hoc networks," *IEEE Symposium on Computers and Communications*, pp. 436–441, Jul. 2008.

[100] J. G. Andrews, F. Baccelli, and R. K. Ganti, "A tractable approach to coverage and rate in cellular networks," *IEEE Trans. Commun.*, vol. 59, no. 11, pp. 3122–3134, Nov. 2011.